EXPERIMENTAL INVESTIGATION OF THE RATE OF PENETRATION OF VIBRATION ASSISTED ROTARY DRILLING

HENG LI

EXPERIMENTAL INVESTIGATION OF THE RATE OF PENETRATION OF VIBRATION ASSISTED ROTARY DRILLING

By

© Heng Li

A thesis submitted to School of Graduate Studies

in partial fulfillment of the requirement for the degree of

Master of Engineering

January, 2011

Faculty of Engineering and Applied Science

Memorial University of Newfoundland

St. John's, Newfoundland

Abstract

A conceptual drilling technology called Vibration Assisted Rotary Drilling (VARD) was experimentally investigated in this study. Similar drilling technologies and their mechanisms were reviewed during this investigation. A laboratory experimental drilling system was developed. This system is capable of providing basic controls over most drilling operating parameters; it is also capable of providing vibrations with adjustable amplitudes near the bit. Relationship between the Weight on Bit (WOB) and Rate of Penetration (ROP), and the effect of drilling fluids were investigated. VARD experiments on coring and full face diamond impregnated bits were then conducted. The effects of vibrations with various amplitudes on the conventional WOB-ROP relationship were studied and discussed.

Acknowledgement

I would like to express my sincere appreciations and respects to Dr. Stephen Butt and Katna Munaswamy for their supervision. I would also like to thank Farid Arvani, the manager of the VARD research project for his continuous support. I deeply appreciate the works done by the work term students Charles Giles, Andrew McHugh and Josh Roberts, for their great dedications during the development of the VARD experimental facility. Also thanks to the assistance from the lab assistants Shawn Organ and Matt Curtis. Their support made the VARD experimental facility possible.

Table of Contents

List of Tables

List of Figures

List of Symbols

Symbol	Description
C_T	Total cost
C_V	Variable cost
D	Drill bit diameter
D_W	Well depth
DTH	Down- The- Hole percussive hammer
f	Frequency of magnetostrictive vibratory drill
F_B	Pump off force
F_{DO}	WOB monitored at surface at drill off point
F_{OB}	WOB monitored at surface when bit is off bottom
F_{Peak}	Maximum impact force of magnetostrictive vibratory drill
K	Constant determined by empirical drilling data
N	Bit rotary speed
ΔP_B	Pressure drop across bit
P_{OB}	Standpipe pressure when bit is off bottom
P_{DO}	Standpipe pressure at drill of point
P_S	Shkaer control setting position
ROP	Rate of penetration
RPI	Rock penetrability index
S	Rock uniaxial strength
T_{FL}	Flat line time (non-penetrating time)
T_D	Drilling time (penetrating time)
MSe	Mechanical specific energy
UCS	Unconfined compressive strength
VARD	Vibration assisted rotary drilling
W	Weight on bit

W_0	Threshold weight on bit
WOB_{true}	Effective weight on bit accounted for pump off force
WOB_{static}	Static weight on bit mechanically stressed by drill system
A_{Po}	Effective pump off area

Chapter 1

Introduction

Rate of penetration (ROP) is an important indicator of a drilling system performance, which is closely related to the overall operation cost in the modern drilling industry. Fast penetrating drill technologies have high demands in the oil and gas industry.

In the modern drilling industry, fast penetration rate is acquired by advanced drill bit designs, extending bit life, reducing well bore diameter, or drilling with low density mud. All these efforts are done based on the existing rotary drilling system. Up to date, fewer investigations were done in these technologies which improve the ROP by fundamentally changing the drilling mechanisms, although these new technologies have been proved to potentially bring advantages to the penetration rates. For example, one technology called percussive hammer drill breaks the rock by high energy impacts in the axial directions. This percussive hammer drill has higher mechanical energy efficiency, and could significantly increase the ROP when drilling with hard rocks. Another technology called ultra sonic drilling vibrates the bit with high frequency with small amplitude and resonates the drill string to increase the dynamic force. Advantages were acquired when this technology is applied in the shallow surface drilling industries.

One of the major issues of these technologies to be applied in the oil and gas industry is that the vibration energy has difficulties to transmit to the bottom hole; whereas the other problem is that high energy impacts could decrease the drill string stability. For these

reasons, developing a new drilling system with moderate frequency and low amplitudes of vibrations based on the existing rotary systems deserves attention.

In the current thesis, a laboratory scale Vibration Assisted Rotary Drilling (VARD) experimental drill rig was established by the author. The effects of these mid-frequency, low amplitude vibrations on the rate of penetrations were then experimentally investigated.

1.1 Organization of the thesis

In chapter 2, there will be a review of conventional land based oil and gas rotary drilling systems. Factors influencing the rate of penetration, such as weight on bit, rotary speed, bit type, and rock properties will be discussed. Drilling technologies which combine axial percussion and vibrations will also be introduced. These technologies have been found to have the potential to increase the rate of penetration throughout laboratory experiments and field trials.

Chapter 3 will report the development of VARD 'Phase I' experimental drill system and provide description of the major components including an electric coring drill rig, a vibration table, and a data acquisition system. Sensors mounted on this system which monitors the axial thrust force, bit travel, vibration displacement amplitude and frequency will also be included in this chapter. Moreover, the investigations of the system properties, such as i) the suspended weight to real weight on bit conversion, and ii) interaction of shaker payload to the vibration displacement and force amplitudes will be presented in this chapter.

VARD experiments based on coring bits will be reported in Chapter 4. These experiments were conducted under 2 different levels of rotary speeds (300 and 600 RPM), with multiple levels of weight on bit and vibration mechanical powers. Significant ROP improvements were revealed under relatively low WOB conditions. The levels of the vibration mechanical power have effects on the shape of the WOB-ROP curves.

Investigation of the drilling fluid flow rate will be reported in Chapter 5. This investigation was conducted to access the effect of drilling fluids on the ROP. Conventional rotary drilling experiments were carried out under various flow conditions while other operating parameters were kept constant. The result showed that two effects, which were i) the pump off force, and ii) bottom hole cleaning interact with each other, and the flow rate was suggested to be kept at 2.5-3.5 US gpm in the later experiments.

Full face bit VARD experiments will be presented in Chapter 6. Rotary speed and drilling fluid flow rate were kept constant, whereas 5 levels of vibration mechanical power were employed instead of 3 levels as in the coring VARD experiments. Compared to the coring bit results, these experiments were conducted under relatively low WOBs, where the WOB-ROP curve is far from saturation. For this reason, a better observation of the positive effect brought by the vibration could be realized. The result showed that the vibration mechanical power could bring a proportional increase to the ROP while the WOB was kept constant.

1.2 Original Contribution

Based on the observations during the laboratory VARD experiments, the vibrations with fixed frequency (at 60 Hz) are found to have brought significant ROP improvements when drilling with moderate Weight on Bit (WOB). The level of vibration energy, which is represented by the control factor 'shaker control settings', was found to have proportionally increased the ROP. The added vibrations also changed the slopes of the original WOB-ROP relationships. Higher vibration energy could result in sharper incline slope of the WOB-ROP curve, and result in an earlier founder point. This may result in reduced WOB operation ranges when vibrations are introduced, however, the peak ROP values (at the founder WOB) are found to be higher with higher level of vibrations.

Chapter 2

Literature Review

2.1 Rotary Drilling Systems

In the oil and gas industry, drilling wells is the only path to reach the underground oil and gas reservoirs. Hundreds of wells may need to be drilled during the exploration and development of one oil reservoir. In the modern drilling industry, most oil and gas wells are drilled with a rotary drilling system. A sketch of land-based rotary drill rig is shown in Fig. 2.1. It consists of the following sub-systems: hoisting system, rotary system, drill string, bottom hole assembly, power system, circulation system, and well control system. The rotating torque from the rotary system at surface is transmitted through the drill string to the bit. The rotary system is powered by the generator at the surface by a diesel engine and the rotary speed can be controlled by a driller. The drill bit is pressed on the bit-rock contact surface by a force called the Weight on Bit (WOB). This WOB, also called drill pressure, is a balance of the self weight of the drill string, the buoyancy force generated from the returning drilling fluid in the annulus, the drilling fluid pump off pressure, and the hook load from the hoisting system. WOB can be controlled by varying the hook load, while keeping all other drilling parameters constant.

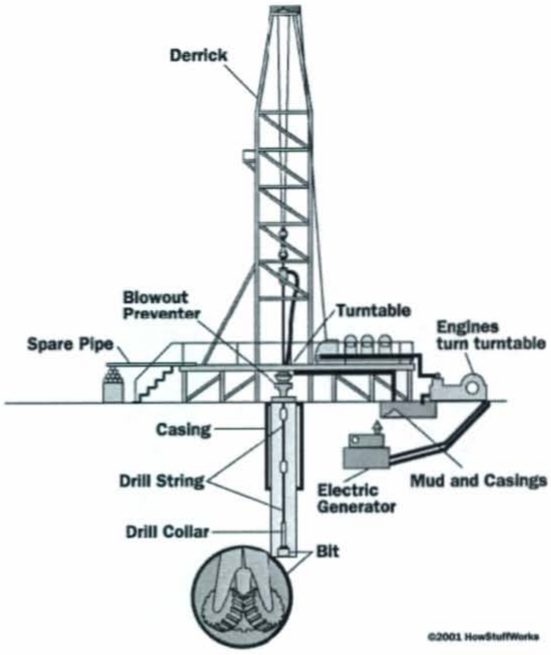

Fig. 2.1 Land based drill rig (from www.howstuffsworks.com)

Drilling fluid is pumped from the surface, starting from the stand pipe into the drill string. Once it reaches the bit, it is ejected by a set of jet nozzles to the bottom of the well bore, then returns from the annulus, (which is the space between the drill string and the well bore), up to the surface. Drilling fluids are crucial in modern drilling operations: flushing away drill detritus created during the bit penetration, cooling down the bit teeth to prevent thermal wear, and balancing the formation pressure to prevent kick or blow outs for well control.

2.2 Drilling Cost Analysis

Penetrating long distance through underground rocks is a costly operation, and the drilling operation cost comprises one of the major expenses in the crude oil production industry. Drilling rate, or called the Rate of Penetration (ROP), is a major indicator to the efficiency of a drilling system. High ROP brought by the technological improvements has great potential to reduce the overall drilling operation costs.

Jean van Wijk (2009) in the VARD drilling research group conducted a series of analysis of the ROP influence to the overall drilling operation cost. The operation cost data were collected based on some field oil and gas drilling operation reports in Newfoundland. A drilling cost function was established.

$$C_t = ((T_D + T_{FL})*C_V + C_0)/ D_w \qquad (2.1)$$

In Eqn. 2.1, Variable cost=total variable cost*24/calculated total time

The sensitivity analysis based on this equation shows that under on-shore oil and gas drilling conditions, increasing the ROP from 15 m/hr to 27.5 m/hr, will reduce the cost per meter from US $620/m to US $415/m. In the mining drilling case, the reduction could be even more significant—cost reduces from US $250/m to US $150/m, while the ROP increases from 4.5 m/hr to 8.7 m/h. Another drilling cost model from Finger (1984) showed a 50% increase in the ROP will result an overall cost reduction of 7.5% during geothermal explorations.

A major trade off to the cost reduction resulted from high ROP is the heavy bit wear under high ROP drilling conditions. This fast bit wear rate would require more frequent

change of the bit, which both increase the bit cost (fixed cost) and the non-penetration time while tripping the bit for replacement. The drilling cost model developed by the VARD team (Van Wijk, 2009) has found that during on shore oil and gas drilling operation, with 100% increase of non penetration time, the drilling cost could increase by close to 11%, from US $700/m to US $790/m. The evaluations of new drilling technologies should be evaluated based on both of these two factors (ROP and bit wear). Maurer (Maurer, 2010) commented that a 25% increase in ROP is a minimum target for new drilling technologies.

2.3 Factors Affecting the ROP in a Rotary Drilling System

The following few sections will discuss the factors affecting the rate of penetration, which is crucial to the overall drilling cost.

2.3.1 Drill Bit

Classified by the rock breakage mechanism (Bourgoyne, et al., 1991), two types of drill bits are widely applied in the oil and gas drilling industry: the drag bit, and the roller bit (Fig. 2.2).

As shown in Fig. 2.2, a roller bit has 2 to 4 rolling cones with inserted teeth. The teeth impact into the rock during the rotation of the roller bit. The rocks were mainly broken by percussion impacts from the tooth. Maurer (1965) and Yang and Gray (1967) examined the exact rock breakage mechanism during the bit tooth impact. Their findings showed that with fixed pore pressure, rock failure mode tends to transform from brittle to psuedoplastic (Maurer, 1965) or ductile (Yang and Gray, 1967).

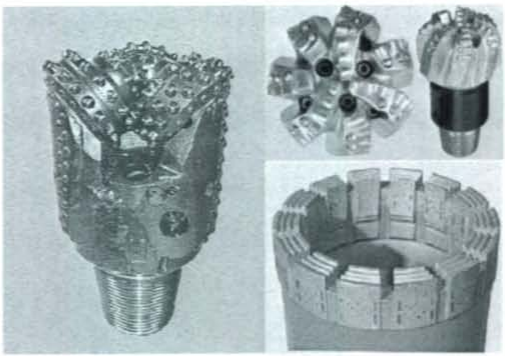

Fig. 2.2 Drill bits for oil and gas drilling operations

Left: roller bit (from Sandvik) Upper right: PDC bit (Greenberg J., 2010)

Lower right: Diamond impregnated coring bit (from archway-engineering)

The drag bit tooth contacts the rock surface with a certain angle. While the tooth is forced to move forward, an area of compressive stress concentration is generated, and this stress concentration will eventually lead the rock to fail in shear, according to Mohr's failure criteria. In recent years, as new types of drag bits, mainly Polycrystalline Diamond Compact (PDC) and Thermal Stable PDC (TSP) bits, were developed. These became more tempting options for their increased durability and ROP compared to roller bits. A laboratory investigation (Black et al. 2008) evaluated the performance comparison of three types of bits (roller bit, diamond impregnated bit and PDC bit). Their results showed that while drilling through a certain type of rock (Crab Orchard Sand-stone) with a same size of the bit (6'' diameter), the PDC bit could reach a ROP close to 15.2 m/h (50 ft/h) at

a low WOB of 8607 kg (19000 lbs), while the diamond impregnated bit had only 2.43 m/h (8 ft/h) at a WOB of 13590 kg (30000 lbs). The roller bit performed the lowest ROP of only 1.37 m/h (4.5 ft/h), while drilling at a very high WOB of 18120 kg (40000 lbs).

2.3.2 Operation Parameters

The following parameters are the factors that could be controlled through the field drilling systems to optimize drilling performance: WOB, bit rotary speed, drilling hydraulic flow rate and pump off pressure. Many researchers have established their empirical functions between the ROP and these operation parameters. The most widely known model is Maurer's drilling model (Maurer, 1962), which is established based on perfect bottom hole cleaning scenario, as shown in Eqn. 2.2:

$$ROP = K\frac{(W-W_0)^2}{D^2S^2}N \qquad (2.2)$$

In this equation, K is a constant which could be determined based on local empirical drilling data; W is the WOB, W_0 is the threshold WOB, which is defined as the minimum bit weight to start the bit penetration; D is the drill bit diameter for full face bits; N is the bit rotary speed; S is described as the 'drillability strength' of the rock.

Among the parameters in Eqn. 2.2, the WOB (W) is believed to be the strongest factor affecting the ROP. In Maurer's model, the ROP proportionally increases with W, until a critical founder point, where ROP begins to decline. This decline is caused by two possible reasons: limitation of the drill motor's torque, or insufficient bottom hole cleaning. A typical model of the WOB-ROP relationship is shown in Fig. 2.3.

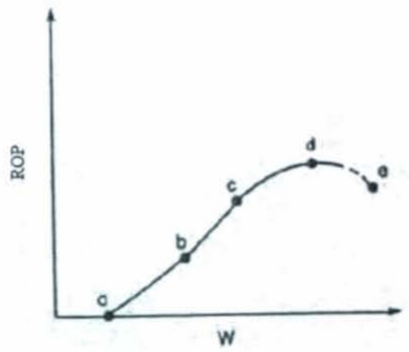

Fig. 2.3 WOB-ROP plot obtained from the experiment verifying the Maurer's model (Bourgoyne Jr, and Millheim 1991)

Another drilling parameter strongly affecting the ROP is the rotary speed. In Maurer's theory, (Eqn. 2.1) the ROP is proportional to the rotary speed. However, Cunningham (1960) concluded that the rotary speed—ROP relationship could be affected by the formation confining pressure (Fig. 2.4). He also recorded the penetration per revolution under different confining pressures, and found that at 5000 psi of confining pressure, the penetration/revolution was reduced with increasing rotary speed, meanwhile, at 0 confining pressure, this value remained constant even if the rotary speed was varied.

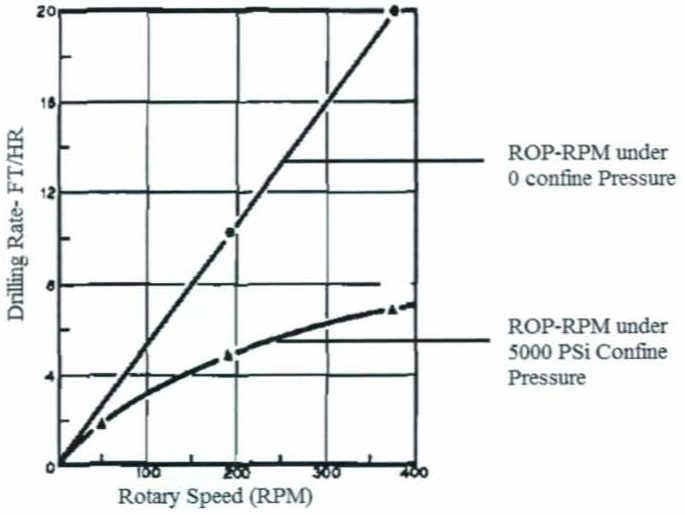

Fig. 2.4 Rotary speed- ROP with and without confining pressure (from Cunningham, 1960)

2.3.3 Rock Properties

In Eqn. 2.2, Maurer suggested that the ROP is proportional to $\frac{1}{S^2}$, where S is interpreted as the 'drillability strength'. This drillability strength is correlated to the rock compressive strength and shear strength. Hoseinie and Ateaei (2009) define 'drillability' as ''the simultaneous influence of physical, mechanical and textural parameters on the penetration rate of drilling systems'', while they attempted to create an index called Rock Penetrability Index (RPI) showing the relationship between drilling performance (ROP) and rock properties. During the establishment of this RPI, 21 rock property factors affecting the ROP were evaluated from previous publications. Based on the frequency

that these rock properties had been mentioned in other publications, the 12 most significant factors for the ROP were selected. Then a statistically calculated number, representing the weight of this factor's influence to the overall drilling performance, was given to each of these parameters. The 12 parameters selected are shown in Fig. 2.5.

Rock characteristics	Total weight
Hardness	0.0998
Compressive strength	0.0883
Young's modulus	0.0862
Matrix type and cementation	0.0874
Quartz content	0.0992
Schmit hammer rebound	0.0834
Texture type	0.0682
Density	0.0738
Abrasiveness	0.0855
Weathering	0.077
Grain size and shape	0.075
Tensile strength	0.0733

Fig. 2.5 Rock properties listed with their weight of influence to the ROP (Hoseinie, 2009)

Gstalder and Raynal (1996) investigated the influence of 4 rock properties that related to rock drillability. Those properties are hardness, specific disintegration (which is very similar to the concept of specific energy, which will be mentioned in later sections), sonic velocity and Young's modulus. Their investigation not only showed that the ROP is correlated to those rock mechanical properties, but they also presented the relationships between the hardness and the other three properties. The relationship between the hardness and the specific disintegration was found to be strong and is shown in Fig. 2.6. The result of this publication showed that under some conditions (drilled by soft rock bit) ROP reduces with increasing of the rock hardness; it also showed a trend of the ROP reduction with the increment of Young's modulus. The sonic velocity was found to have

effects similar to the hardness on the ROP. The ROP/ sonic velocity plot gave a similar trend to the ROP-Hardness plot.

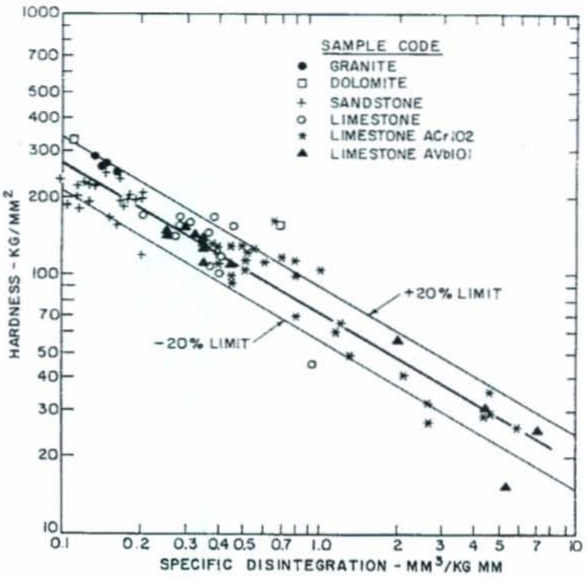

Fig. 2.6 Relationship between hardness and specific disintegration (specific energy) (Gstaider and Raynal, 1996)

Although the drillability research showed many factors potentially affects the ROP, the most widely applied factor to express the resistance to drilling operations from the rock is the unconfined compressive strength (UCS). This was mentioned in Maurer's interpretation to the 'drillability strength'. Spaar et al., (1995) also pointed out that the Unconfined Compressive Strength (UCS) and angle of internal friction are two determinate factors for PDC bit selection.

2.4 Drilling with Vibrations

The above section discussed the factors affecting the ROP in a conventional rotary drilling system. To acquire improvements of the drilling performance, most modern research is focused on optimizing these factors in the existing rotary drilling systems. As a result of these great efforts, the rotary drilling systems have been optimized to such a level that there are few fundamental variables that can be modified to further improve their performance. Up to this stage, it has become necessary and valuable to re-examine the potential of other fundamental drilling mechanisms.

Vibration assisted rotary drilling is one of such conceptual drilling technologies which is believed to have great potential to increase the drilling performance. In 2008 a project called 'Vibration Assisted Rotary Drilling (VARD)' was launched in Memorial University of Newfoundland with the purpose of developing a suitable vibration drilling technology based on the existing rotary drilling systems in order to increase ROP. A wide range of vibration assisted drilling technologies were reviewed. These technologies are:
i) percussive hammer drilling, which is widely applied in shallow hole drilling on hard rocks in mining industry; ii) sonic vibration drilling, which is very suitable to drill in shallow soil formations for civil purposes; and iii) vibration assisted rotary drilling which will be studied by this research.

Although these technologies have some similarities by combining different levels of vibrations to the rotary drilling systems, their drilling penetration mechanisms are quite different. The following section will review these technologies, and the positive and the negative effects they bring.

2.5 Percussive Hammer Drilling

A percussive hammer drill system breaks the rock by creating percussive impacts. Depending on where the percussion hammer is installed, the percussive drill systems are classified into two types—Top hammers and Down the Hole (DTH) hammers. The top hammers have their percussive pistons installed on the surface. The percussive energy transmits a long distance through the drill string to the bit. Because the power efficiencies are not high, when drill strings are long, top hammers are less adopted in many modern drilling operations. In contrast, the DTH drills, which are designed to be compatible with down hole drill strings, have been widely applied for its higher efficiency.

A typical DTH percussive hammer drill assembly consists of a piston between two chambers (upper and lower), a set of valves, a percussive drill head (typically bottom inserted bit) which has some allowance to travel and a chuck which limits the bit movement. A DTH drill assembly is shown in Fig. 2.7. As described by Whiteley and England (1986) the mechanism of this air hammer contains 4 steps of motion: Motion 1—bit pushed by the air pressure and rests on the chuck, air pressure begins to accumulate in the lower chamber; Motion 2—air pressure drives the piston to move upward; Motion 3—upper chamber begins to build pressure, while lower chamber exhausts the remaining air; Motion 4—accumulated energy released and piston strikes on the upper top of the bit.

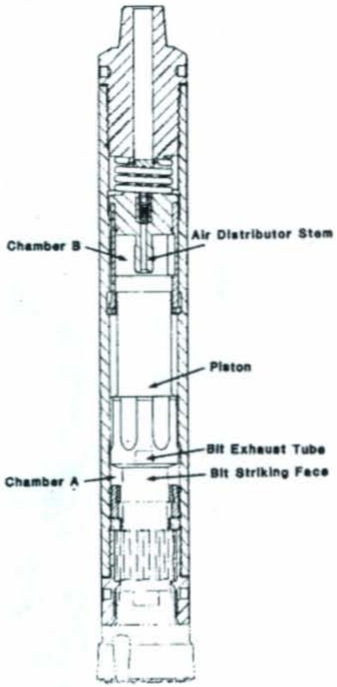

Fig. 2.7 Sketch of down hole percussive air hammer (Whitely, 1986)

These series of motions result in a different rock failure mechanism, compared with the conventional drag bit based rotary drilling system which breaks the rock by shear failure brought by the bit rotation. Han and Bruno (2006), described the rock failure progress while drilling with a percussive hammer: '1) drill bit penetrates rock with compression and vibration; 2) rock receives impact, stress propagates, and damage accumulates; 3) rock fails and disaggregates; and 4) cuttings transport away from the bit and up in the annulus' (p.2). They also studied the rock breakage mechanism and simulated a chisel impacting into a rock surface using Finite Element Modeling (FEM). A strain distribution

plot suggested that a tensile fracture zone which is created by the bit (chisel) impact exists near the compressive zone. Therefore, at least a certain amount of rock material removal is caused by tensile failure instead of shear failure. Paul and Gangal (1969) indicated the existence of tensile failure, through their simulation study using FEM. The location of their tensile fracture zone was slightly different from Han's and Bruno's study. Several other researchers (Rabia, 1985; Lundberg and Okrouhlik, 2001) explained the cause of the tensile failure as reflection of the compressive waves created by the bit. Despite the different approaches explaining the rock failure mechanism, most researchers agreed on the existence of the tensile failure during the percussive drilling. This helps explain the performance improvements brought by the percussive drilling, because in Mohr's failure envelope rock tensile strength is much lower than the shear strength (shown in Fig. 2.8). This implies that percussive drilling requires much less energy to break the rock compared to conventional rotary drilling, which relies on shear failure of rock surface by bit torque (Fossen, 2010).

Due to the unique rock breakage mechanism, and the fact that most percussive drill apparatus use air, foam or other underbalanced drilling fluid as the working fluid as the drilling fluid, a general trend of ROP increment could be observed in most field reports while drilling medium to hard (over 50 MPa of UCS) rocks with DTH percussive hammer drills. Finger (1984) reported a 100% increase of ROP compared with a conventional drilling system, while drilling granites with foam drilling fluids. Pratt (1989) published some air-percussive hammer field results collected in Alberta. These percussive hammers drilled through full depth of the wells. The drilling histories are demonstrated in Fig. 2.9.

In this figure, the hammer drillings reached the target depth in the shortest time compared to mud rotary and air rotary drillings. Eskin et al. (1995), conducted several hydraulic hammer field tests in an exploration field in Bashkiriya, Russia at a depth ranged from 250 to 1300 m. This hydraulic hammer performed the highest ROP at 3.06 m/h compared with 1.95 and 1.76 m/h while drilling with a turbo drill and a rotary system. It also performed a longer bit life at an average of 26.7 m/run, which is more than 100% higher than the other two systems at 11.4 m/run and 10.8 m/run, respectively.

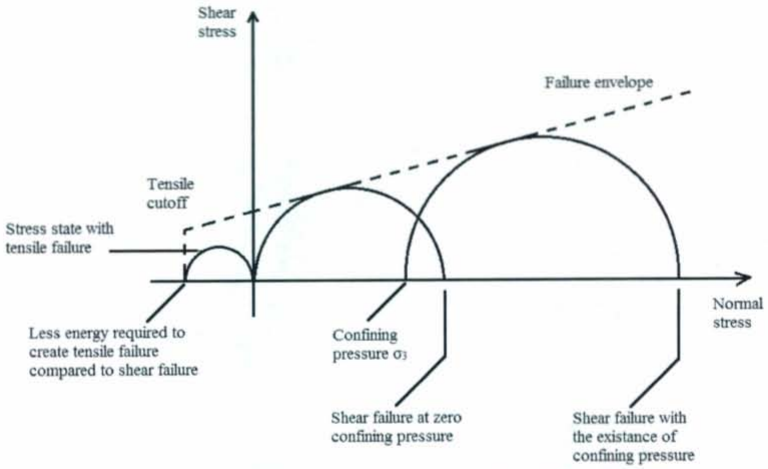

Fig. 2.8 Tensile failure require less energy explained by Mohr-Coulomb failure criterion with tension cutoff

The foregoing sections explained the technological advantage brought by the percussive drills; the next section will discuss the operation parameters of the hammer drills. Compared to rotary drilling systems, percussive drills have two more factors—the piston

impact energy and impact frequency. Meanwhile, because of the change in the drilling mechanism, other parameters, such as WOB, also have a different effect on the drilling performance compared to their functions in the conventional drilling system.

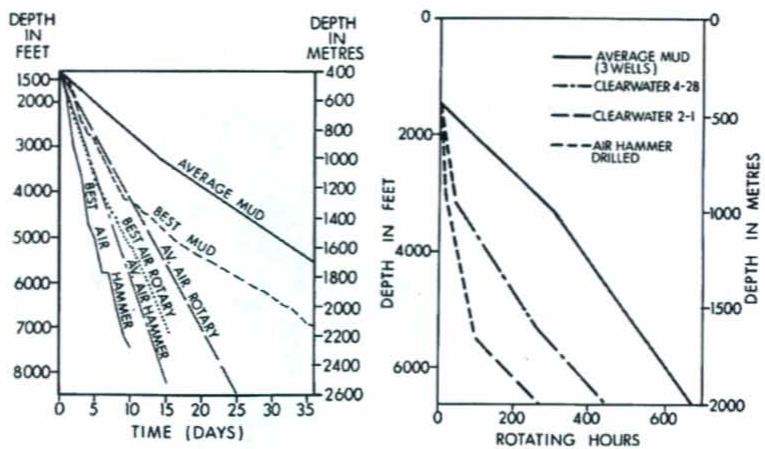

Fig. 2.9 Drill history comparison between air percussive hammer and rotary drill

Jumping Pound area (left) and Clearwater (right) (Finger, 1984)

Pennington (1953) conducted an investigation of the performance of percussive drilling based on the top-hammer system. In their multiple impact tests, an important concept called the indexing angle was developed. This 'indexing angle' stands for the angular rotation between two impacts, and was determined by the ratio between the rotary speed and the impact frequency (impact per revolution). Pennington (1953) found that at a critical indexing angle, the volume of crater per impact could reach 3-4 times more than the single impact crater volume. Some further detailed investigations of this indexing phenomenon were carried out by Hartman (1966). He conducted some parallel indexing

(wedge impact into specimen with different distances) investigations and made the crater volume as the indication of the efficiency of different indexing distances. He found that the wedge geometry, which is related to the bit geometry design, rock type and properties (drillability) are the factors affecting the optimum indexing distance.

Pennington (1953) also conducted field trials with the percussive hammers. High ROP was achieved under low WOB, high RPM, and high dynamic percussive impact force level. The indexing ratio also affected the drilling performance. The optimized ratio between vibration frequency and rotary speed was found to be 200-300 Hz with 60-120 RPM rotary speed with their 4 5/8 inch percussive bottom bit. This result, combined with Hartman's research, suggests that a vibration system including variable frequency will be necessary while drilling through different formations.

Lagreca et al. (2002) presented some field result showing how the WOB affects the ROP while drilling with percussive hammers. In their tests, the driller varied the WOB to 2.25 ton (5 Klbs) in two minutes intervals. A clear instantaneous ROP variation could be observed during the change of WOB, as shown in Fig. 2.10. They also reported that the optimized WOB was around 5-10 Klbs, which was not a high value as their maximum WOB went up to 13.5 ton (30 Klbs). The optimized WOB in such a low value was explained as 'excessive WOB causes loss of impact energy to the cutting face' (p.3). Similar recommendations could be found in many percussive hammer drilling publications which involved studies of the WOB. Pennington (1953) stated that 'no advantage was realized with a dynamic force (vibration percussion force) considerably less than the static load (WOB)' (p.335), because when the WOB is greater than the

percussion force, bit would be forced to keep contact with rock and no actual percussion occurs.

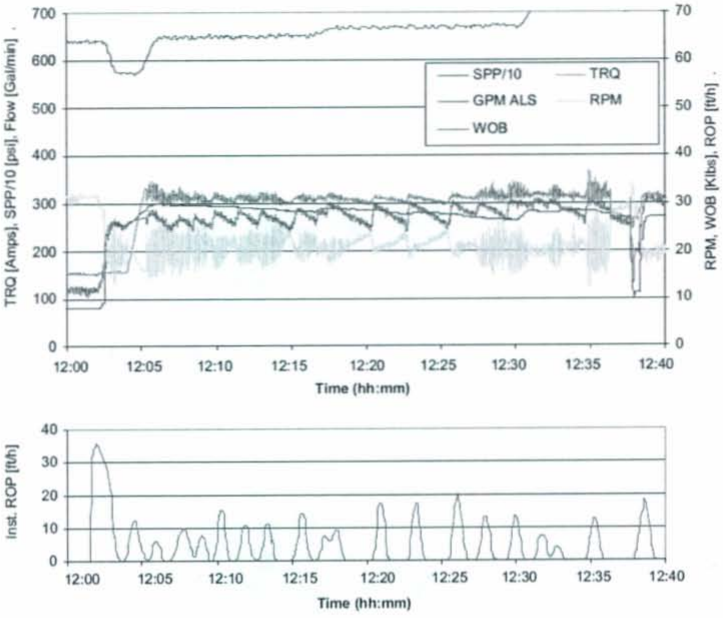

Fig. 2.10 Real-Time drilling data showing WOB affecting the instantaneous ROP (Lagreca, 2002)

Finger (1984) however, pointed that the ROP is less sensitive to the WOB, compared to the impact energy, which could be varied by adjusting the hammer's supply pressure. In Fig. 2.11, he presented a WOB operating envelop which included the variation of the percussion hammer supply pressure. This envelop clearly showed that when doubling the supply air pressure from 125 psi to 275 psi, ROP increased by 100% to 200%. Meanwhile

increasing the WOB from 2.25 ton to 9 ton (5 Klbs to 20 Klbs) only resulted in a 50% increase of the ROP.

The review of percussive drilling, from the control and instrumentation aspect, has come up with following recommendations: to acquire high rate of penetration, a relevantly low WOB (compared to conventional drilling optimized WOB with same scale and bit), combined with high impact force/energy is recommended. The indexing phenomenon should also be noticed. To optimize the indexing ratio (frequency to rotary speed ratio), an experimental based study is necessary for a certain type of rock.

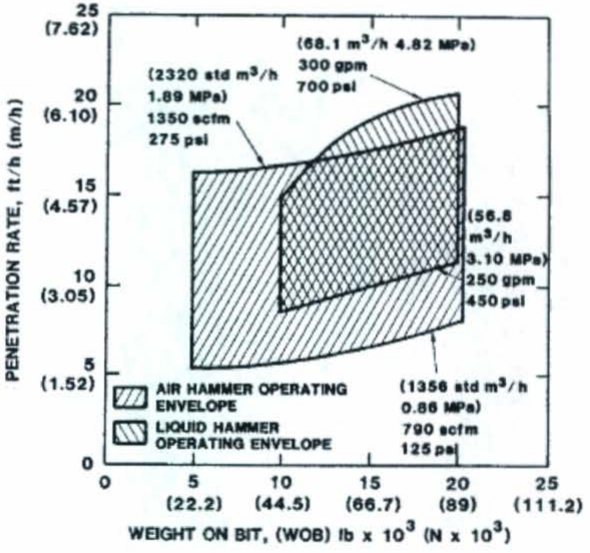

Fig. 2.11 WOB-ROP envelope showing the hammer supply pressure plays a dominant role (Finger, 1984)

2.6 Vibration Assisted Rotary Drilling

The term Vibration Assisted Rotary Drilling (VARD) stands for a technology which places a vibration source near the drill head of a rotary drill system, to achieve a higher rate of penetration than for rotary drilling. Compared to the widely tested percussive drilling, only a few vibration assisted drilling systems have been developed for rock drilling purpose. In fact, in the oil and gas drilling industry, a lot of research has been carried out to limit drill bit vibration on drag bits, because irregular bit friction caused by the vibration and the high WOB result in strong reductions of bit life. Only a few publications were found regarding the vibration assisted rotary drilling; however, performance improvements were found which indicate the potential of this technology. In the following sections, several VARD systems based on their purpose and vibration mechanisms will be reviewed, including the instrumentation setup, effect of operation parameters and the technological advantages they brought.

2.6.1 Resonant Sonic Drilling

A VARD apparatus called ResonantSonic drilling has been introduced (Moad et al., 1995) and tested in the US DOE (US Department of Energy) Handford Site and Sandia National laboratory since 1991. This system was designed to drill subsurface materials for coring, monitoring or remediation wells, and has a similar scale to the conventional cable tool drilling (use the cable to lift and loose the drill string and achieve penetration by low

frequency percussion) which is normally used to drill shallow surface wells. A sketch of a similar system is shown in Fig. 2.12.

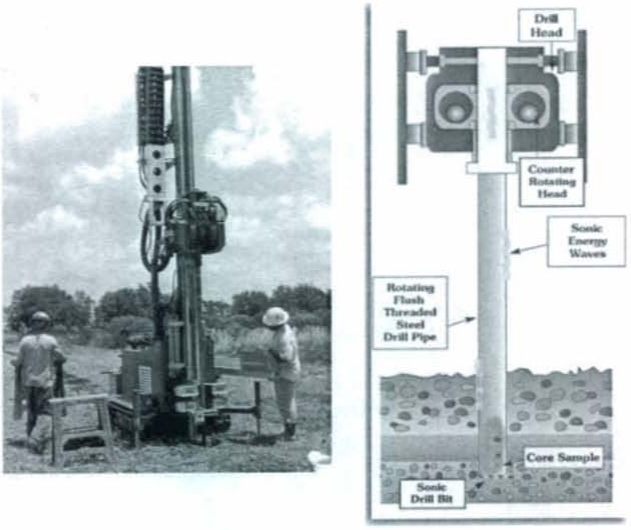

Fig. 2.12 Sonic Drilling instrumentation and technology (From Sonic Samp Drilling ltd)

The essential mechanism of this vibration generator is to have two motor powered rotating masses with synchronized rotation in counter directions. This ensures no horizontal vibration is produced, while vibrations are generated and transmitted into lower drill string in the vertical direction. Vibration frequency could be adjusted to the natural frequency of the drilling string, as a result, resonance will occur and vibration force could be accumulated to a large value. Because of this function, this vibration generator is also called 'resonator'. The DOE report stated that the oscillator could build up the force from 222 kN (50,000 lbs) to 1245 kN (280,000 lbs). In the subsurface

drillings, this resonated energy wave will cause the soil particles surrounding the bit to lose structure and become 'fluidized', thus reducing the resistance to the bit penetration. By adding this vibration instrumentation to a conventional rotary drill tool, three different penetration mechanisms, including shear (by bit rotation), displacement (by resonant), and fracture (by percussion), depending on the type of formation penetrated.

This resonator drill system was field tested from 1991 to 1994 in Hanford and Sandia. During these operations, vibration frequencies were varied from 0 to 150 Hz. Vibration resonance force were varied from 220 kN (50 Klbs) to 880 kN (200 Klbs); a static force which was fed by a hydraulic system plays the role of normal WOB, and was varied from 44 kN (10 Klbs) to 400 kN (90 Klbs). A motor powered the bit rotation and provided 11,524 Nm (8500 ft*lbs) torque. During the drilling, instantaneous ROP was controlled by slightly varying the vibration frequency.

During the test in Hanford, sonic drilling performed an average ROP of 7.26m/day (23.9 ft/day) on soil formations, compared to the cable tool drilling at 3.8m/day (12.6 ft/day) without counting the flat line time (operation time without penetration). Some advantages were also observed in core continuity and sample quality especially on hard rock formations during the coring operations by sonic drilling.

After several years of development, sonic drilling technology has become a mature and popular technology in surface/ shallow depth drilling for many civil applications. Although it could not be directly used in oil and gas drilling due to the compatibility issue and no sufficient power could be transmitted through the long drilling string, the

advantages of adding bit vibration to the large- scale rotary rock drilling systems has been demonstrated.

2.6.2 Surface Mechanical Vibrator and Offshore Sampler

Eskin et al. (1995) reported this surface mechanical vibrator devices to further demonstrate the potential of providing vibrations to rock drilling systems from the surface. As opposed to resonant sonic drilling, no resonance effects were mentioned. The objectives of these systems were to increase drill-string vibrations, therefore increasing the power delivered to the drill bit, as well as the drill performance.

A sketch of the surface mechanical vibrator device is shown in Fig. 2.13. Similar to the sonic drilling, the vibration of this device is also created by opposite rotation of two unbalanced masses. In contrast to sonic drilling, rather than having two motors separately power the unbalanced mass and bit rotation, only one motor is employed to power both systems. The capacity of this system is not mentioned in the report. Although the drilling depth could be increased by adding drill strings, it is possible that this system is as well designed for shallow depth drilling purpose because no well control device or circulation system were found in both the sketch and the original text.

Another similar vibration drilling device reported by Eskin (1995) is the mechanical vibrator offshore sampler (Fig. 2.14). The system has the same unbalanced mass vibration mechanism and as well it uses one single motor to power bit rotation and vibration. One fact to take notice of is that both of these two systems do not have any device to provide a

high level of static drilling pressure. This suggests that for those shallow depth operations with no sufficient feed pressure, such vibration drilling is an ideal solution.

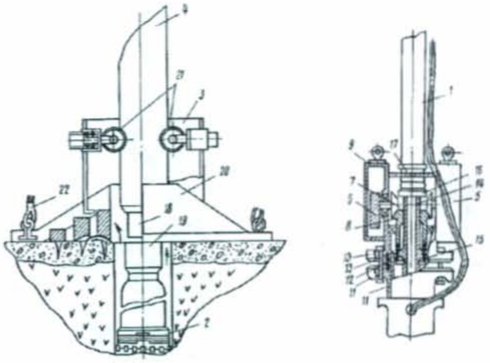

Fig. 2.13 Surface mechanical vibrator (right: lower section; left: upper section) (Eskin et al., 1995)

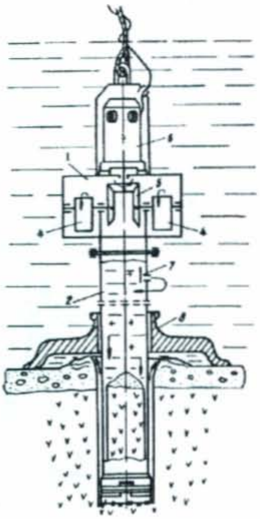

Fig. 2.14 Sketch of offshore sampler with unbalanced mass vibration generator (from Eskin, et al., 1995)

2.6.3 Electro-Magnetostriction Vibratory Drill

Magnetostriction is a phenomenon in which the shape and the dimension of a magnetostrictive material changes when is placed into a magnetic field. Boyd and Donald (1958) developed a VARD system based on this mechanism for the purpose of improving the rate of penetration while drilling in deep well depths. It was developed to be compatible with the down-hole assembly of a conventional rotary drilling system. A sketch of the system is shown in Fig.2.15.

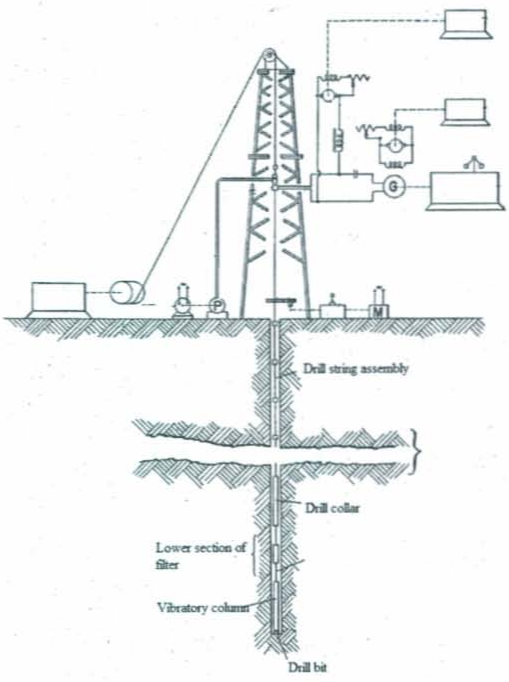

Fig.2.15 Magnetostriction based vibration rotary drilling system (Wise et al., 1958)

The vibratory unit was placed beneath the collar. There was a section of mechanical vibration dampers between the vibration unit and the collar to prevent the vibrations from transmitting to the upper drill strings. The drill bit was placed directly beneath the vibration column. The vibratory unit was designed to be capable of standing the severe down-hole operation conditions (high pressure and high temperature). It was also strong enough to withstand the high tensional force and axial compressive and tensional stress.

A mud pipe traveled through the vibratory unit and conventional mud based drilling could be achieved.

The vibratory unit was powered by an alternating current generator located at the surface. The power line traveled all the way down to the vibrator unit. This vibrator unit was essentially a magnetostrictive type of transducer, supplying 100 KW of electrical energy for the vibrator. With alternating current flowing to the winding, the nickel based magnetostrictive unit would have change in its axial length (shorten and lengthen with the change of magnetic flux through them), thus achieving axial sinusoidal motions while bit was not in contact of rock.

Experiments and field trials were conducted to investigate the effect of the vibration force, frequency and bit contact time on the ROP. The experiments were based on star bits (scratch bits). Single blow impact tests were conducted and the amount of material removal was recorded. It was found that crater volume was dependent on the force of the impact blow, the formation pressure environment and the rock properties. In the multiple impact vibration assisted drilling tests, the rate of penetration were found to be dependent on the vibration frequency, rotary speed, peak value of the thrust force and bit geometry. The experimental and field results showed that at constant rate of penetration, the maximum force and the specific energy has following relationship to the vibration frequency: F_{peak} and MSe $\propto \frac{1}{\sqrt{f}}$.

One example result showed that the maximum force was halved when vibration frequency increased from 80 Hz to 320 Hz, while the ROP maintained constant.

As stated earlier, once the vibrator was turned on, the bit has axial sinusoidal motion when it is not in contact with the rock. However, when the bit is pressed by the static force (WOB) against the rock surface, the bit motion is significantly reduced, resulting in force pulsations of the bit on the rock surface. The peak value of this impulsive force and the contact time is dependent on the vibration characteristics (amplitude and frequency) and the static WOB. The percentage of the bit-rock contact time in one vibration cyclic is called 'on-time'. At exactly 100% 'on-time' (vibration impulsive force equals to static force), the peak force reaches its maximum value. While the static force is larger than the vibration force, the effect of the vibration diminishes and drilling mechanism is similar to conventional rotary drilling. By accounting the effect of bit wear, the optimized 'on-time' value were suggested to be from 50% to 75% while rock strength reduces from hard to soft.

In 1960s and 1970s, similar magnetostriction vibratory drilling technologies were also developed in the USSR (Eskin et al., 1995). A full scale vibration drilling system with an MBS-108 vibrator was evaluated in the late 1960s. A sketch of this vibrator unit is shown in Fig. 2.16.The vibrator works at a fixed frequency of 300 Hz and maximum vibration amplitude of 1.5 mm. The resonance effect was mentioned in the design by applying 'an element with specific dynamic characteristics' to one end of the vibration unit. A crown bit and a rolling cone bit were involved in a comparative drilling test. Rotation speed was varied from 40 to 65 RPM while the 'axial load' (static bit weight) was varied from 100-2200 kg. The result showed a 4 times ROP increment when WOB increases from 600 to 2200 kg for the crown bit. In contrast, the same WOB increment brought only 2 times

ROP increase with roller bits. This implied that the roller bit was less sensitive to the WOB in vibration drillings. The size of the drilling tool assembly was found to be proportional to vibration power, and the optimized bit dimension was 250-300 mm in diameter.

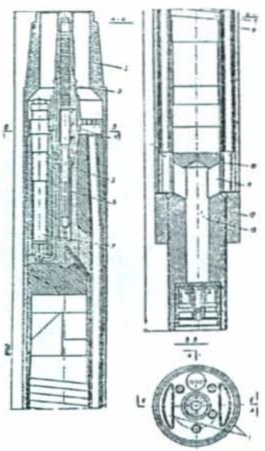

Fig. 2.16 MBS-108 vibration unit (Eskin et al., 1995)

MVS-90 was another magnetostrictive vibrator drill (Fig. 2.17) designed for mining field drilling operations in Ukraine. Instead of nickel, a new type of magnetostrictive material, ferrocobalt alloy 49K2F was used as the essential part of the vibrator. The vibrator works at 1200 Hz with amplitude of 0.6mm. The vibration exciter has 2 meters in length and 90 mm diameter with a weight of 69 kg.

Laboratory tests were conducted with a roller bit as the drill head. The ROP tested compared to conventional drilling, showed a dramatic increase. While drilling with 16

KW power and 90 RPM of vibration drilling, the ROP was 15.8 and 26.0 cm/min, compared with 3.5 and 7.3 cm/min with rotary drilling at two different levels of WOB. The overall ROP was 3.2 to 4.3 times faster than the conventional drilling. Although high ROPs were obtained, specific energy (energy required to remove unit volume of rock) for the vibration drilling was much higher (208 and 215 W/cm^3 compared with 32.4 and 38.6 W/cm^3 of conventional drilling). This suggests that this vibration drilling tool did not have high energy efficiency although much larger amount of energies was introduced by the added vibration.

Three types of bits (roller, crown and full face) were tested during the field trials of the MVS-90 vibrator. The ROP comparative data showed similar result with the laboratory tests (ROP with vibration was 2-3 times higher); a cutter life increment of 5-8 times was obtained while doing vibration drilling on sandstone with a roller cutter bit. However, different from the data shown in the laboratory results, during the vibration drilling the specific energy, which was expressed by KW*h/m in the field test, tended to be much lower than the rotary drilling (around only 30% of the energy consumption compared to rotary drilling). This suggested good energy efficiency during the field tests.

The magnetostriction based vibration drilling tools were widely applied in the shallow drilling operations such as blast hole, wells and excavating machines in the USSR, however no mature instruments were largely applied for oil and gas deep well drilling. During many of these field operations, the magnetostriction vibration drilling showed great advantages compared to conventional or even percussion drilling. The efficiencies compared to air/mud based percussive hammers were 40% -50% higher.

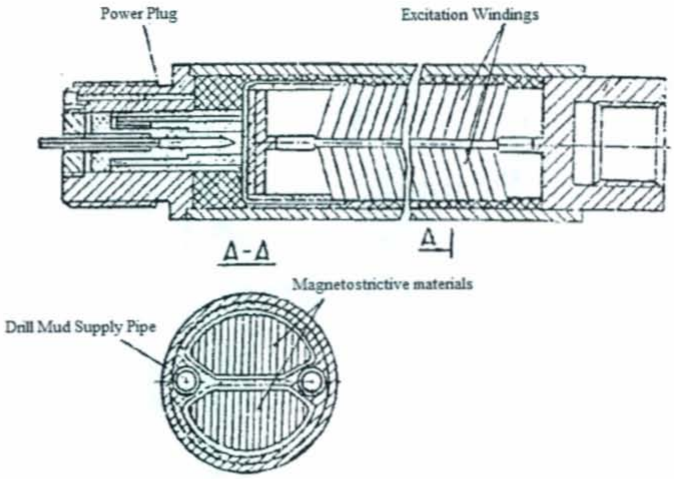

Fig. 2.17 MVS-90 vibrator unit (Eskin et al., 1995)

Chapter 3

Experimental Setup

3.1 Introduction

The objective of the present research was to establish an early stage VARD drilling experimental system including basic controls for most drilling parameters and vibrations near the bit based on existing facilities. After the system was established, the effect of the vibrations and other drilling variables was studied. Preliminary results through these investigations will provide implications for the development of more sophisticated VARD experimental facilities.

This VARD experimental rig was built up based on an electric motor coring drill. A vibration table was mounted on the stand and provides vibrations beneath the sample. Modifications to the electronic drill were done in order to have better control of some parameters, and various sensors were applied on the rig to measure valuable drilling and vibration variables.

3.2 Vibration Velocity Source

A VP-51 electromagnetic shaker table from Syntron Division was chosen as the basis of the vibration velocity source. This shaker table is designed to settle bulk materials or mix cements efficiently in wet and muddy conditions. It also has a suitable size to be installed on the drill stand. For these advantages, it has been adopted and a series of studies to evaluate its performance were carried out.

The sketch and a photo of the VP-51 shaker table are shown in Fig. 3.1. An electromagnetic vibrator is fixed at the bottom of a 0.54 m×0.54 m square plate. Four vibration dampers connect the plate to the main frame; another 4 dampers were placed beneath the frame. The shaker is connected with an external control box. The current input, which is proportional to the mechanical vibration power, could be controlled by a knob on the controller.

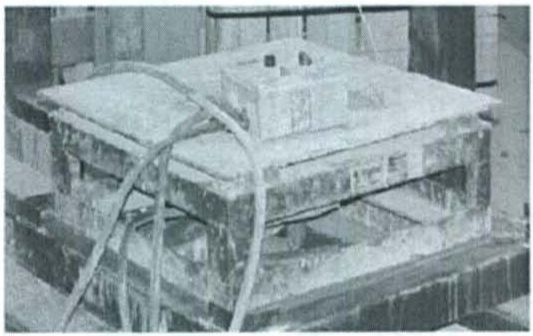

Fig. 3.1 Syntron VP-51 shaker table

The payload capacity of the chosen shaker was 125 kg. The frequency was found to be fixed at 60 Hz, regardless of various load and different current inputs, based on the LVDT and accelerometer data captured during the investigations of the shaker vibration characteristics. The details of these investigations will be presented in Section 3.7.2.

3.3 Rotary Drill System

The essential component of this VARD experimental facility is a 2'' rotary coring drill. The drill is powered by a Milwaukee 4079 electric drill motor which has two levels of rotary speeds (300 and 600 RPM) provided by a mechanical gearbox. The motor is

connected to an ammeter as an indicator of the motor load. A water inlet is located between the drill shaft and the motor; the inlet water pipe guides the drilling fluid to the drill bit. The drill motor travels along a linear gear rail via a small gear wheel installed in the motor part. A set of handle bars are connected to the gear wheel, and the drill pressure (WOB) could be applied through the handle bar by human hand. A fabricated drill stand is connected to the rail beam as the foundation of the whole system. The Milwaukee motor and the initial drill rig setup are shown in Fig.3.2.

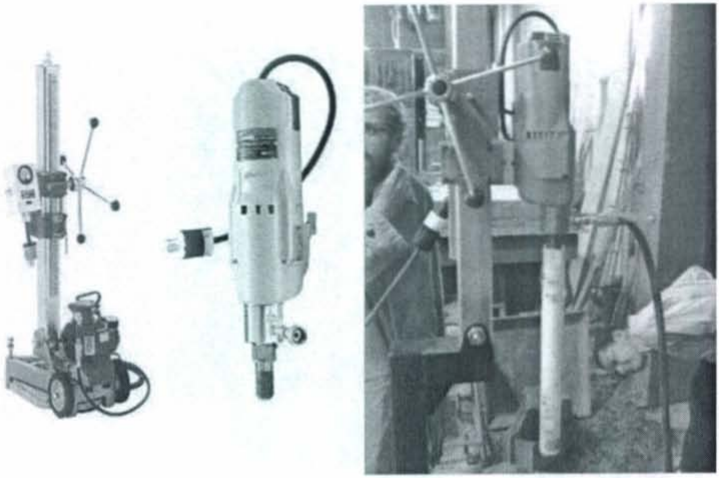

Fig. 3.2 Millwaukee motor and initial drill rig setup

3.4 Modifications to the laboratory VARD testing system

3.4.1 WOB System

As shown in Fig. 3.2, the drill thrust is generated by human hand through the handle bar. Although this is sufficient for normal coring drilling operations, it has inadequate control for research purposes, especially when the WOB has significant influence on the rate of penetration. For this reason, modifications to the handle bar became necessary.

The solution was to install a solid steel wheel with suspended weight at the side instead of the handle bar, which provides constant rotation of force and stable WOB. Initially, a solid steel wheel was designed and fabricated (Fig. 3.3). Because there was no experimental data showing the work range of the WOB for this drill rig, the wheel is designed to be capable to provide the moment arm in two levels. Initial work with this steel wheel showed that it was too heavy for the drill frame, so a light weight replacement was developed. A 26'' bicycle wheel was found to be an ideal replacement for its strength and light weight structure. Some modifications were done so that it could be fixed to the handle bar shaft. The rotating parts in the hub were taken out and the rest of the hub body was bolted to the center of the handle bar set. The experimental setup in this stage is shown in Fig.3.4.

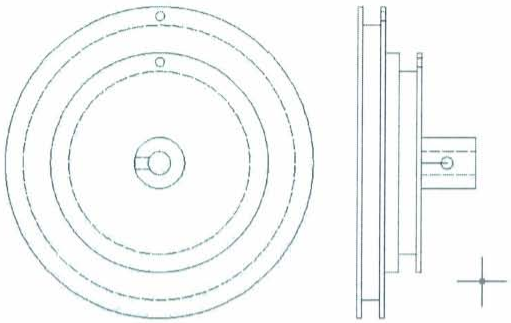

Fig. 3.3 Initial design of the side wheel providing constant WOB with two levels of diameters

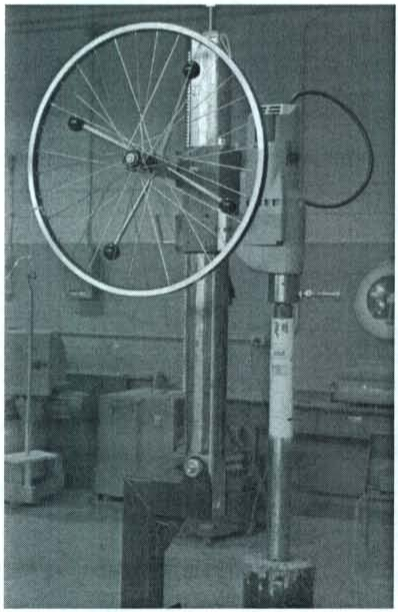

Fig. 3.4 Drill rig installed with a bike wheel to provide constant WOB

Drilling experiments were conducted to test the drill rig after the modifications. The WOB provided by the suspended weights started to rise from 55 kg. A trend of ROP increment could be observed until the maximum suspended weight of 100 kg, after which, a ROP reduction was obtained. The suspended weight was converted into the actual WOB by a conversion equation which was established in the later studies, and the converted WOB varied from 55 kg to 100 kg. The rate of penetration was recorded by a dial-gauge. Two levels of rotary speeds (300 RPM and 600 RPM) were run during the test. The data recorded during the drilling is shown in Table 3.1. The ROP/WOP curve is shown in Fig. 3.5, indicating that the ROP increased with WOB at a similar trend with two set of rotary speeds. The peak ROPs for both occurred at 95.13 kg WOB

Suspended weight (kg)	Actual weight (kg)	Travel time (s)		Bit travel (cm)		Rate of Penetration (cm/s)	
		300 RPM	600 RPM	300 RPM	600 RPM	300 RPM	600 RPM
1.02	55.3	58.7	20.4	4.027	4.207	0.069	0.206
1.22	60.5	31.3	17.5	4.043	4.184	0.129	0.239
1.64	71.5	25.6	13.9	4.01	4.137	0.157	0.298
2.55	95.1	20.3	13	4.258	4.014	0.210	0.309
2.76	100.6	42.5	13.8	3.871	4.185	0.091	0.303

Table 3.1 Drilling data during the test run with the constant WOB system

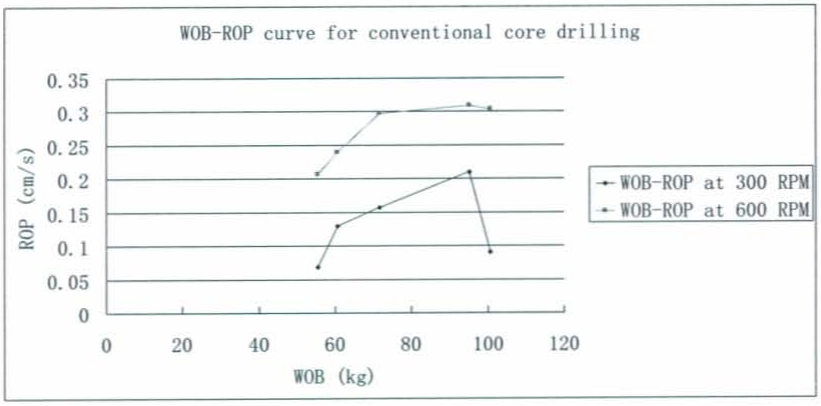

Fig. 3.5 WOB-ROP curve during the test run of modification to provide constant WOB

During the test runs, some problems were found with this bike wheel design. First, because of the relative large wheel size (i.e., 26 inch), bit travel per run was limited to 4.3 cm before the suspended weight touch the ground. Second, some slipping occurred in the connection between the wheel hub and the handle bar shaft. This resulted in occasional sudden drops of the suspended weight and changes in the applied WOB. To resolve this problem, further modification to the WOB system was necessary. A similar wheel with smaller diameter and better connections was purchased. The wheel size is the smallest commercial size, which is 16 inch in diameter. The wheel has a disk brake hub with 6 threaded holes at the outer ring of the hub body, thus realizing a more rigid connection to the exterior shaft. The connecting shaft to the gear wheel was redesigned and the handle bar set was removed. This modification greatly improved the capacity and the quality of the WOB system. The reduced diameter allowed the bit to travel more than 7 cm. It also

resulted in small conversion factors between the suspended weight and the actual WOB, thus increasing the precision of the WOB control.

3.4.2 Installation and Modification of the Vibration Table

The size of the VP-51 vibration table fitted well to the bottom stand of the drill rig. The shaker frame was fixed to the drill stand by 5 C-clamps. Plywood pads were placed between the connecting surfaces of the shaker and the drill stand to isolate the vibrations transmitted from the shaker to the drill stand.

As can be seen from Fig.3.6, the final design includes a sets of brackets designed to firmly fix the sample on the top of the shaker plates. Slots were made on the brackets to provide flexibility to the geometry and the position of the samples. A clamp binds the rock/ concrete sample tightly to the bracket thus resisting rotation and lateral movements during the drilling.

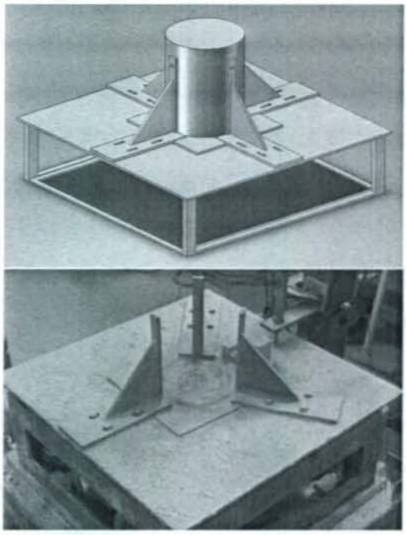

Fig. 3.6 Brackets design and final product to hold the sample

3.4.3 Environmental Protection

The drilling fluids flush the drilling detritus at a flow rate of 3-4 US gpm. The outflow which contains drilling particles needed to be treated in a proper way to maintain the lab environment.

Two phases of modifications were carried out to deal with the drilling mud outflow which contains drilling particles. In the first design, a plastic screen is mounted on the drill stand. All connections between the shaker, the drill stand and the splashing screen are sealed by water proof silicon. Four metallic pans were placed at the bottom and the drill mud out flow was guided into one of the pans. A suction pump was placed in this pan.

With proper operation procedures, this setup could guide the drilling outflow to a sump on the floor. However the plastic screen became a hindrance to operations near the shaker. The re-install and adjustment of the shaker and the sensors have become extremely difficult for the operators. To overcome this limitation, a 1.82 m×1.82 m×17.2 cm wooden basin was placed beneath the drill stand. The same suction pump introduced in the earlier phase was used to drain the out flow accumulated in the basin to the sump. This final setup satisfied the environmental protection requirement.

3.4.4 Modification and Coupling for the Full Face Bit Experiments

The Milwaukee 4079 drill is designed for coring bits. However, some experiments required drilling using a full face bit.

The full face bit has been chosen was an AWJ standard, diamond impregnated bit, produced by Boart Longear. The bit has an 11 cm long drill shaft, with 1 7/8 inch diameter cutting surface and a 1 3/8 inch by 5 threaded coupling. During the coring bit experiments, strong wobbling of the drill shaft was obtained when the bit was initially penetrating into the rock sample. This wobbling issue could be more severe while switched to full face bit due to the increased contact area between the bit and the rock surface. To reduce this wobbling effect, a bushing was fixed outside of the drilling shaft to limit the drill shaft from lateral movement. The bushing was fixed by an arm extended from the drill stand. The location (height) of this arm was finalized mainly with the consideration of spacing issues.

3.5 DAQ- System

VARD drilling performance could be affected by the rotary drilling parameters and vibration variables. To further study these parameters, several sensors were applied to the VARD experimental system. To capture the analog signals from the sensors, data acquisition systems (DAQ) are needed. Alone with the VARD experiments, 2 DAQ-systems were used—Labview and Micro Strain.

3.5.1 NI DAQ-System

All analog signals from the sensors were collected through a PCI 6024E data acquisition board from National Instruments. The board has a maximum frequency of 20 KS/S, which has been found to be practical while recording data at 0.2-1ks/s ranges. This is the major range for the VARD sensors measuring variables to adequately capture the 60 Hz vibrations. A CB-68LP I/O connector board is paired with the PCI board (connected by a R6868 cable). The board has 15 analog inputs and 7 digital I/Os.

NI provides two DAQ- software for this system—Labview and Signal Express. Labview provides a platform to graphically program the input signal. Signal Express is a simplified version of the Labview. It monitors and records the signals with a given voltage and frequency setup. Functions such as filter, count, or clear offset could be selected from the menu. The file outputs could be saved in .csv format and could be further analyzed by excel and matlab.

3.5.2 Micro Strain Wireless DAQ-system

Attempts to examine the drill rig's axial force by a load cell encountered difficulties with the NI DAQ-system due mostly to signal to noise ratio. Attempts to filtering were also unsuccessful since both the noise and the force signal were predominantly at 60 Hz.

A better solution was the SG Link wireless transmitter which consists of a Micro-Strain USB base station, the SG-Link wireless transmitter and Agile-Link software. The whole system is specifically designed for strain gauges and Wheatstone bridge type load cells. Integrated in the transmitter node, there are functions to amplify the signal and make adjustments to balance the bridge.

3.6 Sensors

3.6.1 LVDT

The Linear Variable Differential Transformer (LVDT) is a basic and popular sensor to measure linear displacements. A typical LVDT consists of three sets of coil windings—one primary winding, excited by AC voltage, and two secondary windings connected to the output signal at the two ends (Fig. 3.7). A steel rod travels inside the coil windings with the exterior stroke movement. This motion starts from its center position, produces a tighter coupling between the primary coil and the secondary coil at the side of the rod movement, thus resulting in an increase of signal, in or out of phase with the excitation signal. In the VARD experimental facility, a GHSA 750-250 LVDT from Macro Sensors was mounted at the top of the shaker to measure the vibration amplitude. This LVDT has a linear range of 22 mm.

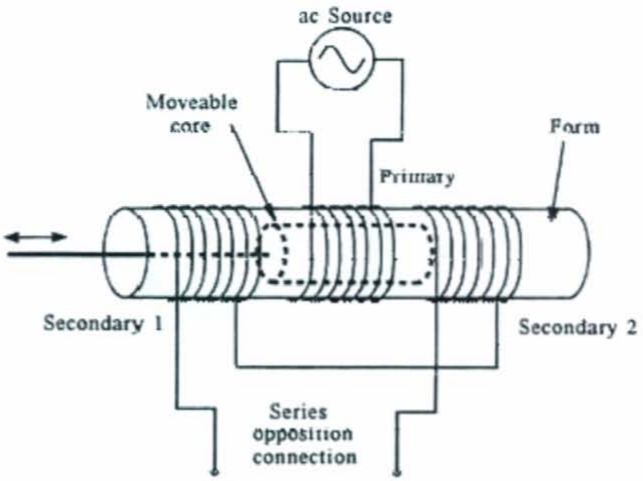

Fig. 3.7 General LVDT assembly (from National Instruments)

As shown in Fig. 3.7, since the primary coil of LVDT needs to be excited by the alternating current, the output signal also needs to be demodulated. A LVDT demodulator provides excitation voltages with a given carrier frequency (usually 5 kHz), and extracts the signal from the output signal of the LVDT. In the VARD experimental setup, the Macro Sensors LVDT is coupled with a Honeywell DLD-V demodulator, which requires voltage input of 18-36 V, and output in ±5VDC. The LVDT and signal conditioner are shown in Fig. 3.8.

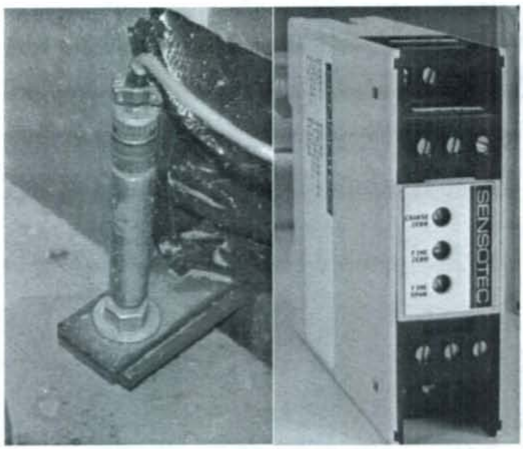

Fig. 3.8 GHSA 750-250 LVDT mounted on VARD setup (left) and DLD-V signal conditioner (right)

The LVDT was calibrated and the calibration curve is shown in Fig. 3.9. The metal pin of the LVDT traveled 11 mm in its linear range. With a 3.14V offset, the calibration factor was found to be 0.618 mm/V, which had been verified several times across different periods during the experiment.

After the calibration works are completed, the LVDT was mounted on the VARD rig by a bracket clamped with plywood to further isolate vibration. The height of the LVDT could be adjusted by two positioning nuts. During the vibration measurements, the sampling frequencies were varied between 500-1000 Hz. The data from the LVDT had shown that the shaker works at 60 Hz frequency and the vibration amplitude could be controlled by the shaker control setting, and the shaker load. Details of the shaker vibration characteristic will be discussed in Section 3.7.2.

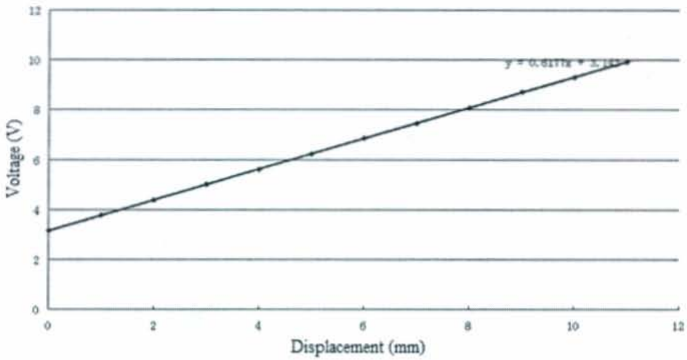

Fig. 3.9 Calibration curve of the GHSA 750-250 LVDT in its linear range

3.6.2 Load Cell

The WOB in general rotary drilling systems is a static force which could be calculated from the weight of drilling string, buoyancy force, pump off force, and hook load. However, for vibration assisted rotary drilling, the thrust force acting on the bit is a combination of the dynamic vibration force and the static load. Because little information could be found regarding the shaker table vibration characteristics, measuring the axial force during the vibration became a valuable measurement for the VARD experimental studies.

In the VARD laboratory setup, a load cell was planned to be placed between the drill motor and drill shaft. The pancake load cell was thought to be an ideal option for such location because of its low profile shape and good water resistance performance. The pancake load cell is essentially a full arm Wheatstone bridge strain gauge based force transducer. The inner structure of the pancake load cell is shown in Fig. 3.10. Strain

gauges were mounted in a symmetric angle (45° to horizontal direction) in pairs on the inner wall of pancake load cell. The outer ring of the pancake load cell is fixed by six to eight bolts on a rigid seat. The center of the load cell undertakes the load. Because of the force stresses at both ends, shear strains occur in the thin connections where the strain gauges are attached. The shear strains of the inner wall lead to extension in one strain gauge and compression in the other. By connecting four of these strain gauges into a Wheatstone bridge (two in compression and two in tension), a voltage output proportional to the axial load could be obtained as shown in Fig. 3.11.

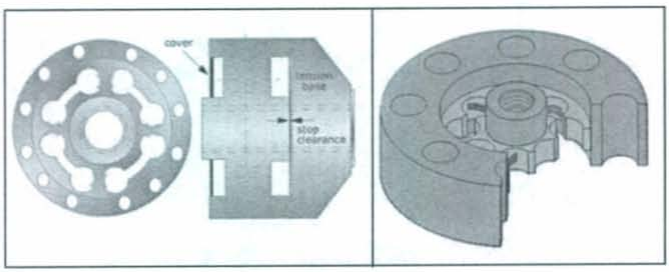

Fig. 3.10 Inner structure of pancake load cell

(left: from Pierson; right: from Honeywell)

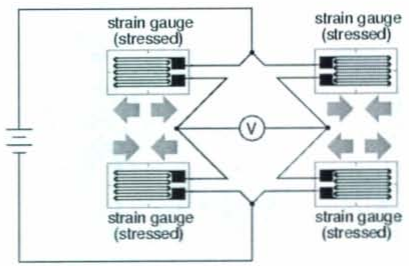

Fig. 3.11 Full bridge strain gauges load cell (from allaboutcircuits.com)

Range of force measurement is a decisive factor while selecting load cells. After the WOB control system was completed, the axial load was measured by a commercial scale. The WOB are found ranging from 28 kg to 130 kg while the suspended weight varied from 0 to 6 kg, which will be the main range of the static WOB in the later VARD experiments. This is because the maximum capacity of VP-51 shaker is 125 kg; and the optimized WOB for the core drill assembly with conventional rotary drilling was found to be 90-100 kg. A pancake load cell from Honeywell (3173-1k) with the lowest available capacity 5 kN was found to have a suitable range.

Two coupling pieces were made to mount the load cell on the drill. The water way was designed to be guided across the load cell so that force measurements with the account of drilling fluid effects could be conducted as well. A plastic shell was made at the top coupling piece so that the wireless node and the battery set could be mounted on this shell. The final load cell unit is shown in Fig. 3.12.

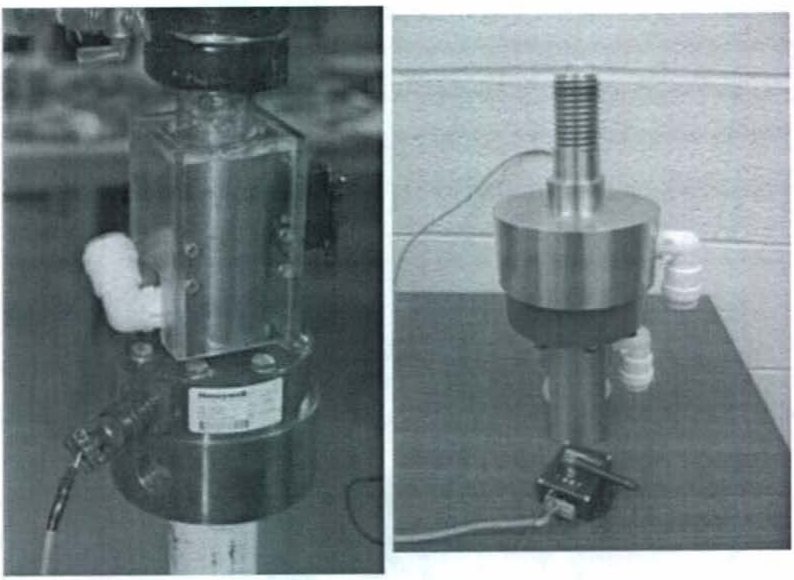

Fig.3.12 Load cell and its mounting unit

(left: with the hosing and node and plastic housing; right: initial status when the coupling units were finished and assembled)

The load cell was calibrated by a servo controlled compressive loading machine. The load cell was connected by the wireless DAQ-system during the calibration. A relationship between the force values and the digital readings from the Agile-link software was established with good linearity. The calibration curve is shown in Fig. 3. 13.

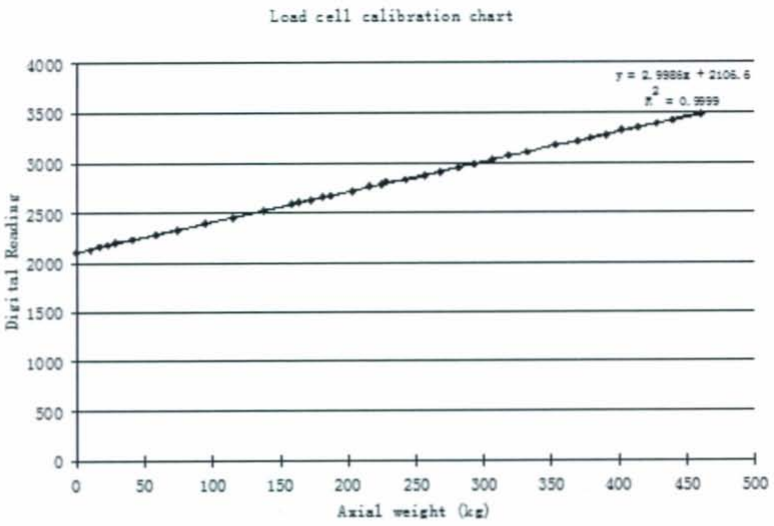

Fig.3.13 Calibration curve of load cell with wireless transmitter

The load cell was then used for confirmation vibration tests. The setup during these tests was similar to actual drilling; however bit rotations were not involved. The vibration forces were recorded at multiple levels of shaker current input and static WOB. The results will be discussed in Section 3.7.3.

3.6.3 Rotary Encoder

A rotary encoder is an ideal sensor to record linear movements, and it was introduced to the drill system to monitor the linear motion of the bit. In this way the ROP could be recorded during drilling. A rotary encoder consists of a rotating disk with two code tracks on it. An optical light sensor faces the track and reads the code. With the disk rotation, the optical sensor generates a pulse signal with every one unit code passing it. For

'quadrature' type encoders, the disk has two coded tracks with 90° out of phase. These two tracks are recorded by two light sensors working on separate channels. Fig. 3.14 describes the principle of a rotary encoder. In this figure, the two code tracks generate two groups of signals (in channel A and channel B). The direction of the rotation could be detected by recognizing which channel is the leading signal.

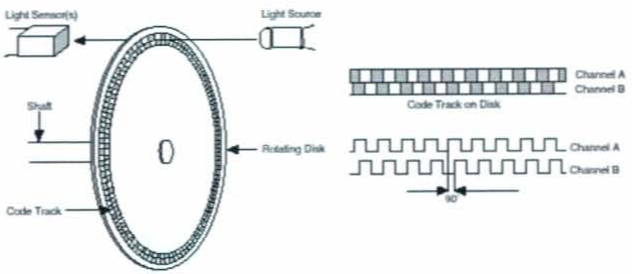

Fig. 3.14 Principle of Quadrature rotary encoder (From National Instruments)

The NI DAQ E-6024 DAQ-board has a counting function designed for rotary encoders. During the setup, the channel A is connected into a 'source input'; whereas channel B is connected to a 'GP_UP_Down' pin. The DAQ- system will count the signal pulses from channel A, and a high/ low statement will be generated from channel B, thus telling the direction of the rotation.

A Nikon RXA 1000-22-1 rotary encoder was modified and mounted on the rig. It has a resolution of 6023 readings for each revolution of its rotation. An alloy disk with a size of 6.3 cm in diameter was fixed with the encoder shaft. Thus a precision of 152 digital points per centimeter could be realized by the encoder while tracking down the linear bit movement.

The encoder was mounted on the rig by a bracket. The alloy disc rotates against the drill stand to record the linear movement. To increase the friction, a rubber ring was embedded on the edge of the alloy wheel, and a sandpaper strip was attached on the frame for the same purpose. The setup of the rotary encoder is shown in Fig. 3.15.

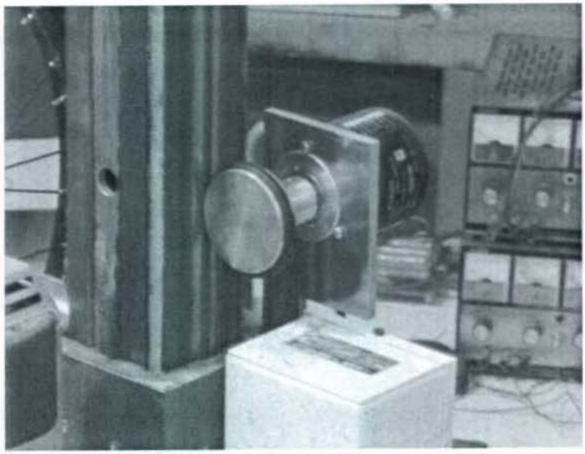

Fig. 3.15 Nikon RXA rotary encoder mounted on the VARD drill rig

The rotary encoder was involved in the VARD test under 600 RPM condition. The bit travel under convention rotary and low level of vibration drilling was recorded. During the test, slip between the wheel and the sandpaper track occurred several times. This sliding issue becomes severe when the vibration was strong. A comparison between the encoder recordings with and without the influence of sliding is shown in Fig. 3.16. At the right column of Fig.3.16, a shift in those curves could be clearly observed. These shifts represent the occurrence of the encoder disk slips.

The slide issue has become a major barricade in the measurement of ROP by the rotary encoder. As more measurements were done, mechanical grease accumulated on the rubber ring, and resulted in stronger slips. The rotary encoder setup was eventually suspended after many efforts.

For this reason, at the current stage, the ROP was alternatively averaged by the bit penetration distance over the penetrating time. The distance was measured by ruler after each drilling run, and the penetrating time was recorded by a stop watch.

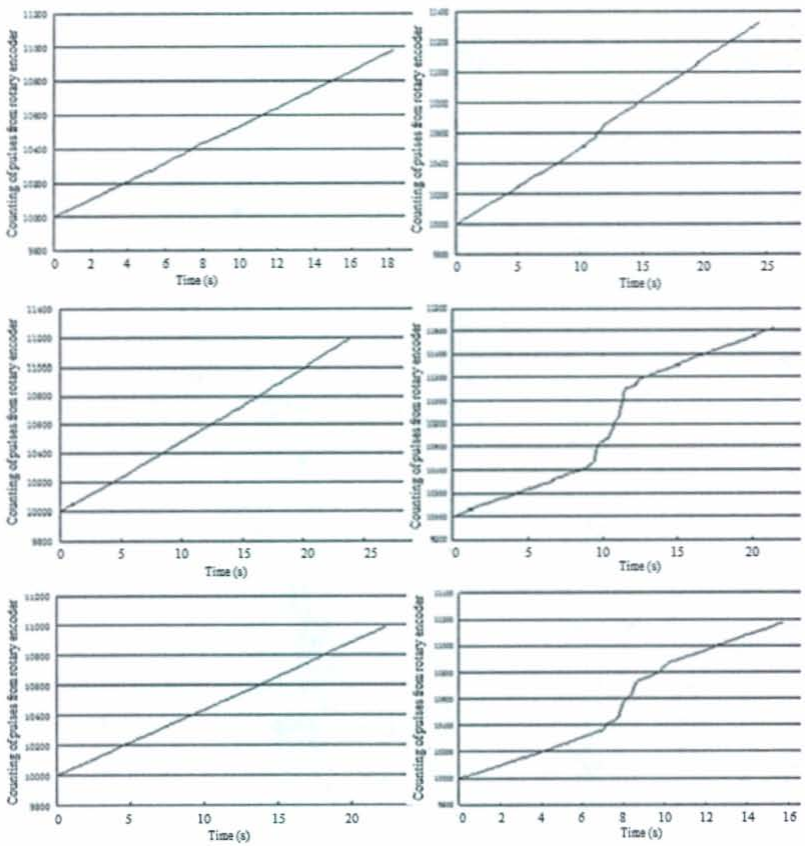

Fig. 3.16 Comparisons of the rotary encoder signal during 'good runs' (left) and runs with sliding issues (right) under low level of vibration VARD drilling

3.7 Drilling System Capacities

In the VARD laboratory setup, the WOB and vibration amplitudes were indirectly controlled. The actual static WOB was transmitted from the suspended weight through the bike wheel and gear wheel assembly, whereas the vibration amplitudes were varied by the shaker control setting and they were also influenced by the loaded mass. To track down the actual values of these variables, the relationships between the control parameters (suspended weight and shaker control setting) and the actual system response (actual WOB, shaker vibration displacement amplitude or force variation amplitude) needed to be established. In the current section, reports and discussions of the work regarding the relationships will be included.

3.7.1 Suspended Weight to Static WOB Conversion

To obtain some general idea of the actual WOB levels, a domestic weight scale was placed between the bit and the shaker. The suspended weight was varied from 0 kg to 5 kg, and the readings were taken from the scale reading panel. During the test, the entire drill section was released at a trivial distance to the bottom surface (scale). The scale readings are found affected not only by the suspended weight, but also the 'falling height', which stands for the space between the bit and the shaker, when the wheel was released by human hand. The influence of this falling height was so strong that minor variation result in ±10 kg fluctuation of the scale reading. After realizing this fact, the falling heights were controlled with extra caution to be maintained at a similarly low level.

The falling height influence on the scale reading was re-investigated later and was found to be a combination of the ratchet effect between the small gear wheel and the gear rail; and the deformation of the shaker surface plate resulted from both the deformation of the surface plate and the four elastomers supporting it. The solution was to turn on the shaker table for several seconds. The vibration force generated by the shaker is sufficient to break the ratchet lock effect. In the subsequent tests with the load cell, good repeatability was obtained by adopting this procedure.

The result of the scale measurements were averaged from 3-4 tests per suspended weight. The suspended weight to actual WOB conversion is shown in Fig. 3.17. The data has showed acceptable linearity.

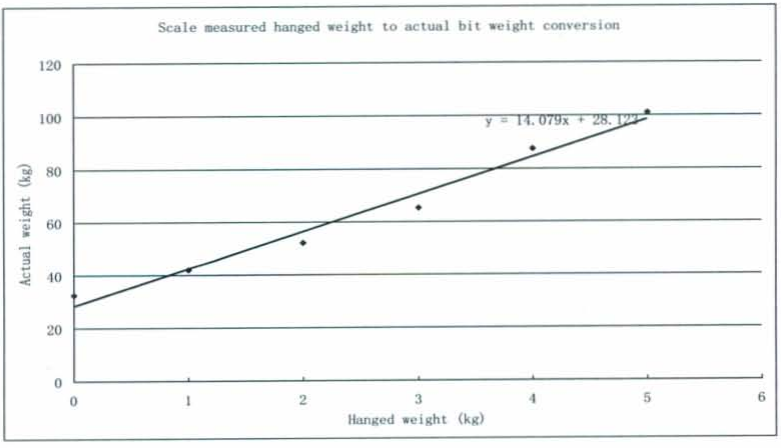

Fig. 3.17 Suspended weight to WOB conversion from the scale test

The load cell introduced in Section 3.6.2 was used to study the suspended weight—WOB conversion relationship for better accuracy compared to the scale. The conversion curve

recorded by the load cell is shown in Fig. 3.18. Because the load cell was placed between the bit and the motor, the result shown in Fig.3.17 is an edited result by adding the weight of the coring bit which was beneath the shaker.

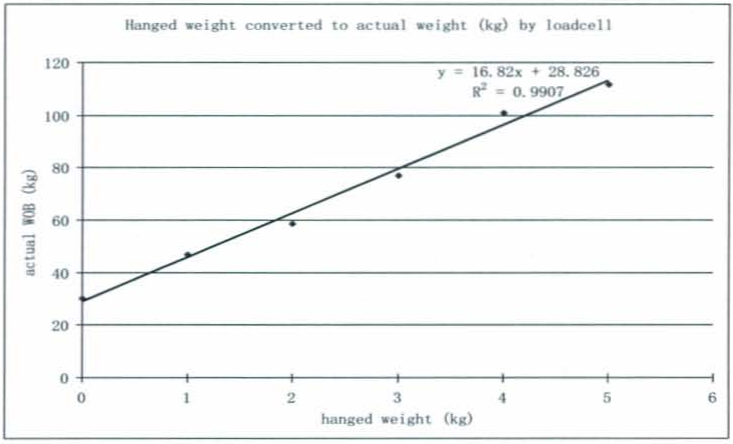

Fig. 3.18 Suspended weight to WOB conversion resulted from the load cell

The result showed some differences in both the slope and the intercept of the conversion curve. These differences could be attributed to the ratchet effect and the error from both means of measurement (mainly from scale). The data acquired from the load cell was believed to be more reliable, because it was calibrated frequently and its output was recorded by DAQ-computer instead of the human eye. The empirical conversion equation obtained from the load cell was adopted in the later experiments.

3.7.2 Study of the Vibration Displacement Amplitude

In the user instruction manual of the Syntron VP-51 shaker, little information about the vibration performance was mentioned, except generally stating that the system has a fixed

frequency and the control is related to the vibration amplitude. Studies were needed to investigate the vibration characteristics in detail under various load and the shaker control settings.

The LVDT in Section 3.6.1 was used to measure the displacement amplitude at the shaker surface. In the shaker controller, 6 levels of shaker control settings were marked from '10' to '60'. The term 'shaker control setting' is defined as the position of the knob on the controller, and is used as a control parameter during the design of the VARD experiments.

During the vibration amplitude measurements, the bit was placed in a pre-drilled sample without rotation; the suspended weights were varied from 1 kg to 4 kg. The shaker was turned on for 20 seconds for each test. The LVDT signal was logged by the NI Signal Express DAQ software at a sampling frequency of 1 kHz. Most of the data presented was close to sinusoidal wave forms, although several data points acquired at high level of shaker control settings presented a small secondary peak. Some fluctuation of the vibration amplitude could be observed and the result of amplitude values were averaged from 10 peak to peak waves randomly chosen from the LVDT signal file. The LVDT recorded displacement waveform vs. time under various combinations of WOBs and shaker control settings are presented in Appendix A. The amplitude versus the shaker control settings and WOB are plotted in Fig. 3.19 and Fig. 3.20.

Fig. 3.19 showed a trend that the vibration amplitudes rise with increasing shaker control settings. No perfect linear trend was observed but the amplitude-shaker control settings at 4 levels of WOB are similar. The influence of the WOB is obvious for the amplitude. Fig.

3.20 presented this influence in a more direct view—the vibration amplitudes are plotted against the WOB. The figure shows that at the lowest level of vibration, the influence of WOB is not strong, however with rising shaker current input, the amplitudes became increasingly influenced by the shaker load (static WOB). For those curves with shaker control settings higher than 40, a significant reduction of amplitude could be observed as the WOB increases. A 3-D displacement amplitude surface is plotted in Fig. 3.21 showing the amplitude as a function of these two factors.

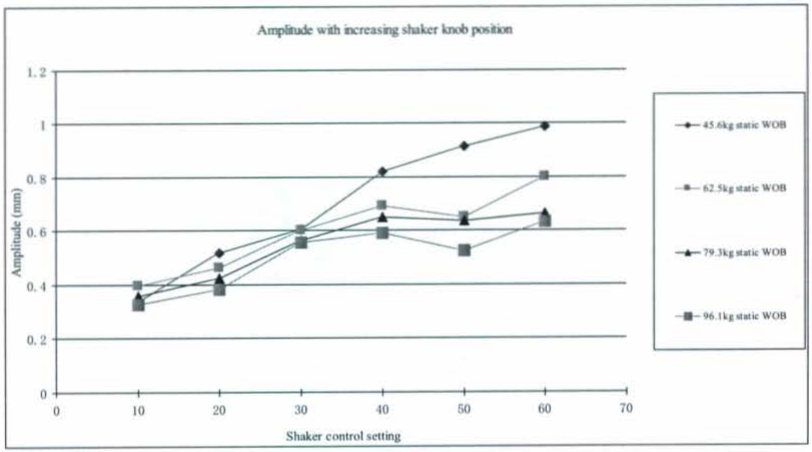

Fig. 3.19 Vibration amplitude measured by LVDT with increasing levels of shaker control settings without drilling

The LVDT test has shown some general trend in shaker vibration characteristics. However, it was hard to establish empirical models between WOB, shaker control settings, and the amplitude based on the result in Fig. 3.19 and 3.20. No curve fitting could be done because of the strong variation of the shapes of the curves. For this reason,

the search for another physical variable, which is independent of the shaker load and could only be affected by the shaker control setting, was conducted.

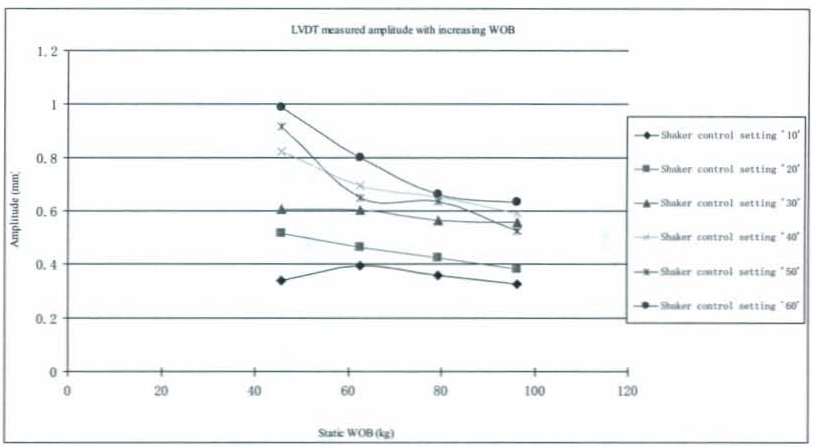

Fig. 3.20 Vibration amplitude at increasing WOB under multiple levels of shaker control settings

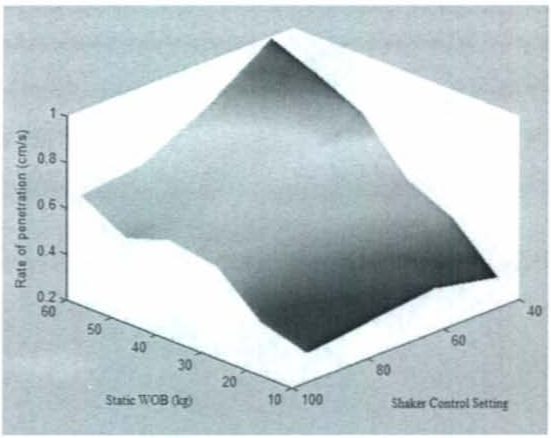

Fig. 3.21 3-D plot of Displacement amplitude dependent to static WOB and shaker control settings

3.7.3 Study of the Vibration Force Variation Amplitude

The force generated by the shaker during the vibration could be a potential variable relevant to the controller but independent of the shaker load. With this speculation, the Honeywell load cell was introduced to measure the vibration forces. The setup of the vibration force tests was similar to the test with the LVDT—the bit was placed in a pre-drilled sample and the shaker is turned on and tested without any rotation.

The data was recorded by the Agile-link software at a frequency of 512 Hz. The signal was then analyzed in the similar method as the LVDT tests. A secondary peak could be observed in all load cell signals when the force reduces from the maximum peak. This may possibly be caused by the gear wheel ratchet effect or the vibration mechanism

inside the shaker motor. The force waveforms measured by the load cell are given in Appendix B.

The force amplitudes versus the WOB under 5 levels of shaker control setting are plotted in Fig. 3.22. The figure shows that the force amplitude was clearly influenced by the payload, especially when WOBs were below 60 kg. However, with the payload over 60 kg, the force amplitudes were not significantly influenced by the payload anymore. Compared to the displacement amplitude-WOB curve measured by the LVDT in Fig. 3.20, the shape of the force amplitude curves tend to be more consistent.

The level of the force amplitudes is a variable which deserves consideration-- it varied from 1300 N to 2800 N. The axial static WOB, on the other hand, were varied only from 300 N to 1000 N. By taking account of the static WOB, the result from this investigation suggested that the instantaneous axial thrust force could reach a maximum of 2500 N.

The third valuable parameter in the load cell testing results is the mean value of the thrust force in the axial direction. In Fig. 3.23, the mean value of each condition was calculated and presented in the form of mean force vs. shaker control settings under variable levels of WOB. The mean force value was found remained approximately constant at all shaker control settings.

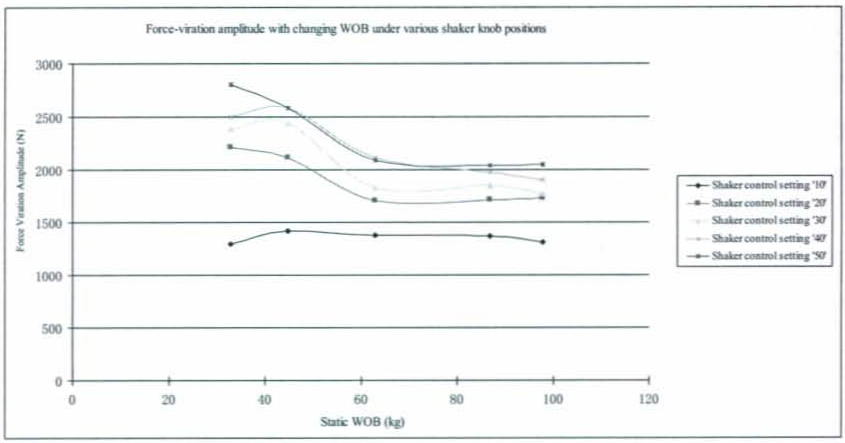

Fig. 3.22 Force variation amplitude with changing WOB under various levels of shaker control settings

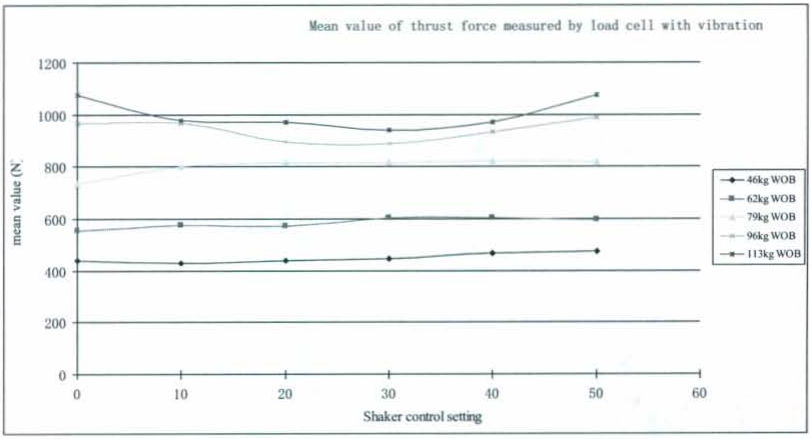

Fig. 3.23 Mean value of thrust force measured by load cell

(Note that '0' in shaker control setting stands for no vibration)

The studies reported in Section 3.7.2 and 3.7.3 attempted to establish relationships between the shaker control settings and the vibration variables. Attempts to establish surface fit equations were made, but the surface were found to be complicated and no suitable 3-D functions were found to establish an equation with acceptable error. Because both the force and displacement amplitude are dependent not only on the shaker control settings, but also the WOB, the 'shaker control setting', in the later experiments, was treated as a control factor which represents the level of vibration amplitudes. When the WOB was kept constant, both vibration variables were proportional to the shaker control settings. This suggested that this factor 'shaker control setting' is an appropriate expression of the vibration power generated by the electromagnetic motor.

Chapter 4

VARD Experiments on Coring Bit

4.1 Objective

The objective of conducting the VARD coring bit experiments was to test run the VARD rig, evaluate the influence of the added vibration on the penetration rate, and provide preliminary results for later investigations and experiment plans.

4.2 Verification of VARD Technology

Shortly after the experimental setup was completed, a VARD test run was conducted to verify the performance improvement brought by the added vibration. The test run was planned to be a demonstration run, and the time required to travel each 1 cm was recorded. The WOB was fixed at a relatively low level (i.e. 45 kg), based on the experiences from other publications (e.g. Pennington, 1953; Lagreca et al. 2002) that vibration drilling has greater potential under relatively low static WOB. The test was replicated once to ensure the validity of the data.

The drilling result is presented in Fig. 4.1. In this figure, bit travel distance vs. time was plotted. The test started with conventional rotary drilling. After several centimeters of travel, the shaker was turned on and vibrations were included in the remaining drillings. A direct change in slope of the travel/time curve implied improved performance brought by the added vibrations. An incensement, from 0.81 mm/s to 1.2 mm/s in ROP occurred while introducing the vibrations.

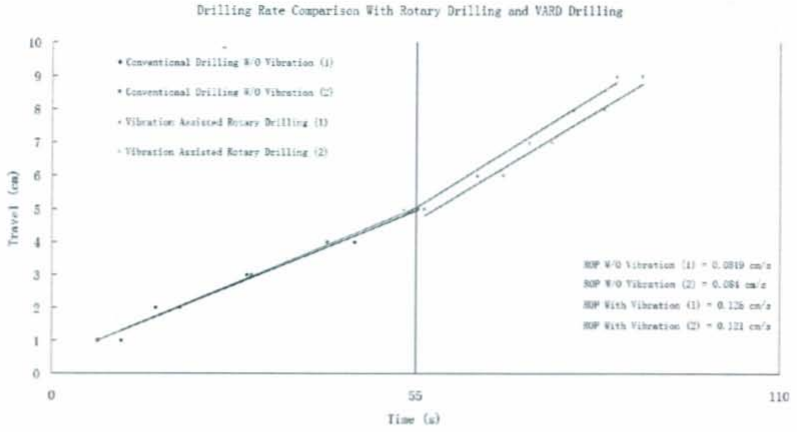

Fig. 4.1 Verification test showing the ROP increment brought by the VARD drilling

4.3 Sample Preparation

For the VARD coring bit tests, the samples were prepared using commercial Quickrete 1004 (a ready mix with cement and aggregate pre-mixed), which is expert in building up strength in a short period. To prepare the mix, all particles larger than 2.36 mm were sifted to improve sample consistency. The sieved mix was mixed with water, then progressively added with 3 lifts and poured into 6'' cylindrical molds to cure. At the 7th day, the samples were taken out from the molds, cored and tested by an Automax C56V4 UCS testing machine. Five samples were tested and the sample strength was ranged from 17 MPa to 22 MPa, with 20 MPa in average. All experiments were finished within 48 hours after the first sample was drilled, in order to guarantee that the results were not affected by the increasing sample strength; the samples were prepared twice for two set of experiments at different levels of rotary speeds.

4.4 300RPM Coring Bit VARD Test

4.4.1 Procedure

A photo of the VARD experimental setup at this stage is shown in Fig. 4.2. During these experiments, splash screens were mounted, and the vibrations were fixed at three levels which are shaker control setting '10', '30' and '50'.

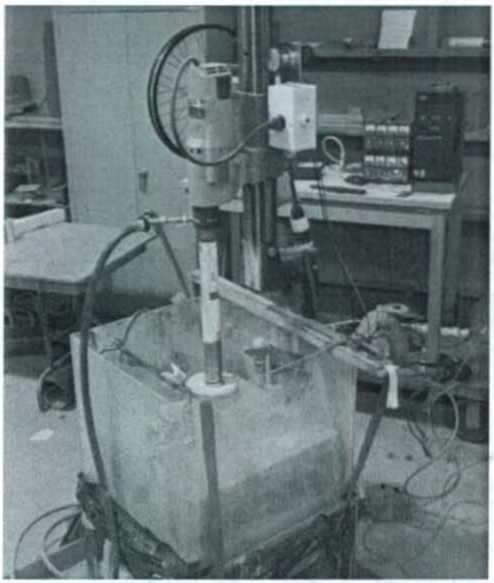

Fig. 4.2 VARD assembly in the condition for the coring drilling experiments

The 300 RPM round of experiments were conducted in November 2009. For each test run the bit travel ranged from 45 mm to 75 mm. The ROP data was computed from the distance the bit traveled. The flow condition was maintained by keeping the same turn

angle of the faucet on the water inlet. The flow was visually controlled to ensure that the concentration of the detritus in the out flow was small.

The experiments started with the rotary drillings without vibration, then the shaker was turned on and the vibration was varied for 3 levels of shaker control settings. The WOB in these tests was varied from 45-146 kg. The WOB was not raised in sequence but was randomly arranged in order to limit the influence of some natural trends (e.g. bit wear, temperature fluctuation or change in sample strength). For each vibration level, the maximum WOB was determined when a reduction of ROP with increasing WOB was encountered. This reduction suggested that the WOB had passed the founder point (optimized WOB) in the WOB-ROP curve, and then the experiment for this level was stopped.

4.4.2 Experiment Result

The data of the 300 RPM VARD experiments are shown are Table 4.1, the WOB-ROP curves under various levels of vibration shaker settings are plotted in Fig. 4.3. The conventional rotary drillings during these experiments showed a good match to the classic WOB-ROP theory (Bourgoyne, et al., 1991). The ROP rose with increasing WOB until the founder point, and then began to reduce. One fact to notice is that although the shape of the WOB-ROP curve came out with a good match to the theory, the point with the maximum ROP does not stand for the exact founder WOB. More data points near the maximum ROP need to be found during the experiments to acquire the exact value of the founder point.

In Fig. 4.3, the VARD drilling resulted in higher ROPs than the conventional rotary drillings under the same WOB. For the curves with low and middle levels of vibration, the inclination portion of the WOB-ROP curves showed a similar shape to the conventional rotary drilling curve. Within these inclined portions, VARD drilling performed a trend to proportionally increase the ROP. With increasing vibration levels, the inclined portions of the VARD curves tend to be shorter, and the ROP reduction started earlier with higher ROP.

The VARD WOB-ROP results with shaker control settings '10' and '30' resulted in proportional ROP increase. The WOB-ROP relationship in shaker control setting '50' was an exception. The test with the shaker control setting '50' vibrations started with 45 kg WOB and obtained a high ROP close to 0.13 cm/s. However, when the WOB increased to 67 kg, a strong ROP reduction was encountered. Two more drillings were conducted at 41 kg and 58 kg. Both corresponding ROPs were lower than the ROP obtained at 45 kg. This implied that the founder WOB under the shaker control setting '50' is near 45 kg.

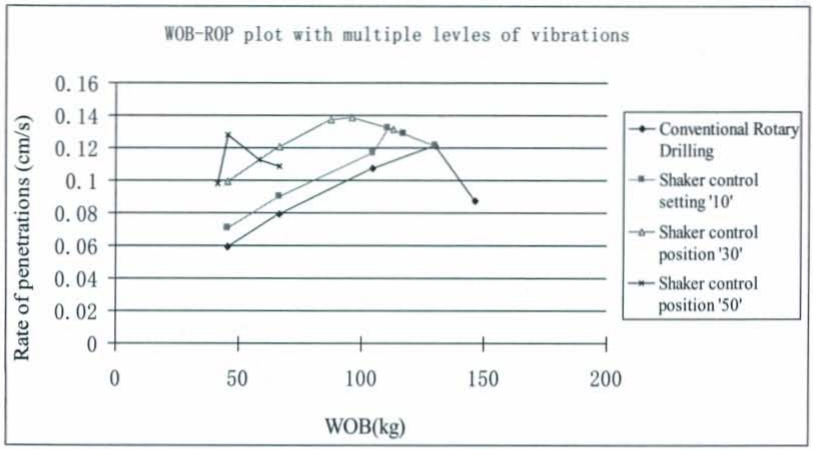

Fig. 4.3 WOB- ROP plot at 300 RPM with and without vibrations

Shaker vibration level	Static WOB (kg)	Bit travel (cm)	Time (s)	Rate of Penetration (cm/s)
No-Vibration	45.646	5.4	90.665	0.060
	104.516	3.95	36.879	0.107
	129.746	4.8	39.541	0.121
	66.671	5.5	69.172	0.080
	146.566	5.65	64.619	0.087
Shaker control setting '10'	66.671	5.1	56.548	0.090
	104.516	5.26	45.175	0.116
	45.646	5.2832	74.83	0.071
	110.5712	4.6	34.915	0.132
	117.131	7.55	58.715	0.129
	129.746	4.5	37.149	0.121

Shaker control setting '30'	66.671	5.44	45.093	0.121
	87.696	4.615	33.552	0.138
	45.646	4.9	49.277	0.099
	96.106	6.805	49.032	0.139
	112.926	4.85	36.909	0.131
Shaker control setting '50'	66.671	7.0	64.459	0.109
	45.646	6.63	51.734	0.128
	41.441	4.55	46.39	0.098
	58.261	6.9	61.334	0.112

Table 4.1 VARD experimental coring bit drilling data with 300RPM rotary speed

The tests were stopped at this point for the excessive vibration resulted in strong bit wobbling. The 4 data points under high level of vibration mechanical power showed that the WOB-ROP curve saturated at very low WOB, compared to the other two WOB-ROP curves generated at lower vibration power.

As mentioned earlier, before the WOB-ROP curves reach the funder point, they tend to have a proportional slope to the shaker control settings. To further demonstrate this proportional trend, additional four ROP data points at 45.65 kg WOB were re-plotted with the rising shaker control settings in Fig. 4.4. Only level of WOB data was selected because at this WOB all data points are below or at the founder point. These data showed a close to linear relationship with increasing shaker control settings.

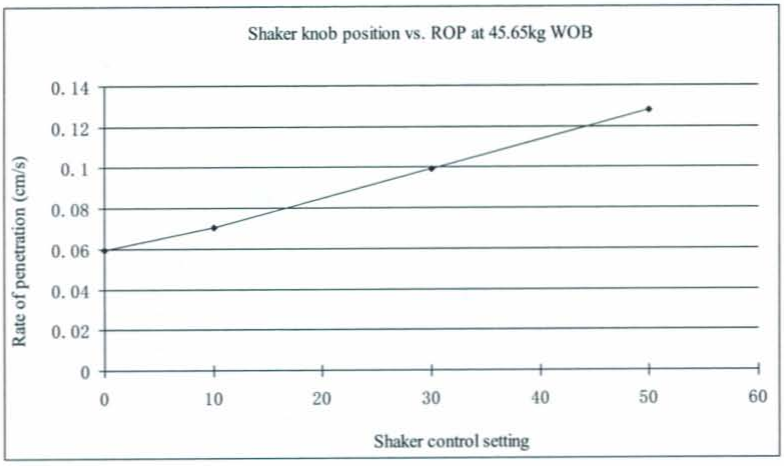

Fig. 4.4 Shaker control setting-ROP plot at 45.65kg WOB, started with zero (no) vibration

4.5 600RPM Coring bit VARD Test

4.5.1 Procedure

In early 2010, a group of VARD experiments was conducted at the high level (600 RPM) rotary speed. The samples were prepared in the same procedure as those 300 RPM experiments and the tests were also carried out at the 7th day after preparation. Based on the operation experience in the previous (300 RPM) experiments, the highest level of vibration was not planned. However, the quantity of the samples were prepared with the same number as the 300 RPM tests. Excess samples were planned to be drilled near the founder point for each WOB-ROP curve in order to gain more details of the curves near

the peak. The WOB was increased in sequence. After obtaining a reduction in ROP, more drillings with small variations of WOB were done near the peak of the WOB-ROB curves.

4.5.2 Experiment Results

The experimental data are shown in Table 4.2 and the WOB-ROP curves with and without vibrations are shown in Fig. 4.5. In this figure, a change in slope in the inclined portion could be found in all three drilling curves (marked with red circles), for drilling with and without vibration. This might be attributed to the increased resolution due to the increased numbers of tests near the founder point, or it might reveal the nature of this coring bit drilling at high rotary speed (compared to oil and gas field drillings which are normally lower than 150 RPM).

Shaker vibration level	Actual Static WOB (kg)	Bit travel (cm)	Time (s)	Rate of Penetration (cm/s)
No-Vibration	45.646	5.85	43.774	0.134
	66.671	5.85	34.133	0.171
	87.696	4.62	21.185	0.218
	112.926	5.9	23.852	0.247
	121.336	6.45	25.397	0.254
	123.018	7.12	25.303	0.281
	124.7	5.69	19.266	0.295
	126.382	5.73	20.28	0.283
Shaker control setting '30'	45.9824	5.69	26.941	0.211
	66.671	5.95	25.241	0.236
	72.558	5.65	19.016	0.297
	74.24	5.25	16.723	0.314
	75.922	4.95	16.442	0.301
	79.286	5.35	18.86	0.284
	87.696	5.95	23.744	0.251
Shaker control setting '50'	45.646	5.49	23.4	0.235
	52.374	5.35	20.936	0.256
	54.056	5.11	18.985	0.269
	55.738	6.8	26.941	0.252
	60.784	5.5	22.791	0.241
	62.466	5.48	22.074	0.248

Table 4.2 VARD experimental coring bit drilling data with 600RPM rotary speed

This phenomenon found during the VARD experiments were rarely mentioned in other experimental based drilling studies. However, many of those WOB-ROP curves were also not perfectly proportional, and little detailed studies were done focusing on the change in slope near the peak. An example showing the imperfection of the curvatures of the WOB curve could be found from Ersoy's et al. (1995) work, as shown in Fig. 4.6. In their work, they tested the performances of 3 types of coring bits at very high rotary speed (above 1000RPM). In Fig. 4.6, a minor increase in slope could be found at the peak of the impregnated bit (which is same type of bit with VARD setup). The other two bits have also showed fluctuations in their WOB-ROP curves. Because these two curves did not reach its founder point, the performance near their peaks were unknown.

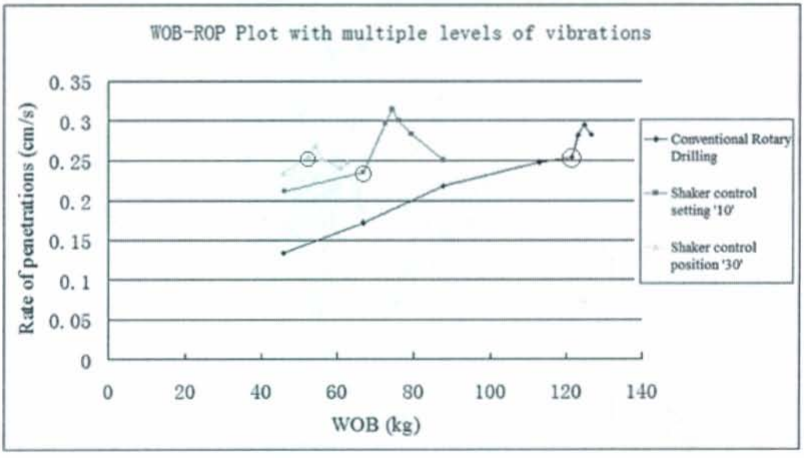

Fig. 4.5 WOB- ROP plot at 600 RPM with and without vibrations

The three red circles mark the points that the slopes of WOB-ROP curves began to change

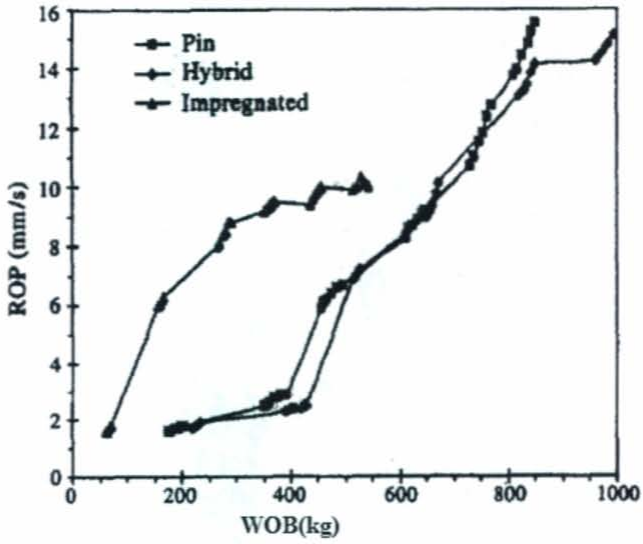

Fig. 4.6 Example of other coring bit drilling experiments at high RPM for 3 different diamond coring bit types (from Ersoy and Waller, 1995)

Other than the above mentioned phenomenon, the 600 RPM VARD experimental results were found to be similar to the 300 RPM's. With added vibrations, the ROP in the incline portion were higher than the ROP without vibration the under same WOB. Compared to the 300 RPM results, the 600 RPM curves were also 'compressed', and they have shorter and steeper slopes. The WOB curve with shaker control setting '30', which was the highest level of the vibrations in 600RPM tests, have showed similar effect of the strongest vibrations (shaker control setting '50') at 300 RPM: the curves were strongly

compressed and the maximum ROP was lower compared to those curves with lower level of vibrations. This implies that for these experiments at relatively high level vibrations, the WOB-ROP curves were saturated for some reason. Furthermore, this saturation happened at lower level of vibrations if the combination of the 'original' rotary drilling parameters could result in high ROP (for example, the doubled rotary speed brought a more than 100% ROP increment in the WOB-ROP curves). This 'saturation' could be attributed to two reasons: the insufficient bottom hole cleaning; or increased bit wobbling brought by the increased vibration force. For this reason, basic studies to the effect of drilling fluids were conducted as outlined in Chapter 5; and modifications to the drill frame were as well carried out when the full face bit was introduced in the VARD experiments to limit the bit wobbling motions during the drilling as mentioned in Chapter 6.

This saturation phenomenon suggests that the operation window of the added vibration could be dependent on the combination of the original rotary drilling parameters. If the combination of rotary drilling parameters already resulted in a relatively high ROP, the benefit brought by the added vibration would then be limited.

Chapter 5

Investigation of the Effect of the Drilling Fluid on Drilling Performance

5.1 Introduction

During the coring bit experiments, drilling fluid was controlled by simply fixing the faucet at the same place when drilling operations took place. This procedure was thought to be coarse and inexact. Previously there was no study done to investigate the flow effects to the drilling performance based on the VARD drilling system. It was unknown whether the drilling fluid was sufficient to meet the requirement of the bottom hole cleaning, and how it influenced the drilling performance. Therefore, some investigations were conducted aiming to gain basic knowledge of the flow effect on drill performance, and providing suggestions for future drilling experiments. These drilling fluid investigations were designed and conducted based on the coring bit which was used in the VARD coring bit experiments described in Chapter 4.

Drilling fluids have several positive effects on a drilling system. The two fundamental functions of the drilling fluids in terms of rock penetration are to protect the bit from thermal wear and to flow away the rock cuttings generated during the drilling to ensure the bit is always in contact with fresh rock surface. The function and the efficiency of the drilling fluid could be also adjusted by adding additives for different purposes, for example, to increase the well bore stability or preventing the loss of circulation for well control purposes.

During the VARD laboratory experiments, only shallow holes were drilled on short concrete samples, and no complex down hole issues existed. For this reason, the only component in the drilling fluid was water, and the only function related to the drilling performance in the rate of penetration aspect is the bottom hole cleaning effect. The insufficient bottom hole cleaning could lead to detritus accumulation at the bottom hole, thus causing regrinding between the bit and the detritus. This will subsequently reduce the contact area between the bit and the rock surface and cause a reduction in the drilling efficiency. According to Bourgoyne Jr., et al. (1991), the insufficient bottom hole cleaning is one of the major reasons leading to reductions of ROP.

Although the drilling fluid is crucial to the drilling systems, its presence also brings interference to the original drilling mechanisms. In an ordinary field rotary drilling system, which uses a full face bit, the drilling fluids are guided through the inner tube of the drilling string, ejected by the drill bit nozzles, and then return to the surface with the generated drilling detritus through the annulus. While ejected from the bit nozzles, the drilling fluids create a force tending to push the bit from the bottom. This force is called 'pump off force', which could greatly affect the WOB. Equation 5.1 shows how the actual WOB is calculated with the pump off force taken into account in the field operations.

$$WOB_{True} = WOB_{Static} - F_B = WOB_{Static} - A_{Po}\Delta P_B \qquad 5.1$$

In equation 5.1, WOB_{Static} is the static WOB determined by drill string weight, hook load and buoyancy force from the mud column in the well bore; F_B is the pump off force; A_{Po} is the effective pump off area; ΔP_B is the pressure drop across bit. A drill off test example

(Bourgoyne Jr., et al., 1991) showed that at the depth of 5747 m with an 8.5 in. diamond bit and a surface pump rate of 285 US gal/min, the pump off force reached to 44903 N (4582 kg), comparing to the static WOB at 7,000 kg. The detailed calculation of the pump off force is in Appendix D.

The above discussion shows that pump off force is a factor which significantly affects the field drilling operations. In the coring bit VARD laboratory setup, the drilling fluid influences the drilling performance in a slightly different way. The main differences between the two systems are in the location of the pump off force acting on the drilling system. As shown in the Fig. 5.1, the core drilling (left) has little space between the rock core and the inner wall of core barrel. This leads to an accumulation of the drilling fluids in the space from the end of the core to the top end of the core barrel; the pump off force which is acting at the top end of the core barrel gives a trend to lift the drill assembly. In contrast, the pump off force under the full face bit pushes the whole drill assembly from the bottom (right of Fig 5.1), as discussed above.

Although these two types of drilling methods have some differences in their pump-off mechanisms, the factors affecting the drilling performances are quite similar – the flow rate affects the bottom hole cleaning efficiency, while the high pump off force balances the actual WOB.

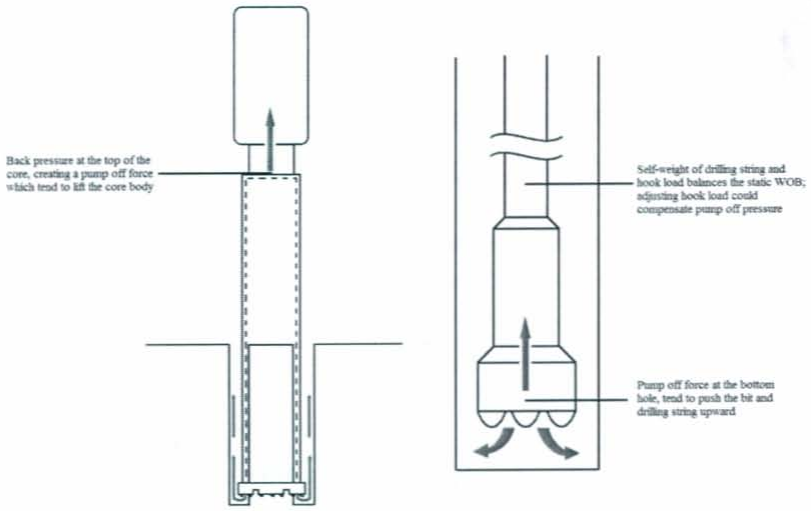

Fig. 5.1 Pump off mechanism comparison of laboratory core drilling and field full face bit drilling

5.2 Experimental Setup for the Coring Bit Drilling Fluid Study

The lack of drilling fluid knowledge during the previous studies was mainly attributed to the lack of appropriate monitoring equipments to the inlet flow. To obtain basic understandings of the drilling fluid effects to the core drillings, both the monitoring of the fluid flow rate and pump off pressure were considered to be necessary: the flow rate is the most relevant factor to the bottom hole cleaning effect, while the pump off pressure is a direct indicator of the pump off force.

To monitor these two parameters, a turbine flow meter with digital readings and a pressure gauge were installed to the drill rig. Because the options of the flow meters were

limited in the market, the turbine flow meter has a best sensitivity of only 1 US gpm. The two gauges were installed at the nearest possible position to the drill bit (Fig. 5.2). During the experiments, the flow rate readings were taken at 1 US gpm increments.

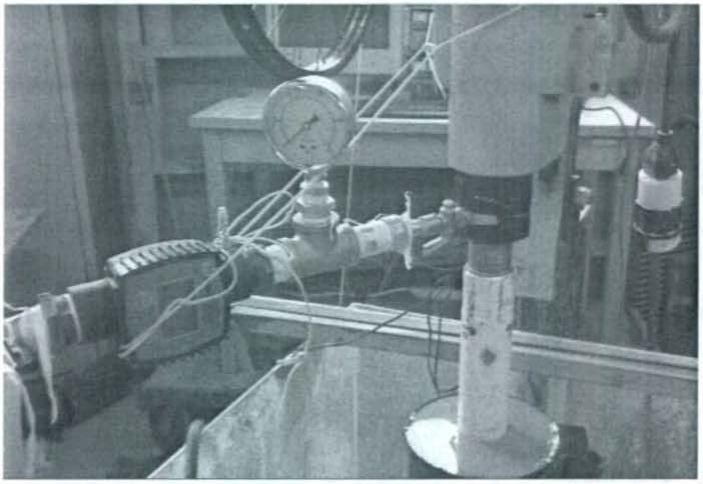

Fig. 5.2 Flow meter and pressure gauge installed on the VARD experimental facility

Some basic study of the flow characteristics was carried out after the gauges were installed. It was found that the maximum flow rate from the lab water was 6 US gpm. The pressure across the pressure gauge is monitored under various flow rates when the drill bit is statically lowered into a pre-drilled borehole to simulate the real drilling condition. The first two columns of Table 5.1 present the recorded pressure reading under different flow rates. It was found that there was no pressure reading until the flow rate reaches to 3 US gpm. This could be explained as the water head in the drill pipe did not reach the pipe

inlet inside the core barrel, where the pressure gauge was located, until the flow rate rise up to 3 US gpm.

5.3 Drilling Fluid Flow Investigation Based on Coring Bit Rotary Drilling Experiments

A set of rotary drilling experiments was carried out after the above tests were done. The drill bit rotary speed was set to 300 RPM. The weight on bit was kept constant at 61.6 kg, which is a mild operation condition. The sample was pre-drilled to 2 cm deep before the test begins. This ensured all the drilling runs started with an existing well bore, and the drilling fluid was under a similar out flow condition. The drilling test started at a flow rate of 1 US gpm, and increased to the maximum flow rate of 6 US gpm. The pressure gauge readings during the drillings were found to be identical to the static pressure test. Each drilling run lasted for 20 seconds. The ROP was recorded and listed in the column 3 of Table 5.1.

Flow rate reading (US gpm)	Pressure gauge reading (psi)	Rate of penetration (cm/s)	Calculated Actual WOB (N)
1	0	0.107	604.073
2	0	0.108	604.073
3	4	0.129	548.222
4	12	0.118	436.478
5	23	0.097	282.821
6	35	0.095	115.227

Table 5.1 Drilling data and drilling fluid readings during the flow investigation

During the experiments, the bottom hole cleaning effect could be visually observed. At low flow rates, the out flow had high concentration of fine grained drill cuttings; with increasing flow rate, the concentration reduced and the out flow became clear water. Some photos (Fig. 5.3) were taken to show the fine grained drill cutting concentration reduction with increasing flow rate.

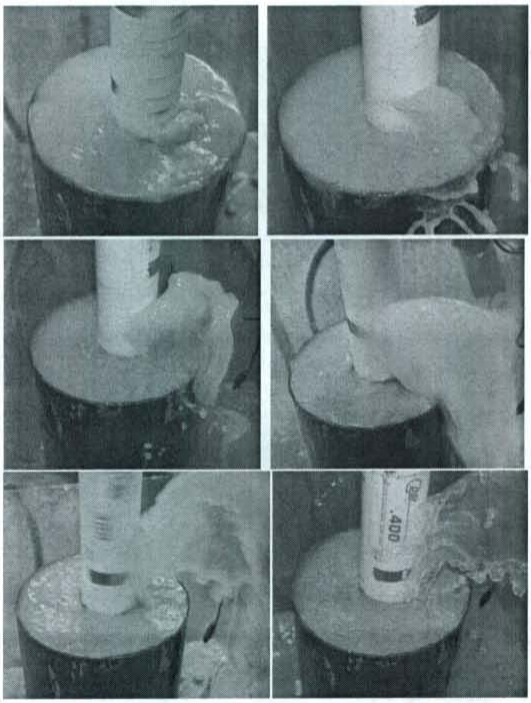

Fig. 5.3 Returned flow to the surface with increasing flow rate from 1 US gpm to 6 US gpm

Fig. 5.4 plotted the rate of penetration as a function of flow rate based on the data presented in Table 5.1. In Fig. 5.4, an increase in ROP from low to middle flow rates was obtained. The photos in Fig. 5.3 showed that from 2 US gpm to 3 US gpm flow rates, a significant reduction of drilling cutting concentration was observed. This implied that the increase in ROP is the effect of better bottom hole cleaning. However, as soon as the flow rate reached 3 US gpm, the ROP began to reduce. An important sign in Table 5.1 showed that the pressure gauge began to capture readings at 3 US gpm. This indicated that the core barrel was saturated with drilling fluid between 2 US gpm to 3 US gpm, and the back pressure inside the core barrel began to affect the drilling performance. As discussed above, the drilling fluid back pressure in the core drilling could significantly affect the actual WOB. Due to the limitation of axial force measurement, the pump off forces under different flow conditions was converted from the pressure gauge readings by a factor of the inner cross section of the core barrel. Then the actual WOBs were calculated by the static WOB (brought by the suspended weight) minus the pump off force. The calculated actual WOB is listed in column 4 of Table 5.1. Fig.5.5 plotted this actual WOB against the ROP. This curve verifies a typical WOB-ROP theory which is similar to previous experiments. The reduction of ROP could be understood as the insufficient bottom hole cleaning, which is a major factor cause the reduction of ROP in Maurer's (1962) WOB-ROP empirical model. This theoretically verifies the results obtained during the experiments.

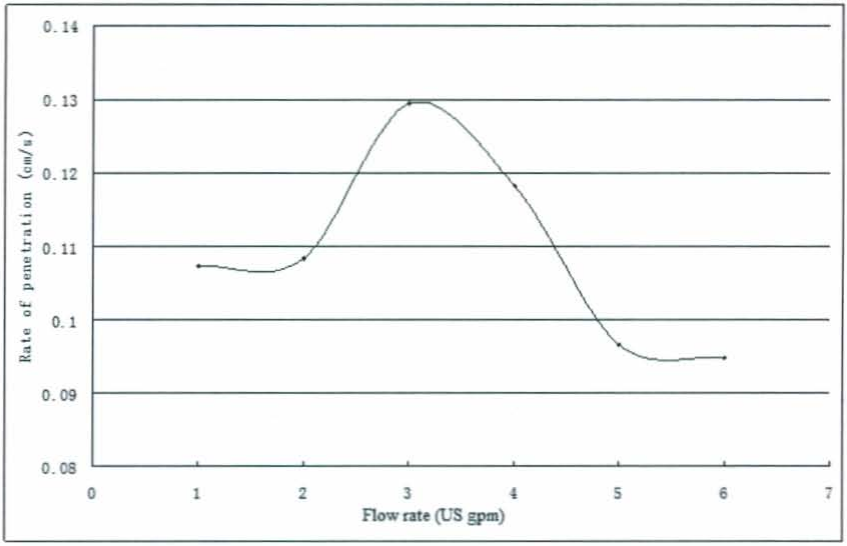

Fig. 5.3 Rate of penetration as a function of flow rate under 61.6 kg WOB

Some suggestions are given for future experiments based on the experiences obtained from this drilling flow investigation, in order to minimize the drilling fluid influences. At the current stage, due to the fact that no actual WOB can be measured during drilling, it is important to minimize the influence of the pump off force. In order not to strongly interfere with the axial thrust force, meanwhile maximize the effect of the bottom hole cleaning effect. With these considerations, the flow rate is suggested to be kept at a low pressure gauge reading (less than 5 psi).

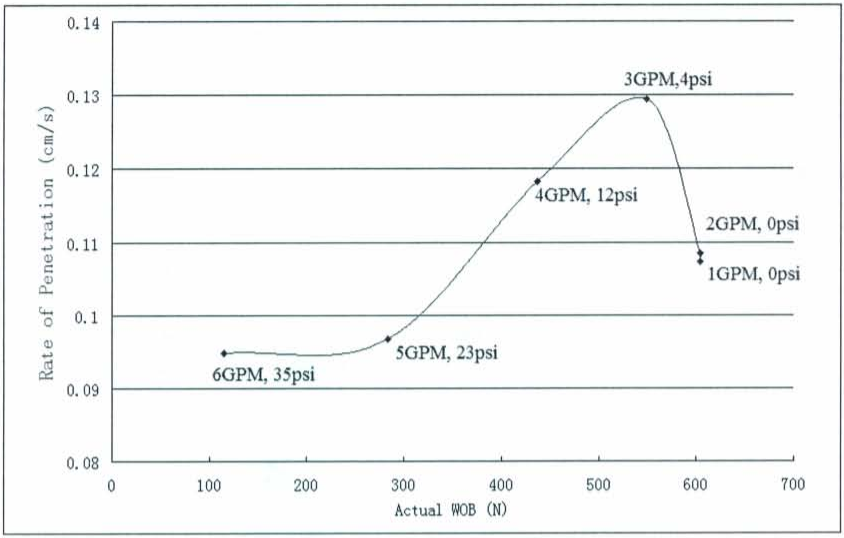

Fig. 5.4 Rate of penetration as a function of actual WOB

Chapter 6

Full Face VARD Experiments

During the coring bit VARD experiments, the peak of the WOB-ROP curves was found to saturate of lower WOB with increasing vibration amplitudes. The shortened curve patterns in high levels of vibrations have created difficulties in further analyzing the effect of the vibrations at the inclined portions of WOB-ROP curves. Only one vibration amplitude-ROP curve was plotted at the lowest level of WOB because the peak of the WOB-ROP curves with the high level of vibrations happened too early. However, this amplitude-ROP curve in the coring bit experiments implied that the vibration amplitudes have a proportional effect on the ROP; and it aroused interest to further investigate the relationship between the vibration amplitude and the ROP.

To further explore the effect of all levels of vibrations on the WOB-ROP curves, the experiments should be conducted using a new drill bit which could undertake higher WOBs before the peak. To meet this requirement, the new bit needs to have larger contact areas, so that the WOB stress on unit bit surface area is lower. Therefore the full face bit drills slower than the thin-wall coring bit under the same WOB, and reaches its founder point at higher WOB.

A full face diamond impregnated bit (shown in Fig. 6.1) from Boart Longyear was selected for this purpose. This AWJ bit has a diameter of 1 7/8'', and it is designed for directional drilling for the oil and gas wells, with good directional stability and durability.

Similar to the coring bit, the full face bit is also a diamond impregnated bit, including three water channels and three nozzles.

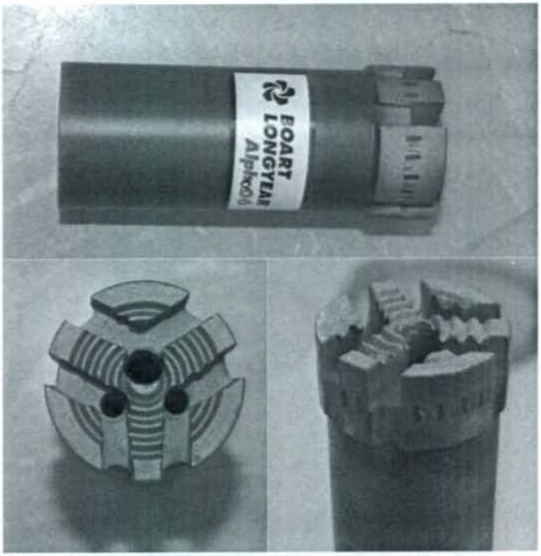

Fig. 6.1 Photo of the AWJ full face bit purchased from Boartlongyear inc.

6.1 Preparation of the Sample

The samples drilled in the VARD experiments reached strength of 20 MPa, which was relatively low compared to most rocks encountered in the oil and gas drilling. During the drilling experiments, these 20 MPa samples were found to be easy to fracture, and small aggregates occasionally fell off from the well bore near the surface. Therefore, improvements in the sample strength are demanded to better simulate the rock properties.

The design of the sample mixture was selected from several different combinations. The final product was mixed with cement, sand aggregate and water. The ratio was 36.5%, 38.7% and 24.8% respectively. The sample has reached to 50.7 MPa at 28th day after mixture, which was the highest UCS value obtained in this study.

Thirty samples were cast in 12'' long, 6'' diameter cylinder molds. These samples allowed 120 drilling runs of 7.5 cm each. The samples were prepared 2 months before the drilling experiments. At the day of the full face bit drilling test, the samples reached 57 MPa UCS value on average.

6.2 Conditioning of the Full Face Bit

The new diamond impregnated bit came with a thin layer of coating on the drill head surface. This layer could wear out shortly after the bit starts drilling. During this wearing progress, the fresh diamond tooth cutters were slowly revealed, followed by changes of the bit surface conditions, which could cause strong fluctuation of the early drilling performance.

To mitigate the influence of this surface coating, a set of drillings called bit conditioning was carried out. The WOB was kept constant at a relatively low level of 64.14 kg, and the flow rate was kept constant with 4.5 psi. The conditioning data is shown in Table 6.1, and the result is plotted in Fig. 6.2.

During the test, the ROP with the new bit was found extremely low. Compared to the ROP close to 0.08 cm/s with the coring bit under the same condition, the ROP for the full

face bit was only 0.003-0.004 cm/s. This was resulted from both the change of the sample properties and the contact area of the drill bit.

Accumulated Travel (cm)	Travel per run (cm)	Time (s)	Rate of penetration (cm/s)
0.85	0.85	273.68	3.11×10^{-3}
1.75	0.9	356.39	2.528×10^{-3}
2.61	0.86	288.22	2.986×10^{-3}
3.78	1.17	270.17	4.333×10^{-3}
4.71	0.93	264.02	3.523×10^{-3}
5.86	1.15	268.00	4.291×10^{-3}
7.06	1.2	268.47	4.478×10^{-3}
8.31	1.25	262.81	4.771×10^{-3}
9.56	1.25	266.89	4.699×10^{-3}
10.81	1.25	264.59	4.735×10^{-3}
12.06	1.25	263.05	4.752×10^{-3}

Table 6.1 Data for the bit conditioning under 2 kg WOB

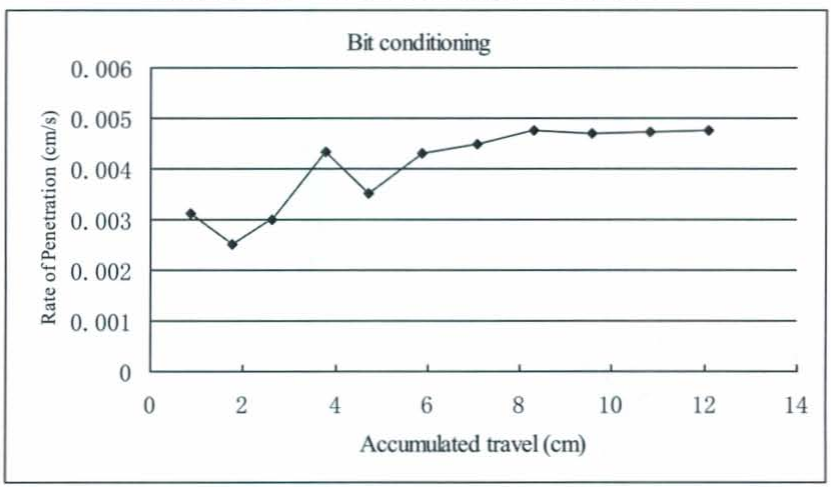

Fig.6.2 ROP variation with accumulated travel during conditioning

Fig.6.2 showed the progress of the bit conditioning. Strong ROP fluctuations could be found at the first several drillings. The ROP data has presented a trend of increasing with longer drilling distance until 8 cm of accumulated bit travel. After this, the ROP stabilized at 0.0047 cm/s for the next 4 cm drill runs. This suggests the influence of the surface coating was gone and the bit conditioning work was completed. A visual observation further verified this hypothesis. A photo of the bit surface before and after the conditioning is shown in Fig.6.3. Before the conditioning, very little diamond teeth could be observed from the surface and the coated surface was trim and smooth. In comparison, after the conditioning, the smooth coating was gone and the diamond teeth could be clearly observed.

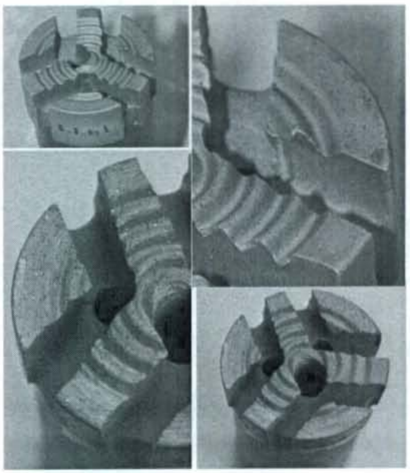

Fig. 6.3 Bit face before (upper) and after (lower) conditioning

6.3 Conventional Rotary Full Face Bit Experiment

Similar to the procedure of the VARD coring experiments, a set of conventional rotary drilling tests was conducted with the full face bit ahead of the full range VARD experiments, so that the founder WOB could be determined.

The sequence of the experiments was set in such a way as to slowly increase the WOB and record the ROP. If any reduction of ROP was obtained, several more tests would be done near this point, in order to verify the result. The drilling flow was kept constant for a pressure gauge reading of 4.5 psi (310 kPa) for all drilling runs.

The drilling history is shown in Table 6.2, and the WOB-ROP data plot is presented in Fig. 6.4. Each data point was obtained by letting the bit run for 7-9 minutes, except some short runs, which were stopped for operation issues. The bit travel distances for most of the drilling runs were only about 1-3 cm, relatively short as compared with 5-7 cm bit travels in the coring experiments. This was because of the extreme low rate of penetration while drilling with full face bit.

Because of the modified test sequence, the experiment was not stopped when a reduction was obtained. Every time a ROP reduction was encountered, drilling was re-conducted at a lower level of WOB. This procedure resulted in repeated drillings under the same WOB for several times, during which fluctuations of ROP values were detected while all controllable parameters were kept constant. It is possible that these fluctuations were caused by the inhomogeneity of the samples. Because of the short drilling distance, minor variations of sample properties in small regions could affect the drilling performance.

Static WOB (kg)	Time(s)	Bit Travel (cm)	ROP (cm/s)
47.316	923	2.2	2.384×10^{-3}
47.316	616	1.3	2.11×10^{-3}
47.316	532	0.76	1.428×10^{-3}
64.136	1090	3.41	3.128×10^{-3}
64.136	825	1.89	2.291×10^{-3}
64.136	300	1	3.333×10^{-3}
64.136	533	1.35	2.529×10^{-3}
80.956	534	1.55	2.903×10^{-3}
80.956	542	1.84	3.395×10^{-3}
80.956	533	1.55	2.917×10^{-3}
80.956	535	1.47	2.75×10^{-3}
97.776	533.3	2.25	4.219×10^{-3}
97.776	533.6	2.35	4.404×10^{-3}
114.596	533.6	2.84	5.322×10^{-3}
114.596	533.6	3.35	6.278×10^{-3}
131.416	534.3	3.65	6.831×10^{-3}
131.416	524	2.7	5.153×10^{-3}
131.416	533.4	2.45	4.593×10^{-3}
131.416	240	1.63	6.792×10^{-3}
148.236	437.1	2.92	6.68×10^{-3}
148.236	337.4	2.35	6.965×10^{-3}
148.236	533.3	3.9	7.313×10^{-3}
165.056	547.2	4.64	8.474×10^{-3}
165.056	356.5	3.53	9.902×10^{-3}
181.876	353.2	4.13	1.169×10^{-2}
181.876	235.8	2.35	9.966×10^{-3}
181.876	281.1	2.387	8.492×10^{-3}
198.696	330.3	3.45	1.0445×10^{-2}

215.516	270	3.3	1.222×10^{-2}
215.516	381.2	3.84	1.007×10^{-2}
232.336	250.3	2.86	1.143×10^{-2}
249.156	295	3.94	1.336×10^{-2}
265.976	286	3.89	1.360×10^{-2}
265.976	230	3.16	1.374×10^{-2}
265.976	150	2.32	1.547×10^{-2}
282.796	183	2.62	1.432×10^{-2}
282.796	245	2.99	1.220×10^{-2}
282.796	300	3.97	1.323×10^{-2}
299.616	200	3.06	1.53×10^{-2}
299.616	215	3.17	1.474×10^{-2}
316.436	335.7	5.23	1.558×10^{-2}

Table 6.2 Drilling data of the full face bit conventional rotary drilling

Although the ROP fluctuated to some extent, an increasing pattern of the WOB- ROP plot could still be observed from Fig.6.4. In order to protect the motor housing which has been damaged previously due to excessively high WOB during a teaching based lab, the WOB did not exceed 300 kg WOB during the experiments. Up to this level of WOB, no sign of peak, or any change in the slope of the increment pattern was found. In Fig. 6.5, the ROP data at each WOB was averaged based on the distance each drill run had traveled. This averaged data better presented the increasing pattern of the WOB-ROP curve.

The full face bit rotary drilling results have shown a long inclined portion in the WOB-ROP performance curve. The ROPs at the range of tested WOBs were relatively low, compared to the ROP of the coring bit experiments. Up to the end of the test, the curve was still rising. These results suggest that there were still potentials for this bit to stand higher WOB.

These results suggested that this diamond impregnated full face bit was properly chosen for the VARD experiment. Its large bit contact surface allows it to sustain high level of bit weight before the limit (optimized WOB). This characteristic made it possible to further investigate the vibration effects on the long climb portion of the WOB curve.

6.4 Full Face Bit VARD Experiment

The full face VARD experiment was designed to involve 6 levels of WOB (from 47 kg to131 kg static WOB) and 5 levels of vibrations (from shaker control setting '10'-'50'). It follows the sequence of increasing the shaker control settings at fixed WOB, then increase the WOB (up to 131 kg WOB) to the limit of the shaker capacity. The drilling

operation went smoothly. The ROP increase could be clearly observed with rising WOB and shaker control settings. Because little fluctuations were encountered during the test with increasing vibration, most data were only drilled for one time, except for several failed drilling runs with lack of proper data recording. For the drilling runs with lower ROP, the drilling times were kept the same for 5.5 minutes. For the higher ROP tests, because of the increased distance the bit has traveled, the drilling times were shortened to 2.5 minutes. For most tests, no more than 2 samples were drilled under one level of WOB so that better consistency of sample quality could be guaranteed.

The drilling data for the VARD full face bit tests is presented in Table 6.3. During the test, the flow was reduced to 2.5 US gpm. This was a compromise to the capacity of the drainage system and pump off effect. The effect of reduced flow could be observed by comparing the conventional drilling data between the results in Table 6.2 and Table 6.3. The ROPs between 47 kg and 131 kg have shifted down by 0.001 cm/s to 0.002 cm/s. The LVDT was mounted on the shaker and the actual amplitudes of the shaker during the drilling were recorded. The recorded displacement wave forms during drillings are presented in Appendix C.

The shaker vibration amplitudes under various levels of WOB and shaker control settings are plotted in Fig. 6.6 and Fig. 6.7 (3-D plot). The LVDT data collected during the drilling test with full face bit responded differently compared with the result presented in Fig. 3.25. In Fig.3.25, the amplitudes were reduced with increasing WOB, and then they tended to be flattened with higher level of WOBs. In comparison, the result presented in Fig. 6.6 showed that the amplitudes reduced while the WOB increased at low level,

(before 81 kg static WOB). Then all amplitudes began to climb to some extent with 98 kg-115 kg static WOB. Up to 131 kg of static WOB, the vibration amplitudes under all levels of shaker control settings have gathered in a very small region (from 0.14 mm to 0.18 mm), which indicated that the shaker vibration was saturated at 131 kg static WOB.

Static WOB (kg)	Time (s)	Travel (cm)	ROP (cm/s)	Shaker control settings	Amplitude measured by LVDT (mm)
47.316	330	0.33	1.0×10^{-3}	No vibration	0
47.316	360	0.48	1.33×10^{-3}	10	0.150
47.316	330	0.78	2.364×10^{-3}	20	0.217
47.316	330	0.96	2.909×10^{-3}	30	0.306
47.316	330	1.31	3.97×10^{-3}	40	0.377
47.316	330	1.26	3.818×10^{-3}	50	0.465
64.136	330	0.44	1.667×10^{-3}	No vibration	0
64.136	330	1.03	3.121×10^{-3}	10	0.072
64.136	330	1.29	3.909×10^{-3}	20	0.150
64.136	330	1.79	5.424×10^{-3}	30	0.279
64.136	330	2.07	6.273×10^{-3}	40	0.320
64.136	330	1.99	6.03×10^{-3}	50	0.340
80.956	330	0.8	2.424×10^{-3}	No vibration	0
80.956	330	1.53	4.636×10^{-3}	10	0.060
80.956	330	2.06	6.242×10^{-3}	20	0.082
80.956	330	2.49	7.545×10^{-3}	30	0.141
80.956	330	3.04	9.212×10^{-3}	40	0.175
80.956	330	3	9.091×10^{-3}	50	0.221
97.776	330	1.1	3.333×10^{-3}	No vibration	0
97.776	330	1.86	5.636×10^{-3}	10	0.069
97.776	330	2.49	7.545×10^{-3}	20	0.010
97.776	330	3.09	9.364×10^{-3}	30	0.155
97.776	330	3.32	1.007×10^{-2}	40	0.230
97.776	330	3.5	1.061×10^{-2}	50	0.290
114.596	330	1.5	4.545×10^{-3}	No vibration	0
114.596	330	2.42	7.333×10^{-3}	10	0.091

114.596	330	2.95	8.936×10^{-3}	20	0.167
114.596	330	3.53	1.068×10^{-2}	30	0.254
114.596	330	4.21	1.276×10^{-2}	40	0.269
114.596	330	4.27	1.294×10^{-2}	50	0.258
131.416	230	1.17	5.087×10^{-3}	No vibration	0
131.416	230	2.05	8.913×10^{-3}	10	0.161
131.416	230	2.25	9.796×10^{-3}	20	0.156
131.416	230	2.65	1.152×10^{-2}	30	0.170
131.416	230	3.15	1.370×10^{-2}	40	0.182
131.416	230	3.5	1.522×10^{-2}	50	0.141

Table 6.3 Drilling data of the full face bit VARD experiments

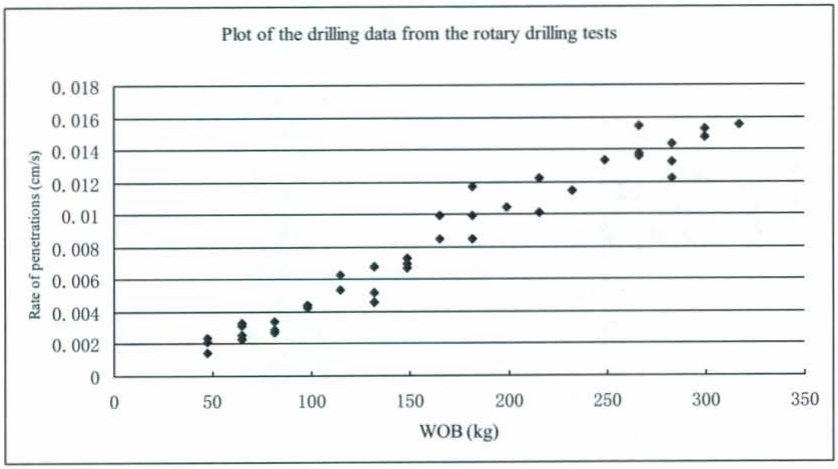

Fig. 6.4 Actual drilling data distribution with increasing WOB

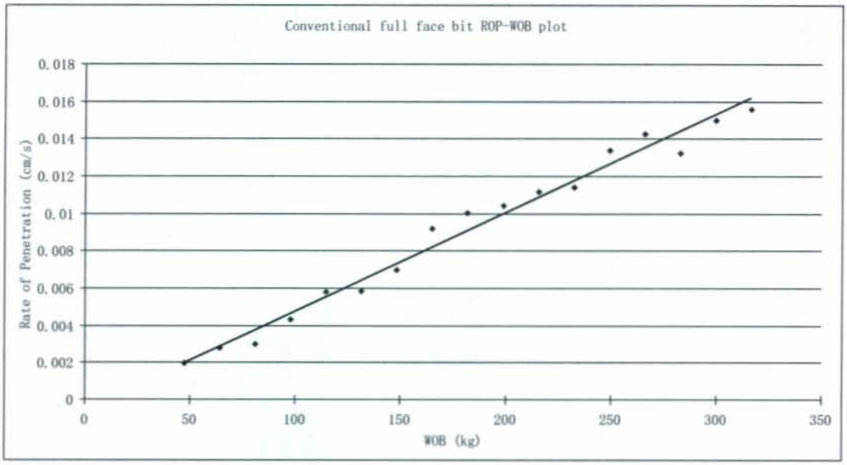

Fig. 6.5 Averaged conventional drilling data with increasing WOB

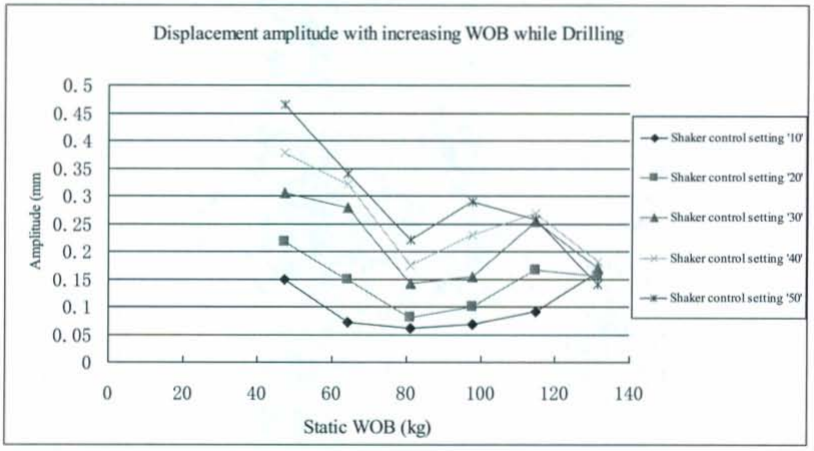

Fig. 6.6 Vibration amplitude measured by the LVDT during the VARD full face bit experiment

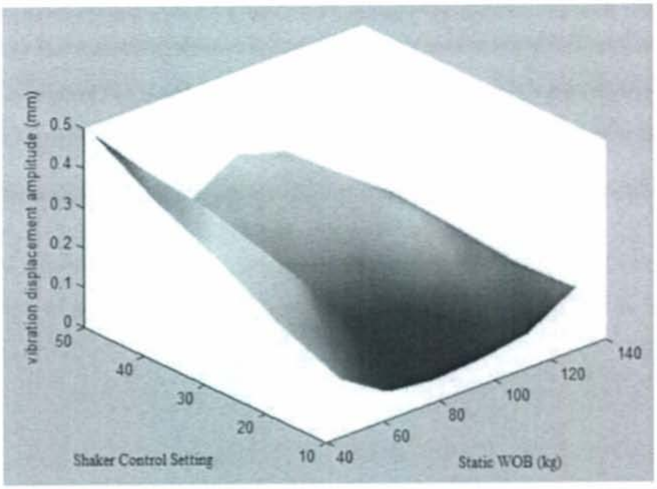

Fig. 6.7 3-D Plot of the shaker amplitude during VARD test

This difference was partially caused by the different setup in the two studies. Compared to the non-drilling shaker vibration characteristic studies in Chapter 3, the bit- rock contact surface was changed; the drilling fluid was introduced; as well as bit penetration. The displacement amplitudes presented in Appendix A and Appendix C also suggested that during the drilling, the bit wobbling also affected the shaker performance. As stated by the supplier of the shaker, the amplitude could be controlled by the shaker knob controller only with certain object fixed on it. When the payload or the weight distribution was changed, the behavior of the shaker amplitude could not be predicted. This explained why the shaker amplitudes increased in most occasions when the shaker control setting increases, but they performed differently with the different configurations used throughout the investigation.

For this reason, the ROP in the VARD full face bit experimental result were mainly presented as a function of the shaker control settings and the WOB. Up to this stage, the shaker control setting was found to be the most direct factor describing the mechanical power of the added vibration to the drilling system, compared to the vibration displacement amplitude and the force variation amplitude. The 2-D result of the ROP against the WOB and the shaker control setting is shown in Fig. 6.8, and Fig. 6.9, and the 3-D response surface of the ROP is shown in Fig. 6.10.

The results shown in Fig.6.8 and Fig. 6.9 marked a milestone in the VARD research. In this group of results, the relationship between the added vibrations on the ROP was clearly obtained. The factor 'shaker control setting', was found to have linearly increased the ROP in all 6 curves with different WOBs, except the highest level of vibration, the 'position 60', which was found to be not in the linear range of the shaker amplitude output. Based on the data presented in Fig. 6.8 and Fig. 6.9, a surface fitting equation is established using linear 3-D models. In the equation, P_S is the shaker control setting factor, which represents the level of the shaker vibration energy. The equation is given in Eqn. 6.1. The linear model was found to have acceptable error of 3.22×10^{-5}.

$$ROP = 9.71\times10^{-5}\times WOB + 1.35\times10^{-4}\times P_S - 6.49\times10^{-3} \quad (6.1)$$

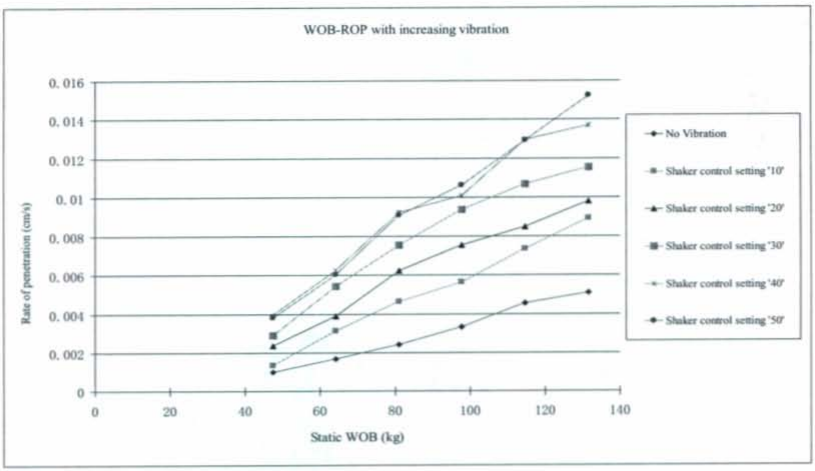

Fig. 6.8 VARD full face experiment result—ROP as a function of WOB with multiple levels of vibrations

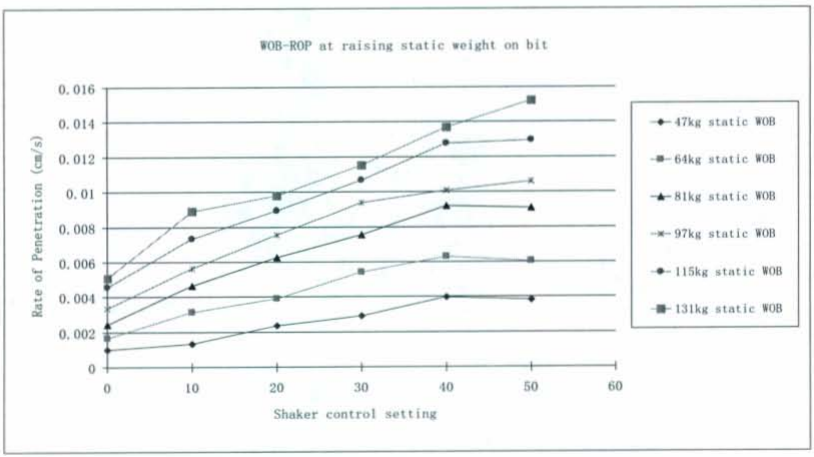

Fig. 6.9 VARD full face experiment result—ROP as a function of vibration with multiple levels of WOB

Another result to take notice is that in Fig.6.9, the added vibration not only shifted up the ROP in the WOB-ROP curve, but also changed its slope. For example, a comparison between the WOB-ROP curves without vibration and with 'shaker control setting 50' vibrations showed that the added vibrations have increased the slope by 100% (1.0E-4 with the 'shaker control setting 50' vibration, compared to 0.5E-5 without vibration). Similar effect could also be found in the coring bit VARD results in chapter 3. During the VARD coring bit tests, the WOB-ROP curves were found to be 'shortened' by the added vibration. However the curves with stronger vibrations tended to climb steeper and reaches to the peak with lower WOB.

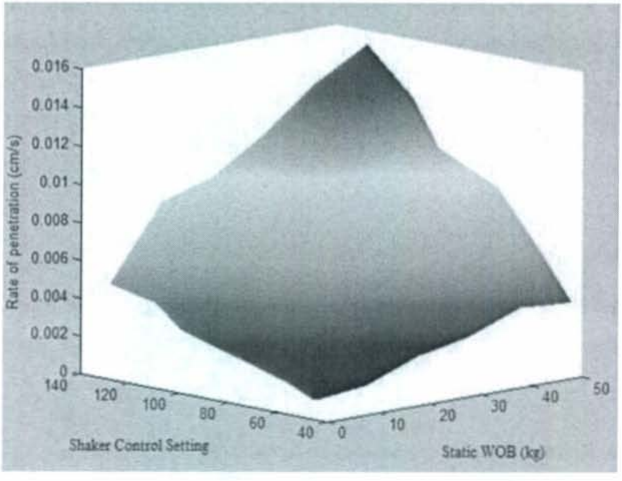

Fig. 6.10 3-D ROP surface as a function of static WOB and shaker control settings

Chapter 7

Conclusion and Discussion

7.1 Conclusions

The development of the VARD experimental system started in the fall of 2008. The main assembly with the rig and the vibration table was completed by May, 2009. Since then, modifications were done to meet the requirements revealed during the experiments. Some of these modifications are still underway today. Fig. 7.1 shows a comparison of the VARD experiments before and after the development and modifications.

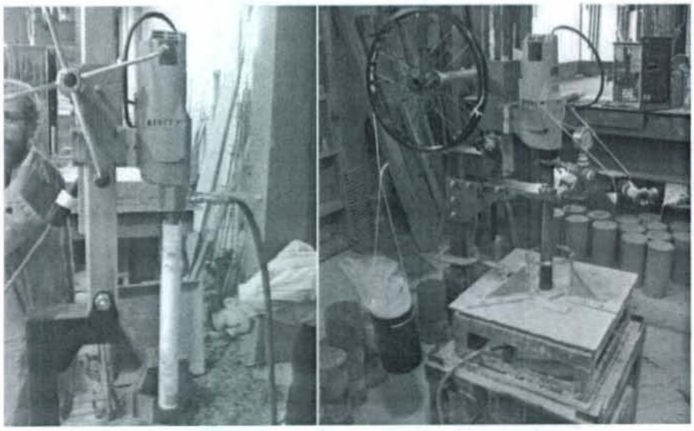

Fig. 7.1 Comparison of the VARD rig in fall, 2008 (left) and August, 2010 (right)

The 'VARD experimental facility' in the VARD project, is a simple but versatile research facility. Most of its operating parameters could be easily controlled and varied to some extent. The simple structure allowed the sensors to be easily installed for necessary measurements. During the later experimental studies, this laboratory drilling rig was proved to be reliable, and generated significant results.

The coring bit VARD experiments were carried out from October, 2009 to February, 2010. The added vibrations were found to significantly increase the rate of penetration before the founder WOB, where the WOB-ROP curves began to saturate. Meanwhile high level of vibrations also led to earlier saturation of the WOB-ROP curve, thus leaving little operation window for the WOB.

The full face bit experiments were conducted in order to investigate the relationship between the vibration mechanical power, and the rate of penetration without encountering the founder points. The conventional rotary drilling experiments showed that the bit served adequately for this purpose. The inclined portion of the WOB-ROP curve for this bit was long, and no founder point was found up to 300 kg WOB. Based on this advantage, subsequent VARD experiments were carried out, and the results clearly revealed the positive effect of the added vibrations on the rate of penetration.

Combining the results from both two groups of experiments, the following effects could be concluded:

The VARD technology could significantly increase the rate of penetrations compared to rotary drilling under same bit operating conditions. This increment is especially obvious while the WOB is relatively low

The mechanical power of the vibration could affect the shape of the WOB-ROP curve. The higher level of vibration mechanical power could result in steeper inclination and earlier saturation of the WOB-ROP curve.

A similar relationship to the WOB-ROP curve is obtained while the 'shaker control setting', which is proportional to the vibration mechanical power, is plotted against the rate of penetration. The vibration shaker control settings were found to be proportional to the rate of penetration.

7.2 Discussions to the future work

Although significant results were generated based on the VARD experimental facility, limitations were also encountered during the experiments. Followings suggestions in both the experimental setup and the experimental design aspects are given for the future experiments.

Up to now, the vibration forces and amplitudes were measured and plotted against the shaker control settings. However, none of these two variables were found to be independent of the shaker load (WOB). The clarification of the vibration mechanical power may need to be continued. The next possible solution is to measure the current input varied by the shaker controller, followed by calculating the electronic power input to the shaker.

Basic studies to the drilling fluids were conducted and recorded in Chapter 5. The temporary solution is to keep the flow constant when the pressure gauge began to have readings. This was done to balance the bottom hole cleaning effect and the influence of the static WOB by the pump off force. In the future experiments, if a load cell with better response to the change in axial forces can be introduced, it is advised to re-investigate the flow effect, and find the maximum flow rate that can provide sufficient bottom hole cleaning so that the WOB-ROP curve can be saturated until it reaches its torque limitation.

The result of this VARD experimental investigation is presented in WOB-ROP and shaker control setting- ROP curves. However, another way to describe the performance improvement of a new drilling technology is to create operation envelopes, instead of analyzing the curves under certain operation conditions. Envelopes could be plotted under various levels of vibrations, with each envelope contain all possible operation conditions, from extremely low levels up to the limitation of the system. The comparison between these envelopes could describe the advantage of the VARD technology in a more exact way.

In particular, the present set of studies suggested that future investigations could further concentrate on the search of new vibration variable independent of the shaker payload, improvement of the WOB control system to balance the pump off force and maximize the bottom hole cleaning effect, and express the performance improvement brought by the VARD technology by creating operation envelopes.

Reference

Allaboutcircuits.com, (n.d.), *Strain Gauges*, Retrieved from http://www.allaboutcircuits.com/vol_1/chpt_9/7.html

Archway-Engineering, (n.d.), *Impregnanted Diamond Core Bits*, Retrieved from http://www.archway-engineering.com/products/corebits_impreg.html

Black, A.D., Bland,R.G., Curry, D.A., Ledgerwood III, L.W. Robertson, H.A., Judzis, A. 2008, 'Optimization of Deep-Drilling Performance—Benchmark Testing Drives ROP Improvements For Bits and Drilling Fluids'. *IADC/SPE Drilling Conference*, SPE 112731-MS, March, 2008.

Bourgoyne Jr, A.T., Millheim, K.K., Chenevert, M.E., and Young Jr, F.S. (1991). *Applied Drilling Engineering*. Richardson, TX: Society of Petroleum Engineers., pp.200, pp.464

Cunningham, R.A., 1960, 'Laboratory Studies of The Effect of Rotary Speed on Rock-bit Performance and Drilling Cost', *Drilling and Production Practice, 1960,* API 60-007, March, 1960, pp.7-14.

Ersoy, A. and Waller, M.D., 1995, 'Textural Characterization of Rock', *Engineering Geology*, *39* (3-4), June, 1995, pp. 123-136.

Eskin, M., Maurer, W.C., Leviant, A. 1995. 'Former-USSR R&D on Novel Drilling Techniques'. Maurer Engineering Inc.

Finger, J.T., 1984, 'Investigation of Percussion Drills For Geothermal Application', *J. of Petroleum Technology*, 36 (12), December 1984, pp.2128-2136.

Fossen, F. (2010). *Structural Geology*. Cambridge: Cambridge University. pp. 127-130

Greenberg, J., 2010. 'Abrasive Formations, Shale Wells Drive New Bit Designs for Hard-Rock, High Temperature Drilling', *Intl. Oil and Gas Conference and Exhibition in China*, SPE 132048-MS, June, 2010.

Gstaider, S., Rynal, J. 1966, 'Measurement of Some Mechanical Properties of Rocks and Their Relationship to Rock Drillability', *J. of Petroleum Technology*, *18* (8), August, 1996, pp.991-996.

Han, G., Bruno, M., 2006, 'Percussion Drilling: From Laboratory Tests to Dynamic Modeling', *Intl. Oil & Gas Conference and Exhibition in China*, SPE 140178-MS, December, 2006.

Hartman, H.L., 1966, 'The Effectiveness of Indexing In Percussion and Rotary Drilling', *Int. J. of Rock Mechanics and Mining Sciences & Geomechanics Abstracts, 3* (4), November, 1996, pp. 265-278.

Honeywell, 1995, *DLD Series LVDT Demodulators*. Retrieved from https://measurementsensors.honeywell.com/ProductDocuments/Manuals/008-0532-00.pdf.

Hoseinie, S.H., Ataei, M., Osanloo, M., 2009, 'A New Classification System for Evaluating Rock Penetrability'. *Int. J. of Rock Mechanics & Mining Sciences*, 2009(46), pp.1329-1340.

Jean van Wijk. 'Exploration Drilling-Market Assessment Research for VARD Tool'. 4 May 2009.

Lagreca, A.J., Santana, D.D., Suarez, G., Rodriguez, M., Mclinnes, M.B., 2002, 'Fluid Percussion Hammer Field Test in the Alocthonous Cretaceous Block, Eastern Venezuela'. *Canadian International Petroleum Conference*, PETSOC 2002-128, June, 2002.

Lundberg, B., Okrouhlik, M., 2001,'Influence of 3D Effects on The Efficiency of Percussive Rock Drilling'. *Int. J. of Impact Engineering*, *25* (4), April 2001, pp.345-360.

Maurer, W.C. 1965, 'Bit-Tooth Penetration Under Simulated Borehole Conditions. Petroleum Transactions'. *J. of Petroleum Technology*, *17* (12), December, 1965, pp.1433-1442.

Maurer, W.C. Pers. Comn. 2010, Collaborating meeting, Nov, 2010, Austin, Texas.

Maurer.W.C., 1962, 'The ''Perfect- Cleaning'' Theory of Rotary Drilling'. *J. of Petroleum Technology*, *14*(11), November, 1962, pp. 1270-1274.

Moad, D., Mclellan, G., Wise, J., Barrow, J., Biancosino, D., Write, J., 1995, 'Resonantsonic Drilling—Innovative Technology Summary Report.' US Department of Energy, April, 1995.

National Instruments, (n.d.) *Using Quadrature Encoders with E Series DAQ Boards*. Retrieved from ftp://ftp.ni.com/pub/devzone/pdf/tut_4623.pdf

National Instruments, 2006, *Measuring Position and Displacement with LVDTs*, Retrieved from http://zone.ni.com/devzone/cda/tut/p/id/3638.

Paul, B. and Gangal, M.D., 1969, 'Why Compressive Loads on Drill Bits Produce Tensile Splitting in Rock'. *Drilling and Rock Mechanics Symposium*, SPE 2392-MS, January, 1969.

Pennington, J.V., 1953, 'Some Results of DRI Investigations—Rock Failure in Percussion'. *Drilling and Production Practice, 1953*, API 53-329, November, 1953.

Pierson, J. (n.d.). *Load/ Force Cells*, Retrieved from http://www.sensorland.com/HowPage005.html

Pratt, C.A., 1989, 'Modifications To and Experience With Air-Percussion Drilling'. *Intl. J. of Rock Mechanics and Mining Sciences & Geomechanics Abstracts*, 27(4), August, 1990, pp.231.

Rabia, H., 1985, 'A Unified Prediction Model for Percussive and Rotary Drilling'. *Mining Science and Technology*, *2* (3), June, 1985, pp.207-216.

Sandvik, (2011). *Roller Cone Bits.* Retrieved from http://www.directindustry.com/prod /sandvik-mining-and-construction/roller-cone-bits-40142-431481.html

Sonic Samp Drill ltd., (n.d.). *Sonic Drilling Theory*. Retrieved from http://www.sonicsampdrill.com/uploads/080623%20Brochure-RotoSonic-How%20does%20it%20work.pdf

Spaar, J.R., Ledgerwood, L.W., Christensen, H., Goodman, H., Graff, R.L., Moo, T.J., 1995, 'Formation Compressive Strength Estimates for Predicting Drillability and PDC Bit Selection', *SPE/IADC Drilling Conference*, API 62-191, February, 1995.

Whiteley, M.C., England, W.P., 1986, 'Air Drilling Operations Improved by Percussion-Bit/Hammer-Tool Tandem', *SPE Drilling Engineering*, SPE 13429-MS, October, 1986, pp.377-382.

Wise, B.A., Cooper, D.E., Thompson, R.L., 1958, 'Well Drilling System', *United States Patent Office*, No. 2,858,108.

howstuffworks.com. (n.d.). *Oil Rig Systems—How Oil Drilling Works*, Retrieved from http://www.howstuffworks.com/environmental/energy/oil-drilling4.htm.

Yang, J.H., Gray. K.E., 1967, 'Single-Blow Bit-Tooth Impact Tests on Saturated Rocks Under Confining Pressure: II Elevated Pore Pressure'. *Society of Petroleum Engineers Journal*, December, 1967, pp.389-408.

Appendix A: Displacement amplitude measured by data without drilling

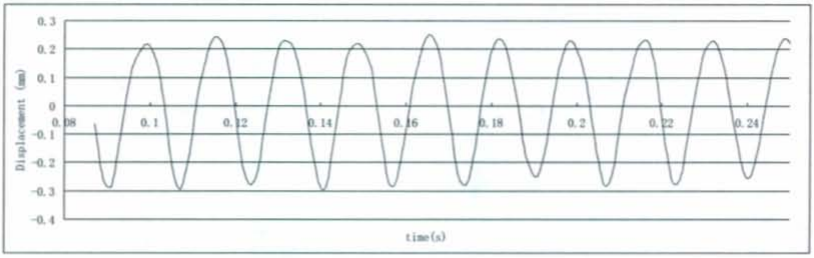

LVDT measured displacement amplitude at 46 kg WOB, shaker control setting '10'

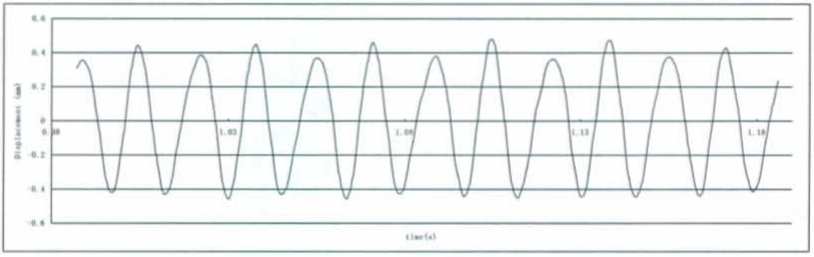

LVDT measured displacement amplitude at 46 kg WOB, shaker control setting '20'

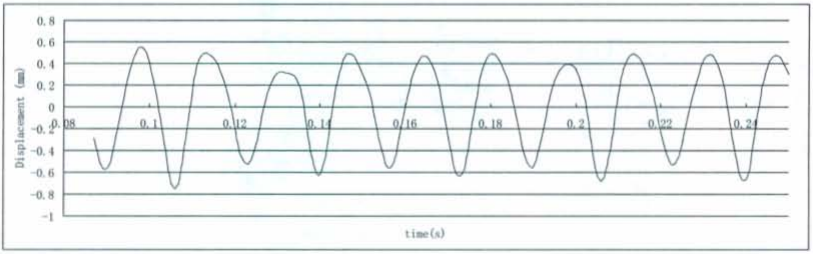

LVDT measured displacement amplitude at 46 kg WOB, shaker control setting '30'

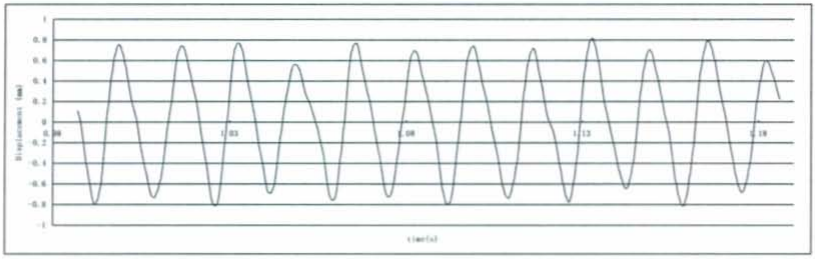

LVDT measured displacement amplitude at 46 kg WOB, shaker control setting '40'

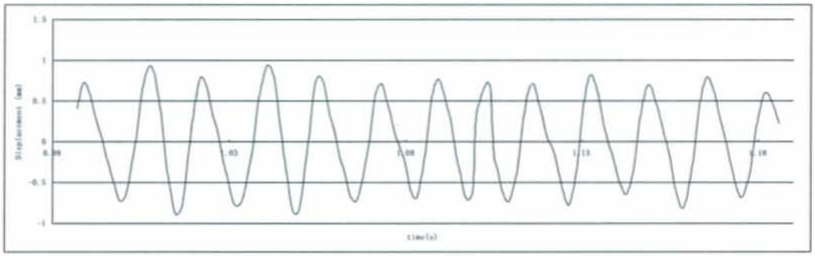

LVDT measured displacement amplitude at 46 kg WOB, shaker control setting '50'

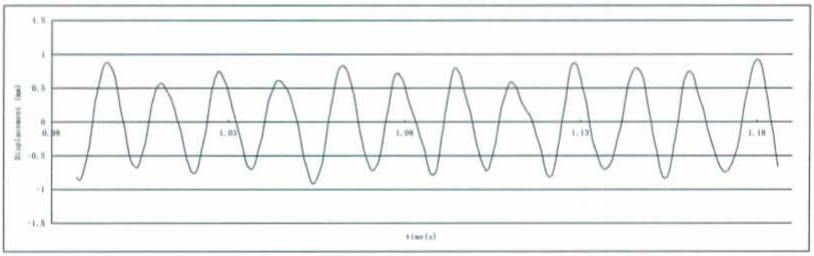

LVDT measured displacement amplitude at 46 kg WOB, shaker control setting '60'

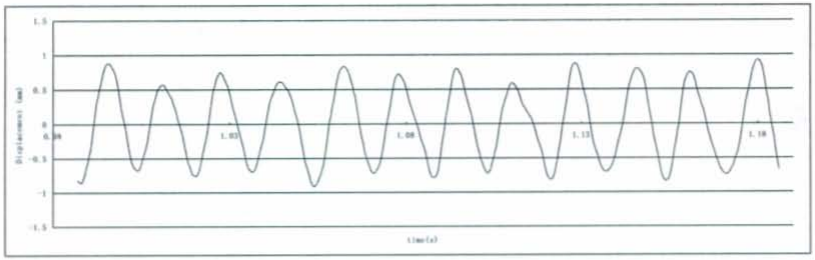

LVDT measured displacement amplitude at 62 kg WOB, shaker control setting '10'

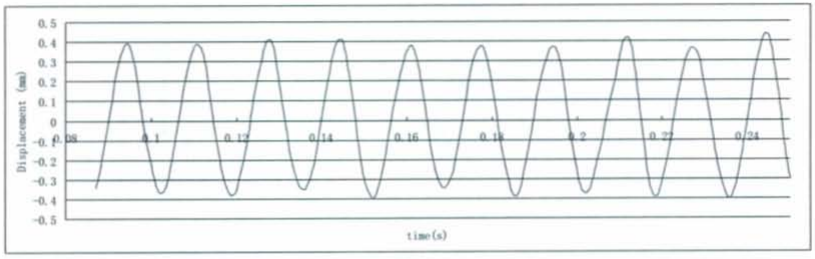

LVDT measured displacement amplitude at 62 kg WOB, shaker control setting '20'

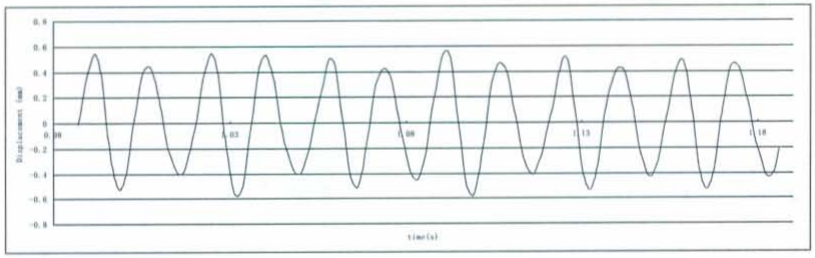

LVDT measured displacement amplitude at 62 kg WOB, shaker control setting '30'

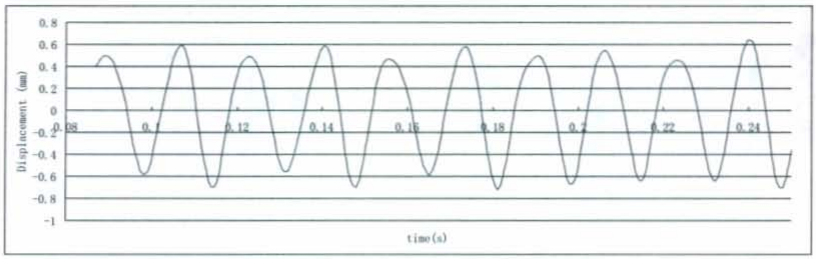

LVDT measured displacement amplitude at 62 kg WOB, shaker control setting '40'

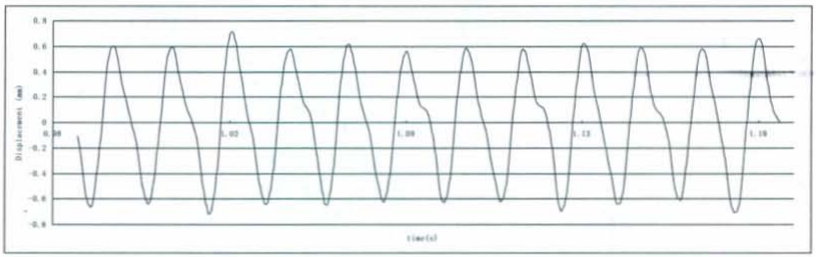

LVDT measured displacement amplitude at 62 kg WOB, shaker control setting '50'

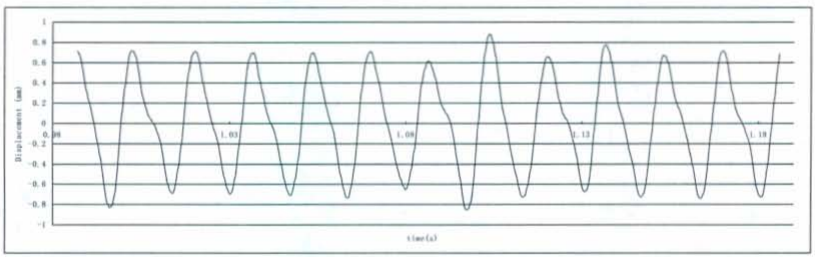

LVDT measured displacement amplitude at 62 kg WOB, shaker control setting '60'

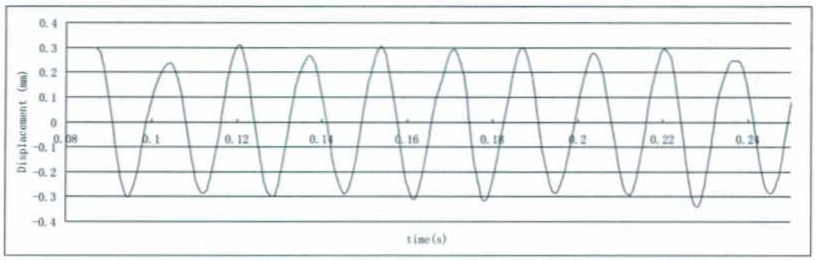

LVDT measured displacement amplitude at 79 kg WOB, shaker control setting '10'

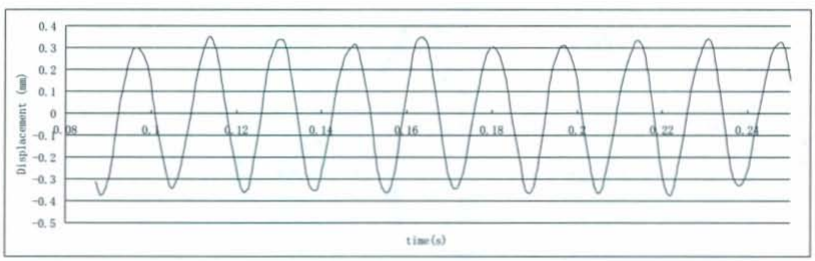

LVDT measured displacement amplitude at 79 kg WOB, shaker control setting '20'

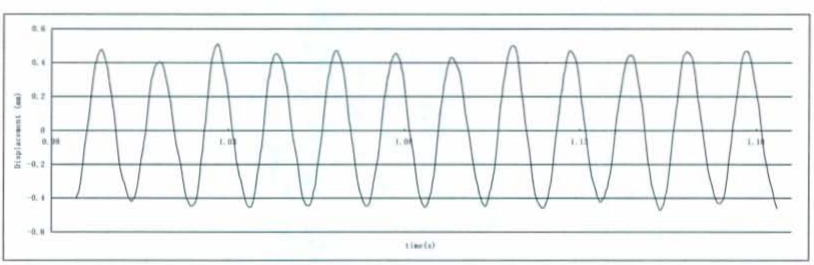

LVDT measured displacement amplitude at 79 kg WOB, shaker control setting '30'

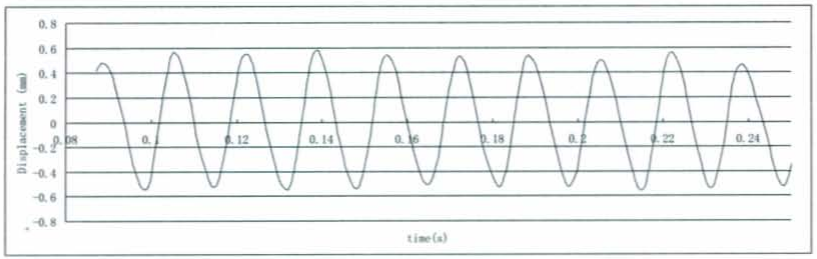

LVDT measured displacement amplitude at 79 kg WOB, shaker control setting '40'

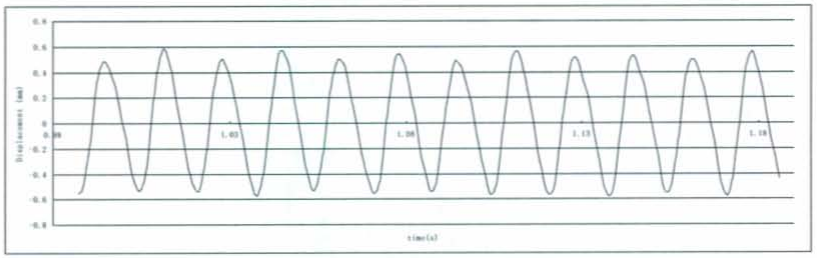

LVDT measured displacement amplitude at 79 kg WOB, shaker control setting '50'

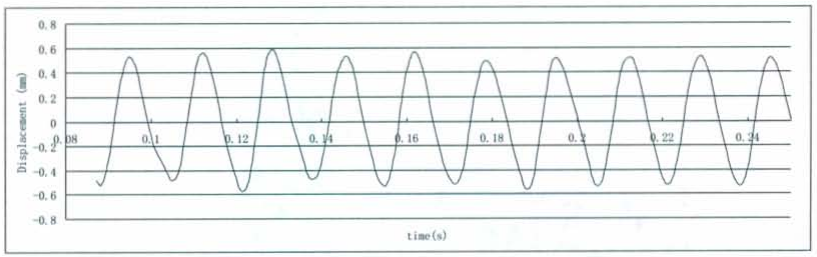

LVDT measured displacement amplitude at 79 kg WOB, shaker control setting '60'

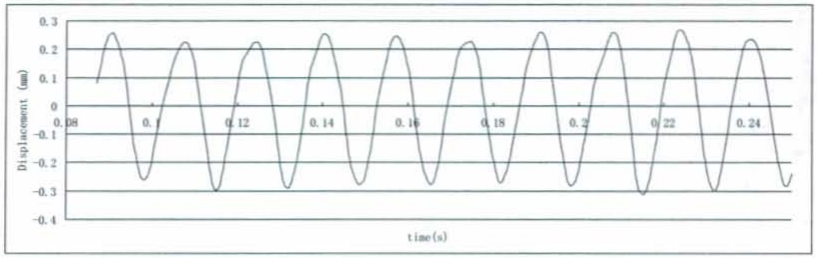

LVDT measured displacement amplitude at 96 kg WOB, shaker control setting '10'

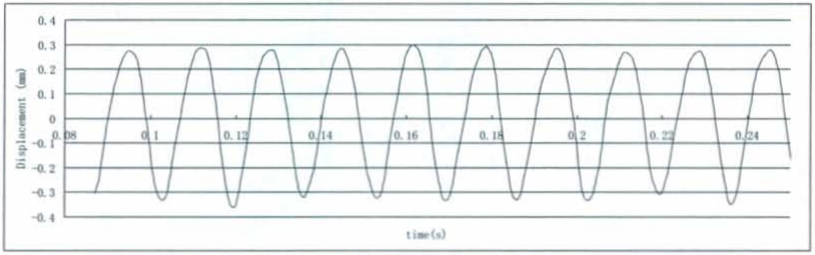

LVDT measured displacement amplitude at 96 kg WOB, shaker control setting '20'

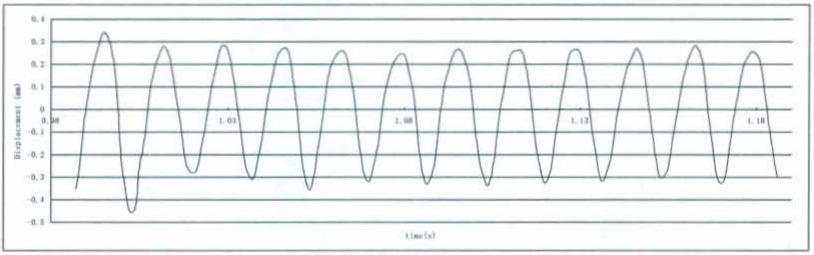

LVDT measured displacement amplitude at 96 kg WOB, shaker control setting '30'

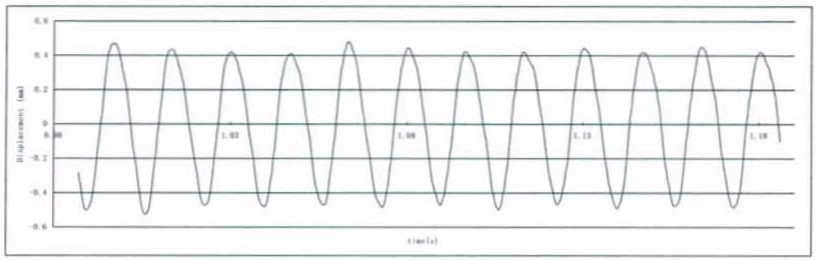

LVDT measured displacement amplitude at 96 kg WOB, shaker control setting '40'

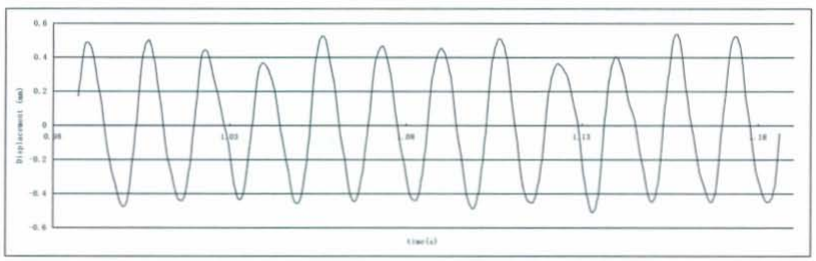

LVDT measured displacement amplitude at 96 kg WOB, shaker control setting '50'

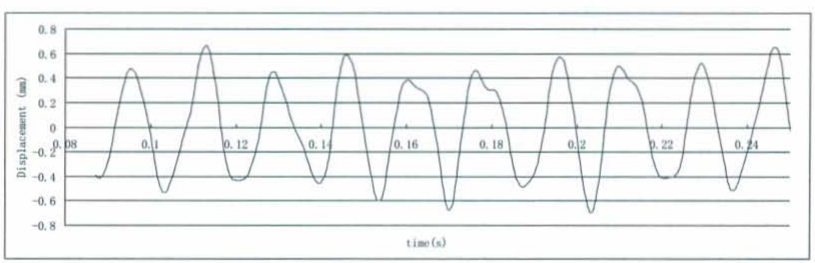

LVDT measured displacement amplitude at 96 kg WOB, shaker control setting '60'

Appendix B: Force amplitude recorded by load cell without drilling

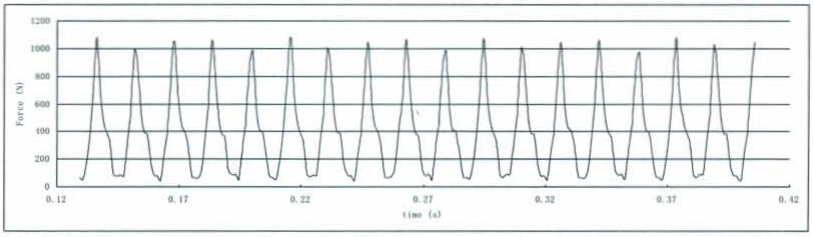

Load cell measured force amplitude at 46 kg WOB, shaker control setting '10'

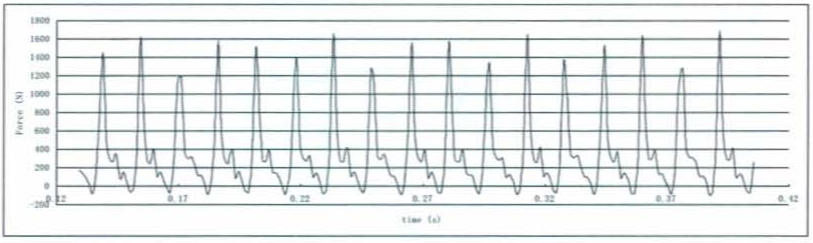

Load cell measured force amplitude at 46 kg WOB, shaker control setting '20'

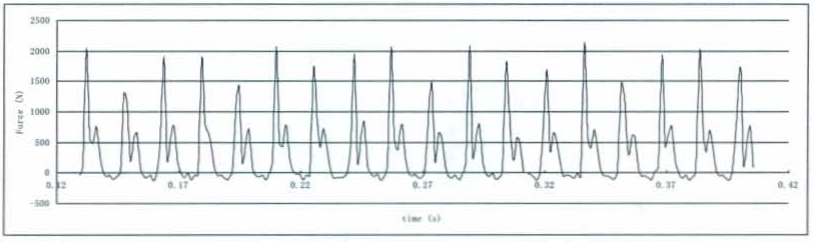

Load cell measured force amplitude at 46 kg WOB, shaker control setting '30'

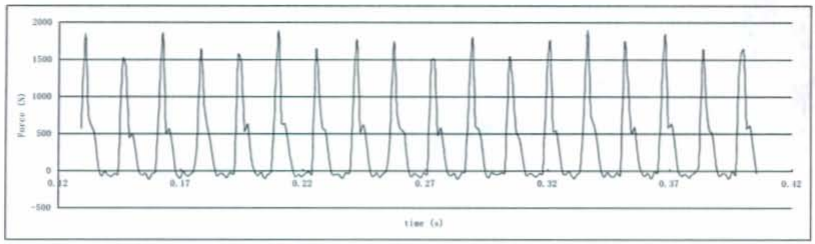

Load cell measured force amplitude at 46 kg WOB, shaker control setting '40'

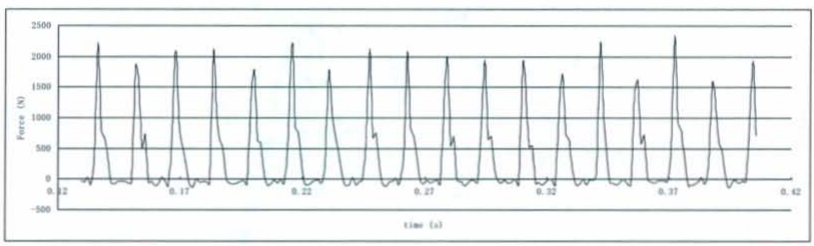

Load cell measured force amplitude at 46 kg WOB, shaker control setting '50'

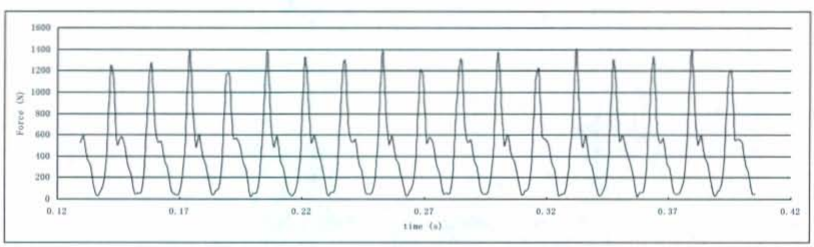

Load cell measured force amplitude at 62 kg WOB, shaker control setting '10'

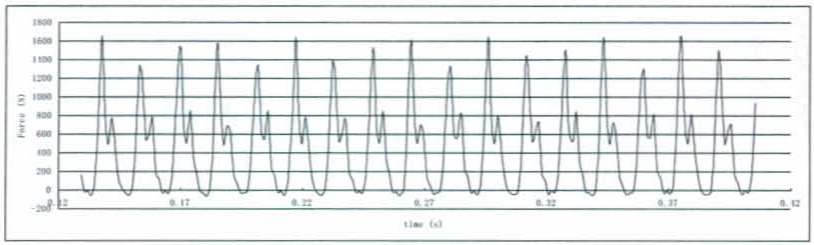

Load cell measured force amplitude at 62 kg WOB, shaker control setting '20'

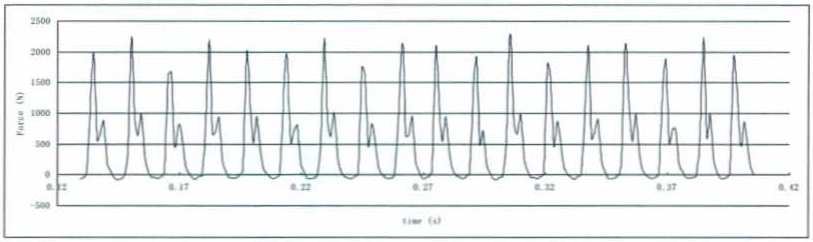

Load cell measured force amplitude at 62 kg WOB, shaker control setting '30'

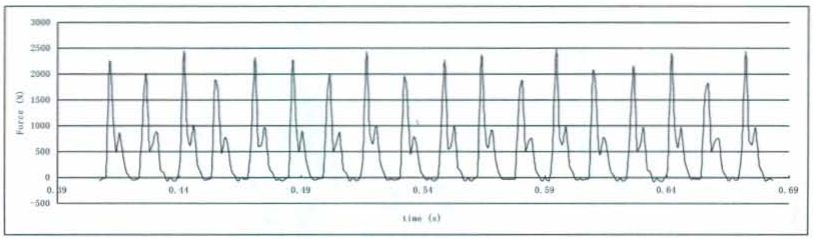

Load cell measured force amplitude at 62 kg WOB, shaker control setting '40'

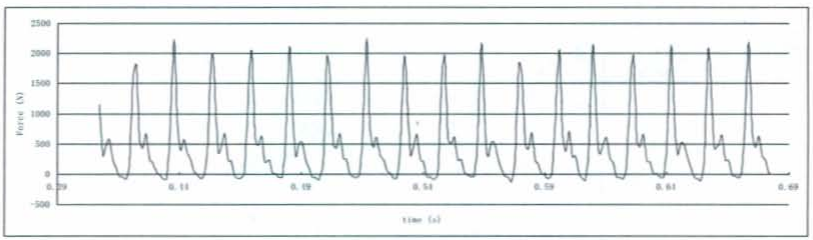

Load cell measured force amplitude at 62 kg WOB, shaker control setting '50'

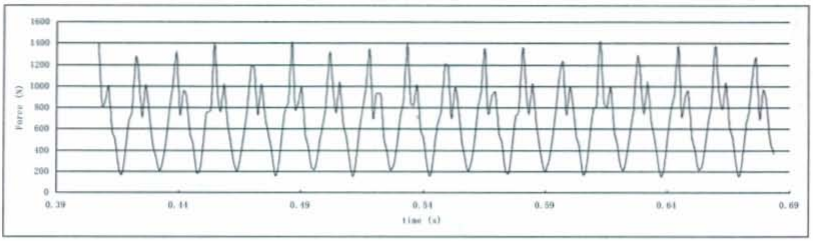

Load cell measured force amplitude at 79 kg WOB, shaker control setting '10'

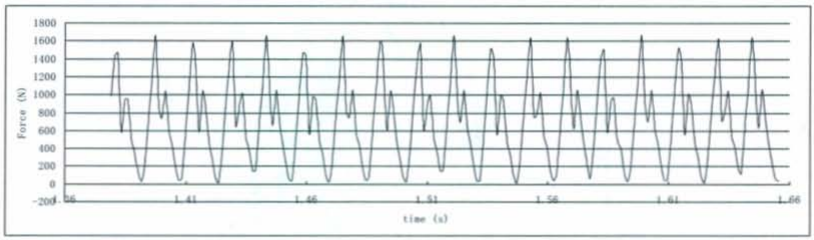

Load cell measured force amplitude at 79 kg WOB, shaker control setting '20'

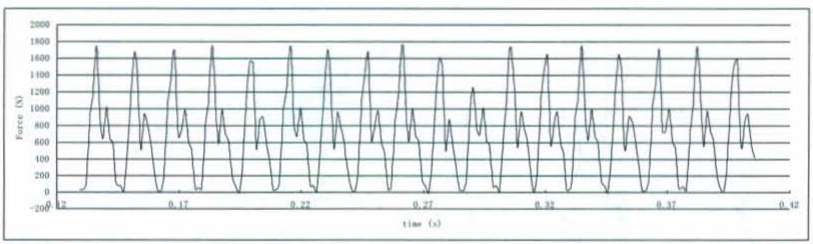

Load cell measured force amplitude at 79 kg WOB, shaker control setting '30'

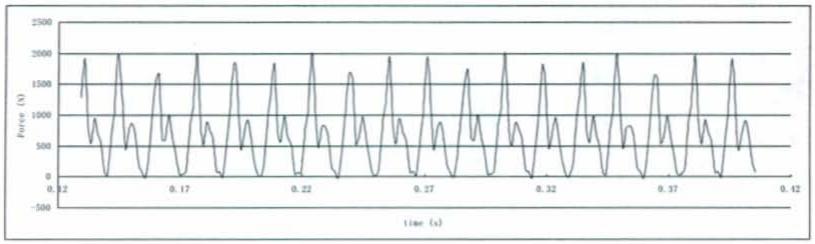

Load cell measured force amplitude at 79 kg WOB, shaker control setting '40'

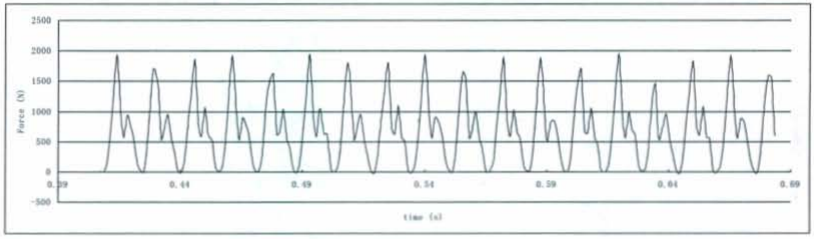

Load cell measured force amplitude at 79 kg WOB, shaker control setting '50'

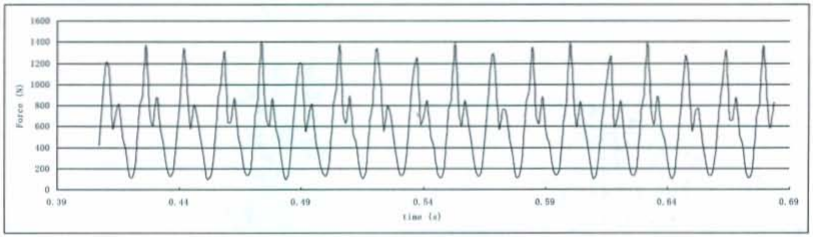

Load cell measured force amplitude at 96 kg WOB, shaker control setting '10'

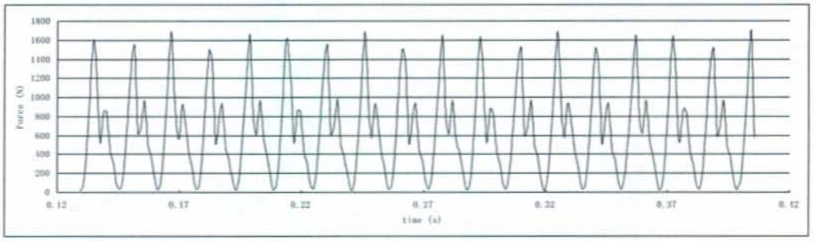

Load cell measured force amplitude at 96 kg WOB, shaker control setting '20'

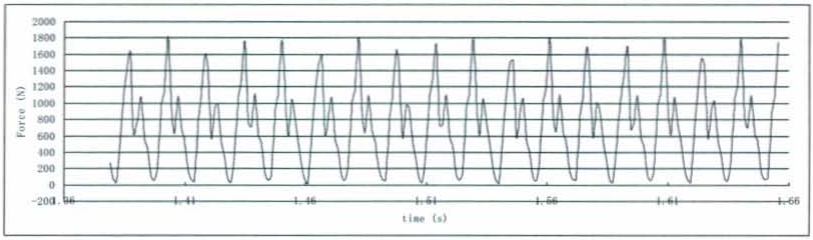

Load cell measured force amplitude at 96 kg WOB, shaker control setting '30'

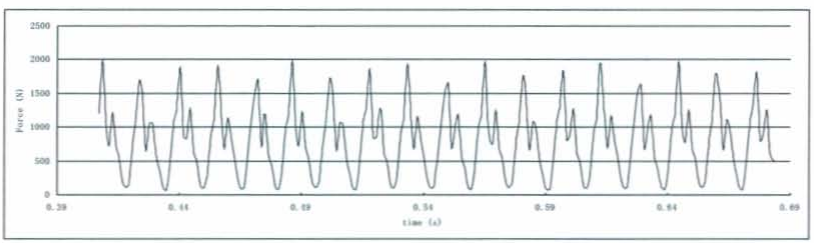

Load cell measured force amplitude at 96 kg WOB, shaker control setting '40'

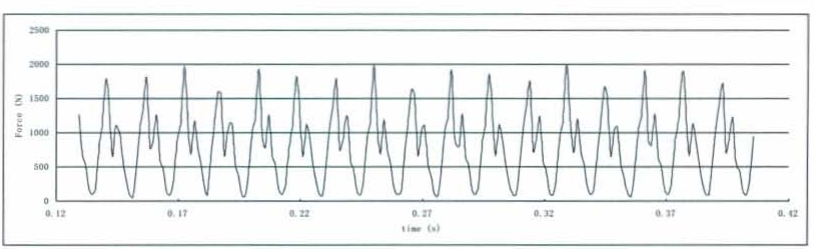

Load cell measured force amplitude at 96 kg WOB, shaker control setting '50'

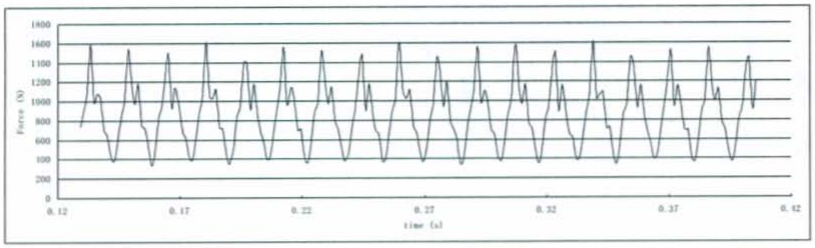

Load cell measured force amplitude at 113 kg WOB, shaker control setting '10'

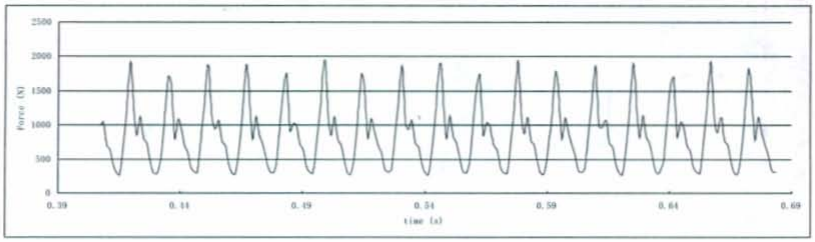

Load cell measured force amplitude at 113 kg WOB, shaker control setting '20'

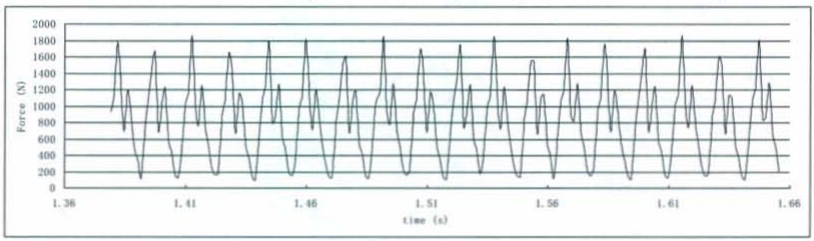

Load cell measured force amplitude at 113 kg WOB, shaker control setting '30'

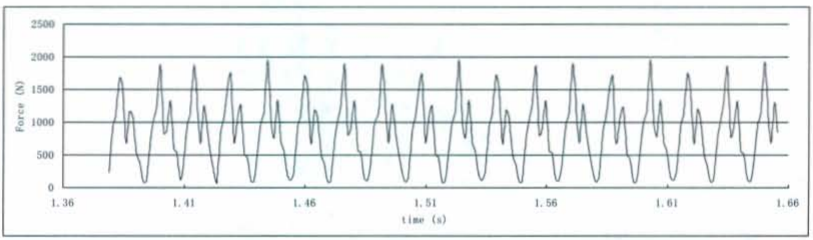

Load cell measured force amplitude at 113 kg WOB, shaker control setting '40'

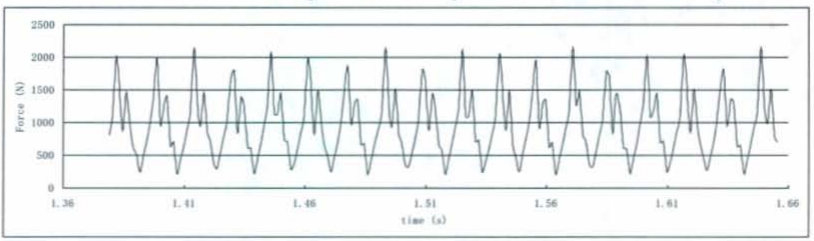

Load cell measured force amplitude at 113 kg WOB, shaker control setting '50'

Appendix C: Displacement amplitude measured by data while drilling

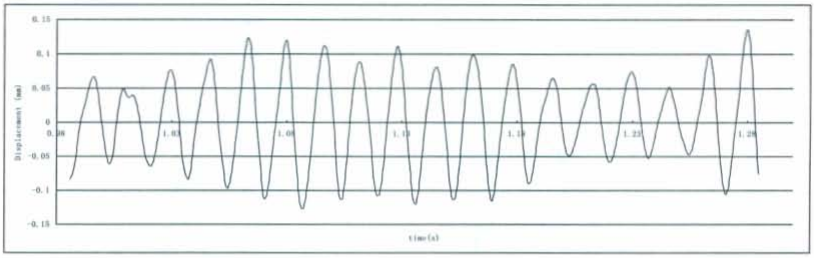

LVDT measurement of displacement amplitude at 47 kg WOB during drilling, shaker control setting '10'

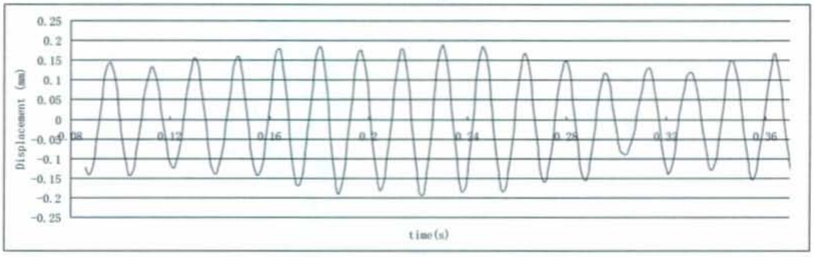

LVDT measurement of displacement amplitude at 47 kg WOB during drilling, shaker control setting '20'

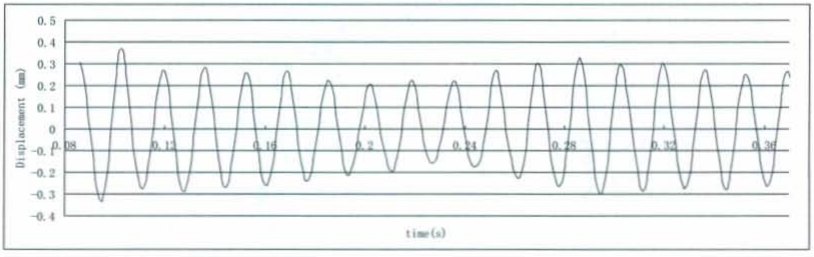

LVDT measurement of displacement amplitude at 47 kg WOB during drilling, shaker control setting '30'

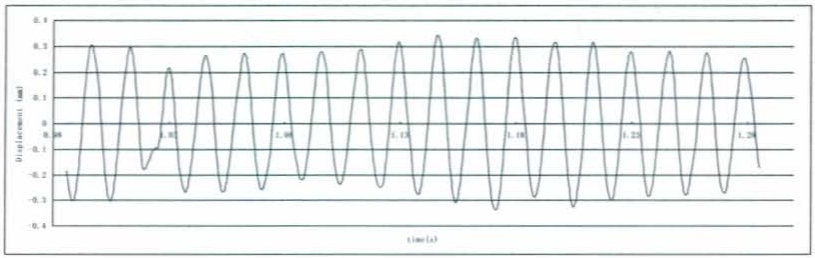

LVDT measurement of displacement amplitude at 47 kg WOB during drilling, shaker control setting '40'

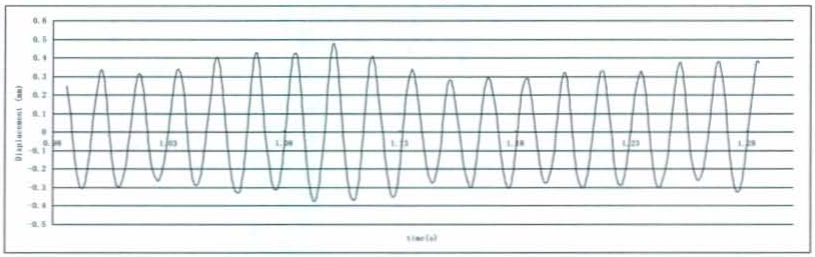

LVDT measurement of displacement amplitude at 47 kg WOB during drilling, shaker control setting '50'

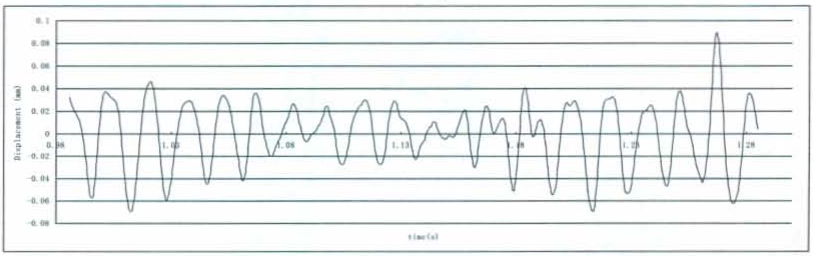

LVDT measurement of displacement amplitude at 64 kg WOB during drilling, shaker control setting '10'

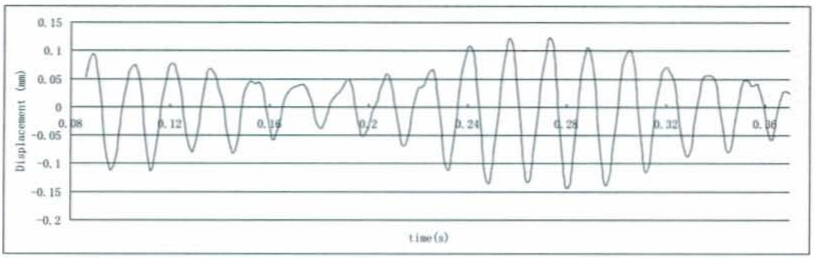

LVDT measurement of displacement amplitude at 64 kg WOB during drilling, shaker control setting '20'

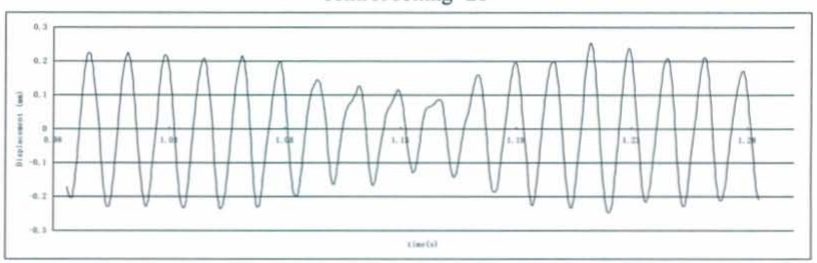

LVDT measurement of displacement amplitude at 64 kg WOB during drilling, shaker control setting '30'

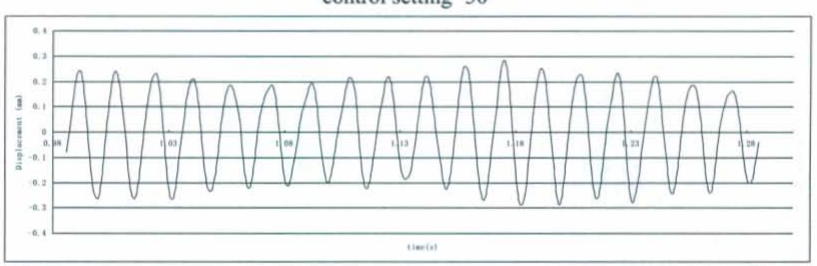

LVDT measurement of displacement amplitude at 64 kg WOB during drilling, shaker control setting '40'

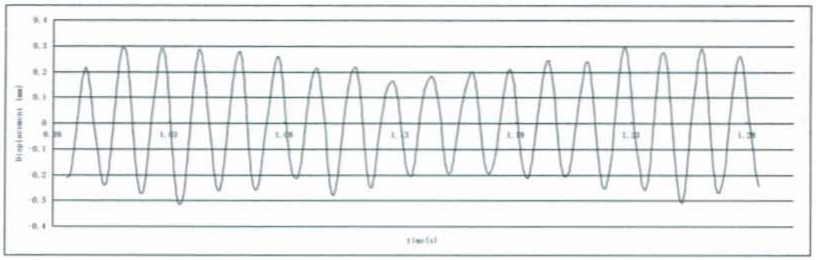

LVDT measurement of displacement amplitude at 64 kg WOB during drilling, shaker control setting '50'

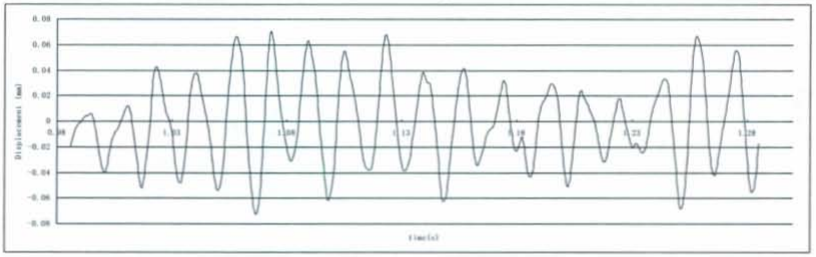

LVDT measurement of displacement amplitude at 81 kg WOB during drilling, shaker control setting '10'

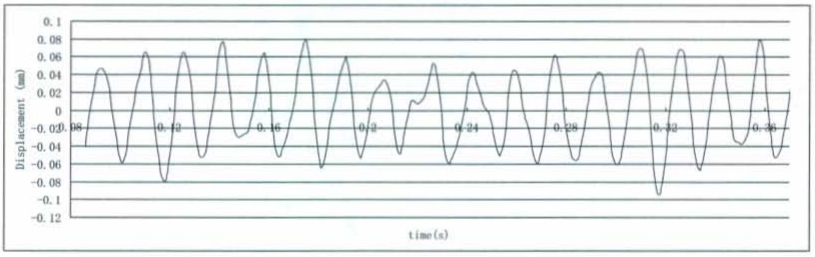

LVDT measurement of displacement amplitude at 81 kg WOB during drilling, shaker control setting '20'

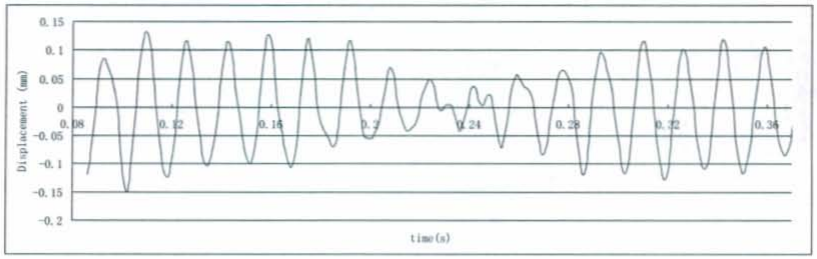

LVDT measurement of displacement amplitude at 81 kg WOB during drilling, shaker control setting '30'

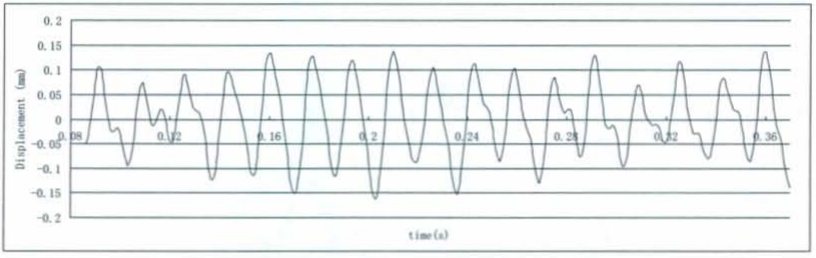

LVDT measurement of displacement amplitude at 81 kg WOB during drilling, shaker control setting '40'

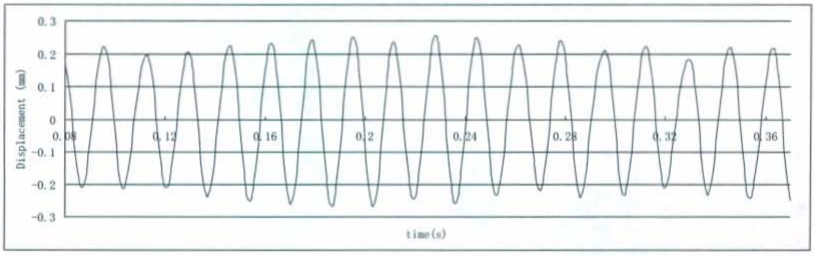

LVDT measurement of displacement amplitude at 81 kg WOB during drilling, shaker control setting '50'

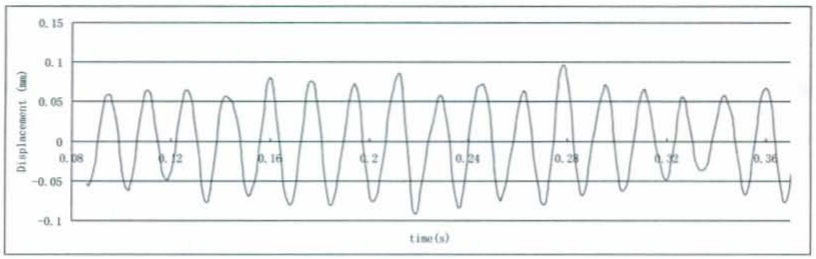

LVDT measurement of displacement amplitude at 98 kg WOB during drilling, shaker control setting '10'

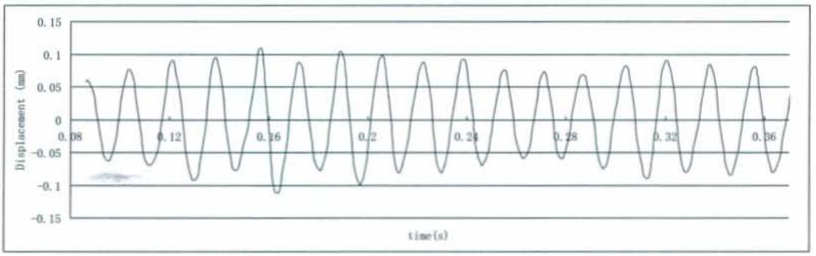

LVDT measurement of displacement amplitude at 98 kg WOB during drilling, shaker control setting '20'

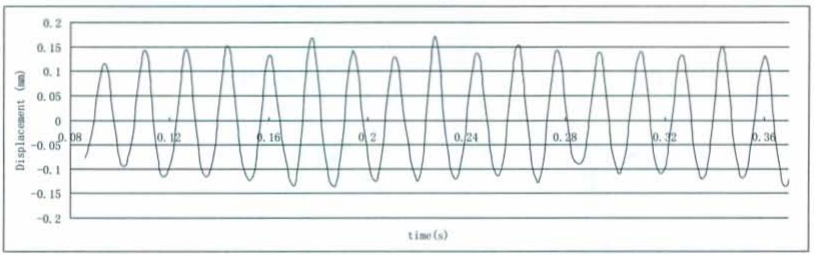

LVDT measurement of displacement amplitude at 98 kg WOB during drilling, shaker control setting '30'

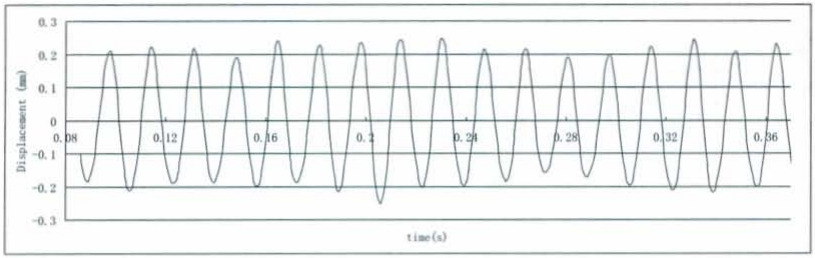

LVDT measurement of displacement amplitude at 98 kg WOB during drilling, shaker control setting '40'

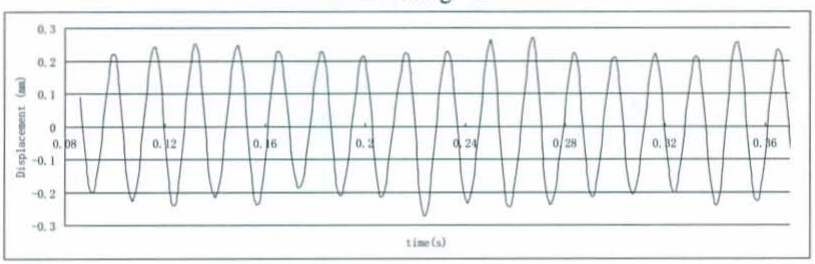

LVDT measurement of displacement amplitude at 98 kg WOB during drilling, , shaker control setting '50'

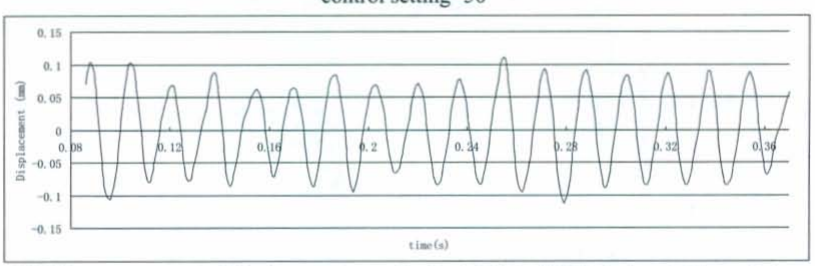

LVDT measurement of displacement amplitude at 115 kg WOB during drilling, shaker control setting '10'

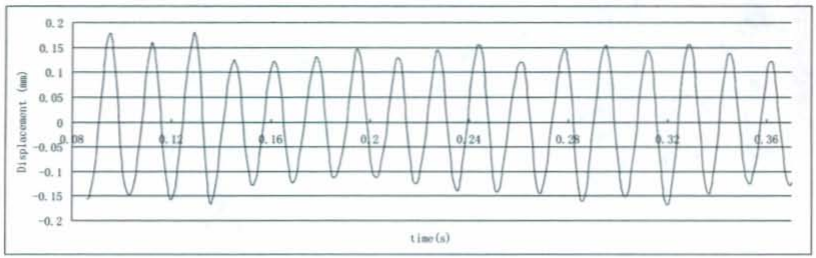

LVDT measurement of displacement amplitude at 115 kg WOB during drilling, shaker control setting '20'

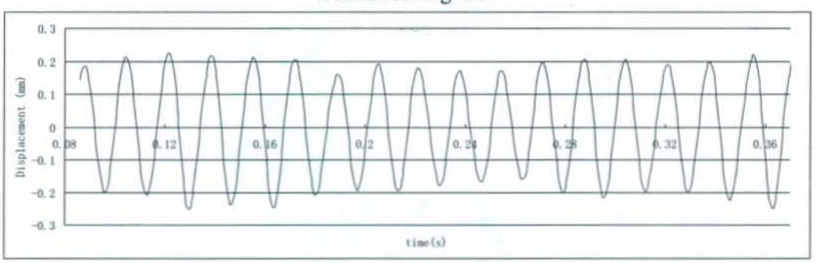

LVDT measurement of displacement amplitude at 115 kg WOB during drilling, shaker control setting '30'

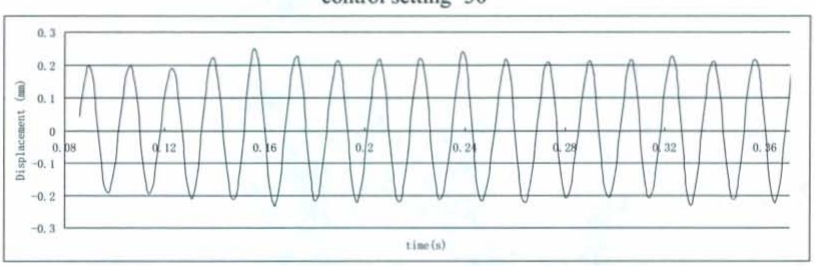

LVDT measurement of displacement amplitude at 115 kg WOB during drilling, shaker control setting '40'

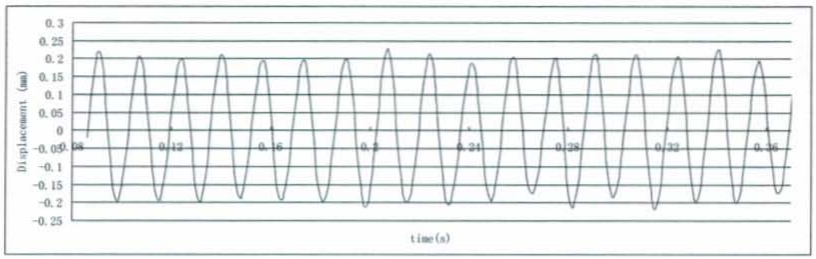

LVDT measurement of displacement amplitude at 115 kg WOB during drilling, shaker control setting '50'

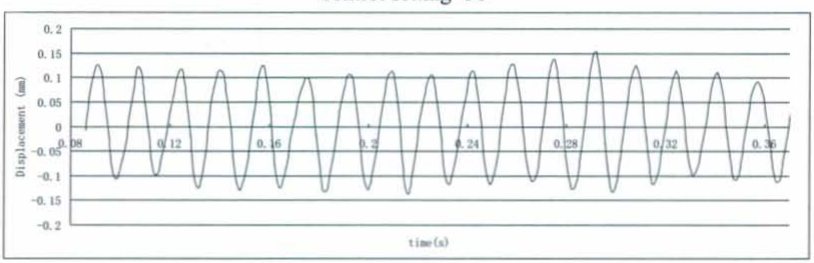

LVDT measurement of displacement amplitude at 130 kg WOB during drilling, shaker control setting '10'

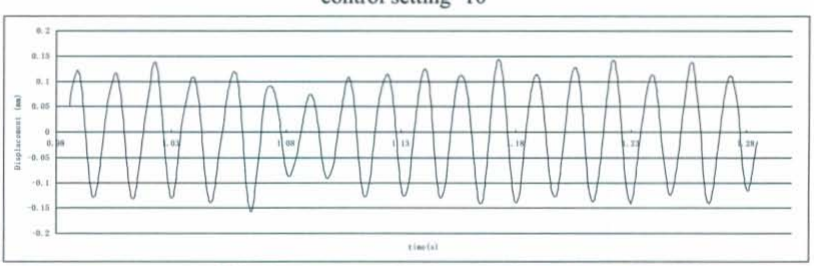

LVDT measurement of displacement amplitude at 130 kg WOB during drilling, shaker setting '20'

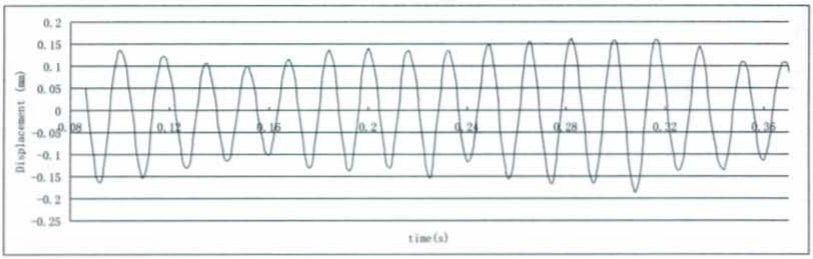

LVDT measurement of displacement amplitude at 130 kg WOB during drilling, shaker control setting '30'

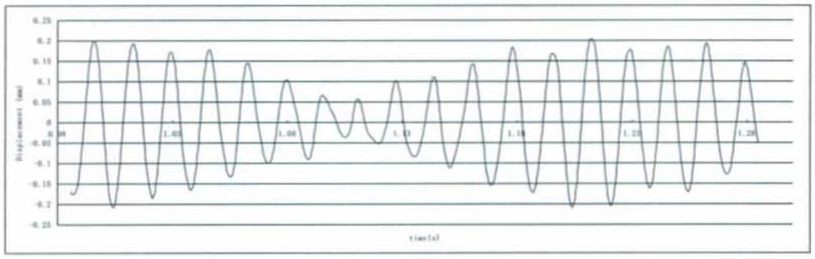

LVDT measurement of displacement amplitude at 130 kg WOB during drilling, shaker control setting '40'

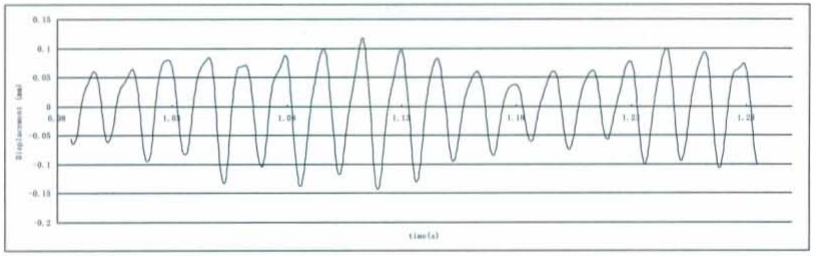

LVDT measurement of displacement amplitude at 130 kg WOB during drilling, shaker control setting '50'

Appendix D: Calculation of the Pump Off Force During a Drill Off Test

Drill- off test is a field operation procedure to locate the optimized operation parameters. The founder WOB and the pump off force could be determined through this test. A passive drill off test begins by locking the drill string at the surface with a strong WOB, then start the bit rotation. When bit penetration starts, the drill string which is compressed by the WOB starts to stretch. This will result in a reduction of WOB; and eventually penetration will stop. As soon as the penetration stops, the bit will be slightly pushed off from the bottom by the pump off force, and the WOB indicator at the surface will have a 0 reading. The elapsed time and bit penetration is recorded during the test so that founder WOB could be located. The following example (Bourgoyne Jr., et al. 1991) shows the calculation of pump off force in a typical drill off test.

A drill-off test is performed with an 8 ½ in natural diamond bit at a depth of 18,858 ft. The TFA of the bit is 0.40 sq in. the drilling mud is oil based, has a density of 1.6 kg/m^3 (13.5 lbm/gal), and is being pumped at a rate of 285 US gal/min. the rotary table is turning at 100 rpm. At an indicated WOB of 6530 kg (14000 lbs), the draw works is locked and a drill-off test is run to measure the bit's pump-off force. The following table records the WOB and standpipe pressure during the test.

Elapsed time (min)	WOB Indicator (lbs)	Standpipe Pressure (psi)
0	14,000	2,490
3	13,000	2,490
10	12,000	2,485
15	11,500	2,485
19	11,000	2,485
22	10,500	2,480
30	10,000	2,480
38	9,000	2,475
52	9,000	2,475
(off bottom)	0	1,650

Force at pump off point

$$F_B=F_{DO}-F_{OB}=9000-0=9000\text{lbs}$$

Pressure drop across bit

$$\Delta P_B=P_{DO}.P_{OB}=2475-1650=825\text{psi}$$

Pump off area

$$A_{PO}=F_B/\Delta P_B=9000\text{lbs}/825\text{psi}=10.91\text{in}^2$$

Standpipe pressure at 14000lbf WOB

$$P_P=2490\text{psi}$$

Pressure drop across bit at 14000lbf WOB

$$\Delta P_B=P_P-P_{OB}=2490-1650=840\text{psi}$$

Pump off force at 14000lbf WOB

$$F_B=A_{PO}\times \Delta P_B=10.9\text{in}^2\times 840\text{psi}=9164.4\text{lbs}$$

susu

Heng Li_s thesis version 3_5_pdf
04/23/11 08:21 AM